CASE FILE
COPY

NACA RM L55K15

NACA

RESEARCH MEMORANDUM

THE ORIGIN AND DISTRIBUTION OF SUPERSONIC STORE INTERFERENCE FROM MEASUREMENT OF INDIVIDUAL FORCES ON SEVERAL WING-FUSELAGE-STORE CONFIGURATIONS

V - SWEPT-WING HEAVY-BOMBER CONFIGURATION WITH LARGE STORE (NACELLE). MACH NUMBER 2.01

By Harry W. Carlson and Douglas J. Geier

Langley Aeronautical Laboratory
Langley Field, Va.

Declassified February 8, 1963

NATIONAL ADVISORY COMMITTEE
FOR AERONAUTICS
WASHINGTON

February 13, 1956

NACA RM L55K15

NATIONAL ADVISORY COMMITTEE FOR AERONAUTICS

RESEARCH MEMORANDUM

THE ORIGIN AND DISTRIBUTION OF SUPERSONIC STORE INTERFERENCE FROM MEASUREMENT OF INDIVIDUAL FORCES ON SEVERAL WING-FUSELAGE-STORE CONFIGURATIONS

V - SWEPT-WING HEAVY-BOMBER CONFIGURATION WITH LARGE STORE (NACELLE). MACH NUMBER 2.01

By Harry W. Carlson and Douglas J. Geier

SUMMARY

A supersonic wind-tunnel investigation of store interference has been performed in the Langley 4- by 4-foot supersonic pressure tunnel at a Mach number of 2.01 in which separate forces on a store and a swept-wing—fuselage combination were measured. The store was separately sting-mounted on its own six-component internal balance and was traversed through a wide systematic range of spanwise, chordwise, and vertical positions. This report presents data on a configuration which simulated a heavy-bomber airplane with a large external store.

The interference effects measured for the heavy-bomber configuration at a Mach number of 2.01 were similar in character and magnitude to those reported previously at a Mach number of 1.61. In general, the maximum interference force coefficients at the higher Mach number are slightly less and the curves are displaced in the direction of the Mach line shift. Linearized-theory calculations of the effect of the wing-fuselage flow field on store drag have been made.

INTRODUCTION

A systematic series of wind-tunnel investigations have been conducted at the Langley 4-foot supersonic pressure tunnel to determine the effect of some configuration variables on the aerodynamic forces incurred by wing-fuselage-store configurations. This report presents the results of one phase of this series in which a large store (a body of revolution

having an equivalent frontal area of a twin-engine nacelle) was tested at a Mach number of 2.01 over a wide range of positions in the vicinity of a swept-wing—fuselage combination simulating a heavy bomber. Separate forces and moments were measured on the sting supported store (six components) and on the wall-mounted half-span wing-fuselage combination (four components). An analysis of the data similar to that presented in references 1, 2, and 3 has been made. In addition, linearized theory calculations of the effect of the wing-fuselage flow field on store drag have been made.

SYMBOLS

$C_{D_{wf}}$ drag coefficient of wing-fuselage combination, $\frac{\text{Drag}}{qS}$

$C_{L_{wf}}$ lift coefficient of wing-fuselage combination, $\frac{\text{Lift}}{qS}$

$C_{m_{wf}}$ pitching-moment coefficient of wing-fuselage combination $\left(\text{about } \frac{\bar{c}}{4}\right)$, $\frac{\text{Pitching moment}}{qS\bar{c}}$

$C_{l_{wf}}$ wing bending-moment coefficient (about fuselage center line, positive up), $\frac{\text{Bending moment}}{qS\frac{b}{2}}$

C_{D_s} drag coefficient of store, $\frac{\text{Drag}}{qF}$

C_{L_s} lift coefficient of store, $\frac{\text{Lift}}{qF}$

C_{m_s} pitching-moment coefficient of store, (about nose unless otherwise indicated), $\frac{\text{Pitching moment}}{qFl}$

C_{Y_s} side-force coefficient of store, $\frac{\text{Side force}}{qF}$

C_{n_s} yawing-moment coefficient of store (about nose), $\frac{\text{Yawing moment}}{qFl}$

C_{D_t} total drag coefficient of complete configuration (wing-fuselage plus store) based on wing area, $C_{D_{wf}} + C_{D_s} F/S$

C_{L_t} total lift coefficient of complete configuration (wing-fuselage plus store) based on wing area, $C_{L_{wf}} + C_{L_s} F/S$

q dynamic pressure, lb/sq ft

P pressure coefficient

P_B base pressure coefficient

$\bar{c}$ mean aerodynamic chord

S total area of wing semispan, 0.5 sq ft

$b/2$ wing semispan, 12 in.

F maximum frontal area of store, 0.0123 sq ft

l store length, in.

x chordwise position of store midpoint, measured from fuselage nose, in.

y spanwise position of store center line, measured from fuselage center line, in.

z vertical position of store center line, measured from wing chord plane, positive downward, in.

β cotangent of Mach angle, $\sqrt{M^2 - 1}$

α wing-fuselage angle of attack, deg

Subscripts:

w wing

wf wing-fuselage combination

s store

t total, for complete configuration (wing-fuselage-store)

MODELS AND EQUIPMENT

The models and the general arrangement of the test setup are shown in the drawing of figure 1 and the photograph in figure 2. Additional information and model dimensions are given in table I.

The wing-fuselage half-span model was constructed of metal and was mounted on a boundary-layer bypass plate. A four-component strain-gage balance housed within the plate measured normal force, chord force, pitching moment, and wing bending moment.

The store, (a body of revolution scaled to have the equivalent frontal area of a twin-engine nacelle) was constructed of metal and was mounted on a six-component sting-supported internal strain-gage balance. The store support equipment allowed translational motion in a plane parallel to the plane of the wing, and in addition, through a remotely operated crank provided a vertical movement. Since the store and balance rotated as they moved from one height to another, resolution of forces was necessary to obtain values in the vertical and horizontal plane. The store chordwise location was varied by changing the length of the support sting during shutdown between tunnel runs. Store base pressure was obtained by measurement of the pressure in the store balance cavity.

TESTS

This investigation was performed in the Langley 4- by 4-foot supersonic pressure tunnel at a Mach number of 2.01 and a Reynolds number of 3.62×10^6 per foot. The positions in which the store was tested are shown by the "test grid" of figure 1. The store and wing-fuselage both remained at zero degrees angle of attack when the store was at vertical positions $z = 1.15$ and 1.67. At $z = 2.09$ tests were made with the wing-fuselage at 0° and 4° angle of attack while the store remained at $\alpha = 0^\circ$.

A 1/4-inch-wide strip of number 60 carborundum grains in shellac was located on both surfaces of the wing along the 10-percent chord line, on the fuselage nose 1/2 inch from the tip, and on the store nose 1/4 inch from the tip, in order to insure boundary-layer transition from laminar to turbulent.

A discussion of the extraneous support interference encountered and the ability of this technique to reproduce the data obtained on full-span models is discussed in reference 1.

Precision of Data

An estimate of the relative accuracy in the present data as determined from an inspection of repeat test points and static-calibration deflections is presented below:

Store Position

x, in.	±0.025
y, in.	±0.05
z, in.	±0.05

Store		Wing Fuselage	
C_{D_S}	±0.005	$C_{D_{wf}}$	±0.0005
C_{L_S}	±0.010	$C_{L_{wf}}$	±0.005
C_{m_S}	±0.005	$C_{m_{wf}}$	±0.002
C_{Y_S}	±0.010	$C_{l_{wf}}$	±0.002
C_{n_S}	±0.005	α, deg	±0.1
α_S, deg	±0.2		

PRESENTATION OF TEST DATA

All of the test data (both on store and wing-fuselage) have been adjusted to correspond to the condition of free-stream static pressure at the model base.

Isolated Store and Wing-Fuselage Data

These data are presented so that the interference effects can be evaluated in terms of the isolated forces and equivalent angle of attack.

Figure 3 shows lift, drag, and pitching-moment coefficients referred to the wind axis for the store alone at angles of attack up to 10°. The store was tested in pitch in both the plane of the pitch beam and in the plane of the side force beam. The forces and moments thus obtained agree within the stated accuracy of the tests.

Figure 4 presents the isolated wing-fuselage data. Lift, drag, pitching-moment and wing bending-moment coefficients based on the wind axis are shown for angles of attack from -1° to 4°. Limitations of the test apparatus prevented a greater α range.

Chordwise Plots of Basic Data

The measured test data are presented in the form of plots of force and moment coefficient against chordwise position of the store midpoint. Offset vertical scales are used so that data for the 11 spanwise positions can be shown in a single figure. On the right and left margins the zero for each curve is identified with the line symbol corresponding to that spanwise position. On each figure is a sketch of the configuration showing the store positions at which measurements were obtained. The use of the chordwise position parameter, $x-\beta y$, facilitated the fairing of the curves.

Drag, lift, side force, pitching moment, and yawing moment for the store in the presence of the wing-fuselage are presented in figures 5 to 9. Figure 10 gives the measured store base pressures used in adjusting the above-mentioned data. Parts (a) through (d) of each of the above figures show data for three store vertical locations and two angles of attack, (four conditions). In figures 11 to 13, drag, lift, and pitching moment of the wing-fuselage combination are presented for the four conditions. In figure 14, wing bending moment for three conditions is presented. Total drag and total lift of the complete configuration (wing-fuselage-store) are shown in the four parts of figures 15 and 16.

Contour Maps of Basic Data

The bulk of the basic data has been repeated in the form of contour maps (figs. 17 to 27). The number assigned to the contour line is the force or moment coefficient of the store or wing-fuselage with the store midpoint at any point on that line. Maps are presented for each of the forces and moments at two vertical heights and two angles of attack (three conditions).

Two other contour maps which have been prepared from the basic data are presented. In figure 28 the slope of the store lift coefficient with wing-fuselage angle of attack is shown in the form of a contour map, and the slope of the store side-force coefficient is shown in figure 29. The slopes were computed assuming a linear variation of the particular coefficient between 0° and 4° angle of attack.

Comparison Figures

Figures 30 to 36 show the effect of a reduction in Mach number on the store and wing-fuselage forces and, in addition, on the slope of store lift and side force with wing fuselage angle of attack. The Mach number 1.61 data are reproduced from references 1 and 2.

The effect of changes in vertical store displacement on store drag, store lift, store side force, wing-fuselage drag, and wing-fuselage lift can be seen from an inspection of figures 37 to 41. At each of four representative spanwise positions, coefficients for three vertical positions are shown on the same plot.

In the same fashion, the effect of wing-fuselage angle of attack on these forces is shown in figures 42 to 46.

The relative contribution of the store and the wing fuselage to the total drag and total lift is shown in figures 47 and 48.

DISCUSSION OF RESULTS

Store Drag

The results for store drag are similar to those obtained at a Mach number of 1.6 and reported in reference 1. The interference values at a Mach number of 2.01 are slightly smaller; that is, lower maximum and higher minimum drag coefficient values are encountered, as shown in figure 30. Figure 30 also shows that the drag reduction that occurs when the store base is in the positive pressure region between the bow wave and the leading edge of the wing is smaller and occurs farther aft at a Mach number of 2.01. This trend is as would be expected when the rearward shift of the Mach line is considered.

Increasing the separation distance (z) between the store and the wing causes relatively large changes in store drag as shown in figure 37. This is most evident when the store midpoint is near the quarter chord of the local wing section. For instance, at $y = 3.0$ in., the maximum drag reduction due to increased separation is of the same size (40 percent of the isolated store drag) as the maximum change due to variation in chordwise position.

For some chordwise positions, large increases in drag occur with an increase in wing-fuselage angle of attack as shown in figure 42. However, this result is not general and for some locations decreases are shown, particularly when the afterbody of the store is in the region of increased pressure about the wing leading edge.

Store Lift

As shown in figure 31 the positive interference lift on the store at a Mach number of 2.01 is somewhat smaller than at the lower Mach number. The effect of store vertical location and wing-fuselage angle of attack on store lift (figs. 38 and 43) is similar to that shown in reference 2 for a Mach number of 1.61. At some chordwise positions the decrease in lift due to increasing z is about 3/4 of the maximum change due to variations in chordwise position, which as was the case for store drag is most pronounced when the store midpoint is near the quarter chord of the local wing section. Decreases due to an increase in wing-fuselage angle of attack to 4° are as large as 2/3 of the chordwise variation. However, as was pointed out in reference 2 and as will be shown later in this report, store interference lift is only a small part of the configuration total interference lift.

Store Side Force

Variations in store side force at zero angle of attack occur with the change in Mach number as shown in figure 32. The contour map of the slope of store side force with wing-fuselage angle of attack (fig. 29) shows a marked similarity to the one in reference 2 at a Mach number of 1.61. This indicates that the development of spanwise flow is not greatly affected by the Mach number change from 1.61 to 2.01.

The effect of vertical location is less on store side force (fig. 39) than on store lift or drag (figs. 37 and 38). Maximum changes due to vertical location are only half those due to chordwise position.

Store Pitching Moment and Yawing Moment

Comparison figures are not presented for store pitching moment and yawing moment. As shown in the basic data, the store moments were referenced to the nose. However, that data, being based on an unrealistic center of gravity, cannot be used to show the effects of the variables on store moments. An examination of the moment data referred to the store midpoint showed that the moments are less affected by changes in vertical location and angle of attack than the forces. For instance, the maximum change in store yawing moment due to the 4° change in angle of attack is one-third the maximum change due to chordwise position. In the case of side force the two variables had equal effects. This result is in agreement with that obtained at a Mach number of 1.61.

Wing-Fuselage Drag

Figure 33 presents a comparison of wing-fuselage drag in the presence of the store of the two Mach numbers. No explanation could be found for the substantial and unexpected increase in drag-coefficient level at a Mach number of 2.01. The interference, however, is somewhat less pronounced at the higher Mach number. Only small changes in the interference pattern occur with an increase in z (fig. 40). Of course, at angle of attack (fig. 45) the whole curve is at a higher level and more severe interference forces are exhibited.

Wing-Fuselage Lift

The curves of wing-fuselage lift in the presence of the store at the two Mach numbers (figure 34) show reasonable agreement, except at x = 18 for the inboard stations. The effect of vertical height on the lift is relatively small, see figure 41. At the increased angle of attack, (fig. 46) although the level of the curve increases, the interference pattern changes little.

Total Drag

Figure 47 shows that both store and wing-fuselage contribute almost equally to the total interference drag. Notice that, in general, store positions that give high store drag also result in high wing-fuselage drags, as was also the case at a Mach number of 1.61. Total drags 16 percent higher and 10 percent lower than the sum of the isolated store and isolated wing-fuselage drags were encountered.

Total Lift

Figure 48 shows that the total lift is composed almost entirely of the wing-fuselage lift. The maximum interference lift obtained corresponds to lift generated by the wing-fuselage at 1^{o} angle of attack. A comparison with figure 47 shows that almost this amount of lift can be generated at a store position that produces no interference drag penalty, (y = 3.0 in., x = 28 in.).

Wing-Fuselage Flow Field

In an attempt to predict the interference drag of the store in the vicinity of the wing-fuselage, linearized theory has been used to calculate the longitudinal static pressure distribution at two spanwise positions, and these pressures have been used to calculate the buoyant force on the

store. The pressure distributions for $y = 5.4$ and $y = 9.0$ are shown in figure 49. A comparison of the resulting drag values and the experimental interference store drag is also shown.

The buoyant force experienced by the store is dependent on the combined flow field of the wing and the fuselage (including wing-fuselage interference) and on the reflected field of the store itself with the wing or fuselage acting as a reflecting surface. The pressure distributions due to the wing and fuselage were determined separately and were added, the effect of the interference between the wing and the fuselage being neglected. The effect of the image store field was investigated and found to be negligible in the cases considered.

The familiar equations of linearized theory were used in evaluating the pressures. However, because of the complexity of the configuration, graphical integration was employed. The following equations were used:

Wing

$$P_w = -2\phi x$$

$$\phi = -\frac{1}{\pi}\iint \frac{f(\xi,n)\,d\xi\,dn}{\sqrt{(x-\xi)^2 - \beta^2\left[(y-n)^2 + z^2\right]}}$$

$$f(\xi,n) = \lambda$$

Fuselage

$$P_f = \frac{1}{\pi}\int \frac{f(\xi)\,d\xi}{\sqrt{(x-\xi)^2 - \beta^2 y^2}}$$

$$f(\xi) = \frac{d^2S}{d\xi^2}$$

where

ϕ velocity potential

λ slope of wing surface in streamwise direction

S cross-sectional area of fuselage

x,y,z field point location in Cartesian coordinates

ξ,n source location in Cartesian coordinates

The graphical method used did not completely take into account the singular nature of the distance functions,

$$\frac{1}{\sqrt{(x-\xi)^2 - \beta^2\left[(y-n)^2 + z^2\right]}}$$

and

$$\frac{1}{\sqrt{(x - \xi)^2 - \beta^2 y^2}}$$

their maximum value being arbitrarily limited in the plotting. The maximum error in the calculated pressure coefficient due to that omission and to plotting and integrating errors is estimated to be ±0.02. An error of 0.02 in pressure coefficient along the length of the store (positive over the forebody, negative on the afterbody) produces an error in the integrated drag coefficient of 0.032. However, that represents an extreme case not likely to be encountered.

The infinite slope at the leading edge of the 65A006 wing section was treated in the same manner as the infinity of the distance function, being arbitrarily limited to a slope of 0.3. This treatment of the leading edge is one of many possible adjustments for a condition which violates the assumptions of linearized theory. As will be shown later, this is one region where the theory as used here is inadequate. The velocity potential was found by a double integration involving a continuous distribution of sources over the surface of the wing within the fore Mach cone from the point in the field. The resulting velocity potentials were plotted against x and were differentiated to obtain the pressure coefficient due to the wing alone along a line parallel to the wing-fuselage axis.

The wing was treated as being symmetrical about $y = 1.375$, the fuselage surface being considered to act as a reflection plane. However, the contribution of the image wing is small for the cases treated, amounting to 0.015 in pressure coefficient at the maximum. The pressure distributions due to the wing, the fuselage, and the combination are shown in the upper portion of figure 49. The experimental and the calculated theoretical drags are also shown in this figure.

The sharp break in the theoretical drag curve at $x = 17.5$ in part (a) and at 21.5 in part (b) occurs when the base of the store moves into the positive pressure region at the wing leading edge. In both cases, it can be seen that better agreement would result if the positive pressure jump appeared as a bow wave some distance ahead of the leading edge. An examination of the store drag data and store base pressures indicates that the bow wave is present at this Mach number and at a Mach number of 1.61. Another sharp break occurs in both curves when the increase in pressure at the trailing edge of the wing first affects the store afterbody. This causes a pronounced disagreement between experiment and theory. Apparently, this pressure buildup is not nearly as sharp as the theory predicts. These seem to be the two major causes of the disagreement between experiment and theory.

On the whole, the calculations do predict the proper trends in store drag although the quantitative agreement is poor. A more exact theoretical solution and a more appropriate treatment of the wing leading edge quite possibly would show better agreement with experiment.

CONCLUSIONS

The results of a supersonic wind-tunnel investigation at a Mach number of 2.01, in which separate forces were measured on a store and a swept-wing—fuselage combination for a wide range of store positions, provide the following conclusions:

1. The interference effects measured at a Mach number of 2.01 are similar in character to those previously reported at a Mach number of 1.61 in references 1 and 2.

2. The principal effect of the change in Mach number was to slightly reduce the maximum interference effects when expressed in coefficient form and to shift the occurrence of these peaks in the directions of the Mach line change.

3. The interference store drags calculated from linear theory showed but limited agreement with experiment. The major areas of disagreement, however, are explainable in most cases by the well-known limitations of linearized theory in predicting the wing-body flow field.

Langley Aeronautical Laboratory,
National Advisory Committee for Aeronautics,
Langley Field, Va., November 17, 1955.

REFERENCES

1. Smith, Norman F., and Carlson, Harry W.: The Origin and Distribution of Supersonic Store Interference From Measurement of Individual Forces on Several Wing-Fuselage-Store Configurations. I. - Swept-Wing Heavy-Bomber Configuration With Large Store (Nacelle). Lift and Drag; Mach Number, 1.61. NACA RM L55A13a, 1955.

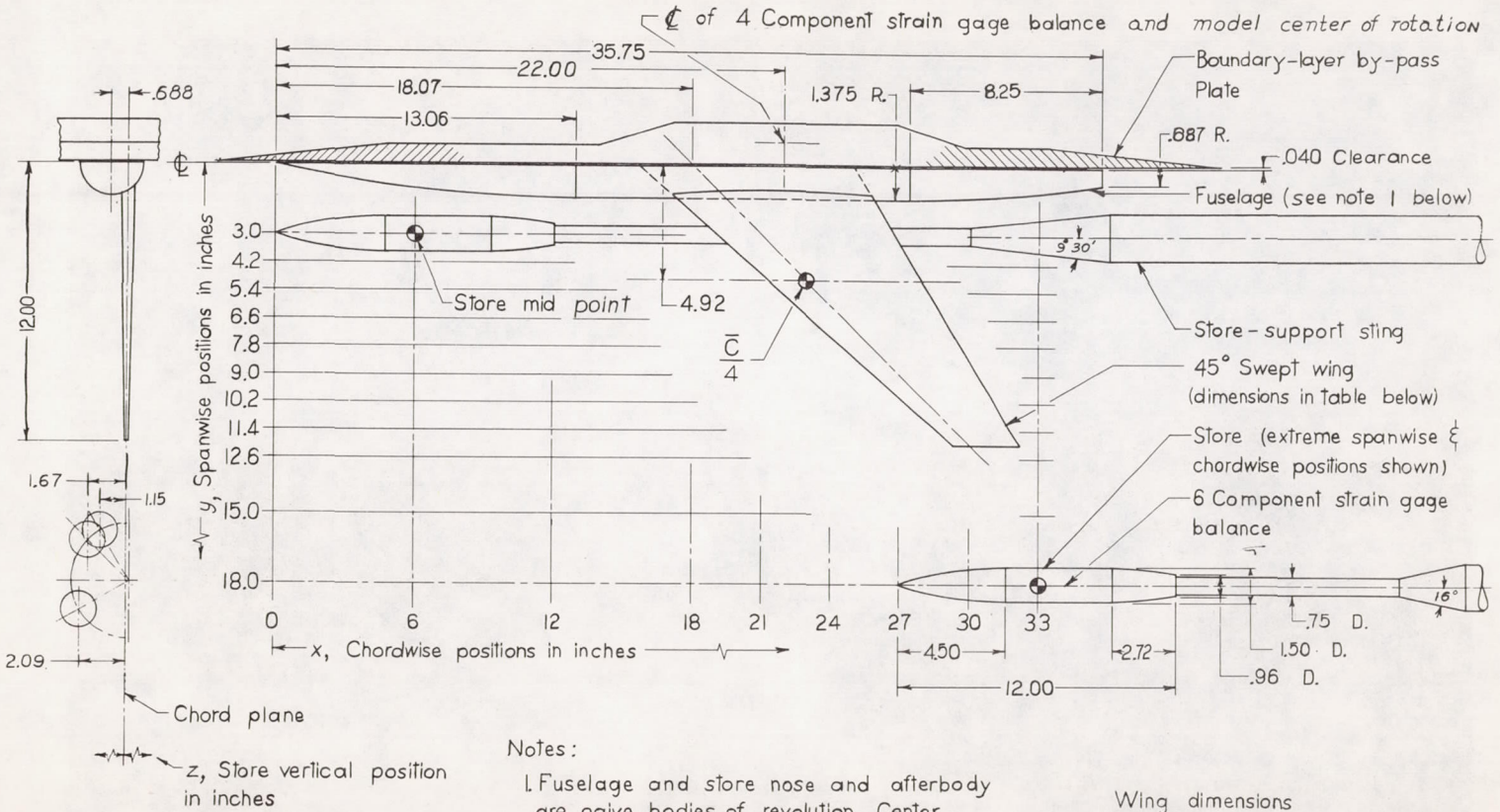
2. Smith, Norman F., and Carlson, Harry W.: The Origin and Distribution of Supersonic Store Interference From Measurement of Individual Forces on Several Wing-Fuselage-Store Configurations. II. - Swept-Wing Heavy-Bomber Configuration With Large Store (Nacelle). Lateral Forces and Pitching Moments, Mach Number, 1.61. NACA RM L55E26a, 1955.

3. Smith, Norman F., and Carlson, Harry W.: Some Effects of Configuration Variables on Store Loads at Supersonic Speeds. NACA RM L55E05, 1955.

TABLE I

Pertinent Model Dimensions

Store:	
Maximum diameter, in.	1.5
Maximum frontal area, sq ft	0.0123
Base diameter, in.	0.96
Base area, sq ft	0.0050
Over-all length, in.	12
Nose fineness ratio	3
Afterbody fineness ratio	1.82
Over-all fineness ratio	8
Ratio of wing area to store maximum frontal area	40.6
Fuselage:	
Maximum diameter, in.	2.750
Maximum frontal area (semicircle), sq ft	0.0206
Base diameter, in.	1.372
Base area (semicircle), sq ft	0.0051
Over-all length	35.75
Nose fineness ratio	4.75
Afterbody fineness ratio	3
Over-all fineness ratio	13
Swept Wing:	
Semispan, in.	12
Mean aerodynamic chord, in.	6.580
Area (semispan), sq ft	0.500
Sweep (c/4), deg	45
Aspect ratio	4
Taper ratio	0.3
Chord, in.	9.23
Section	NACA 65A006



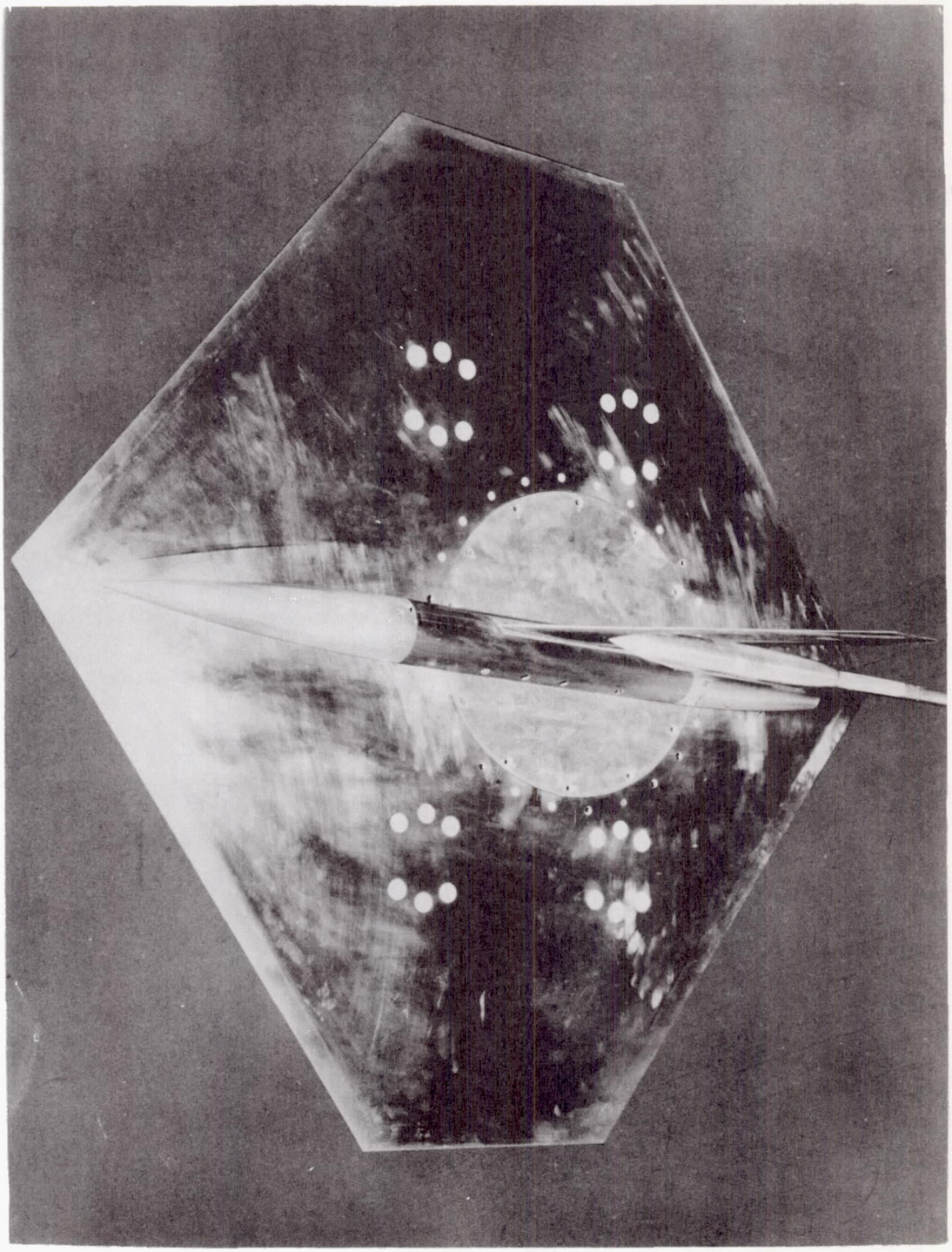
Notes:

1. Fuselage and store nose and afterbody are ogive bodies of revolution. Center sections are cylindrical
2. All dimensions in inches.

Wing dimensions

Semi-span	12
Sweep $\frac{c}{4}$	45°
Aspect ratio	4
Taper ratio	0.3
℄ Chord	9.23
Section	65A-006

Figure 1.- Layout of models showing dimensions of components and ranges of store positions investigated.



L-87526

Figure 2.- Photograph of models. Transition strips not shown.

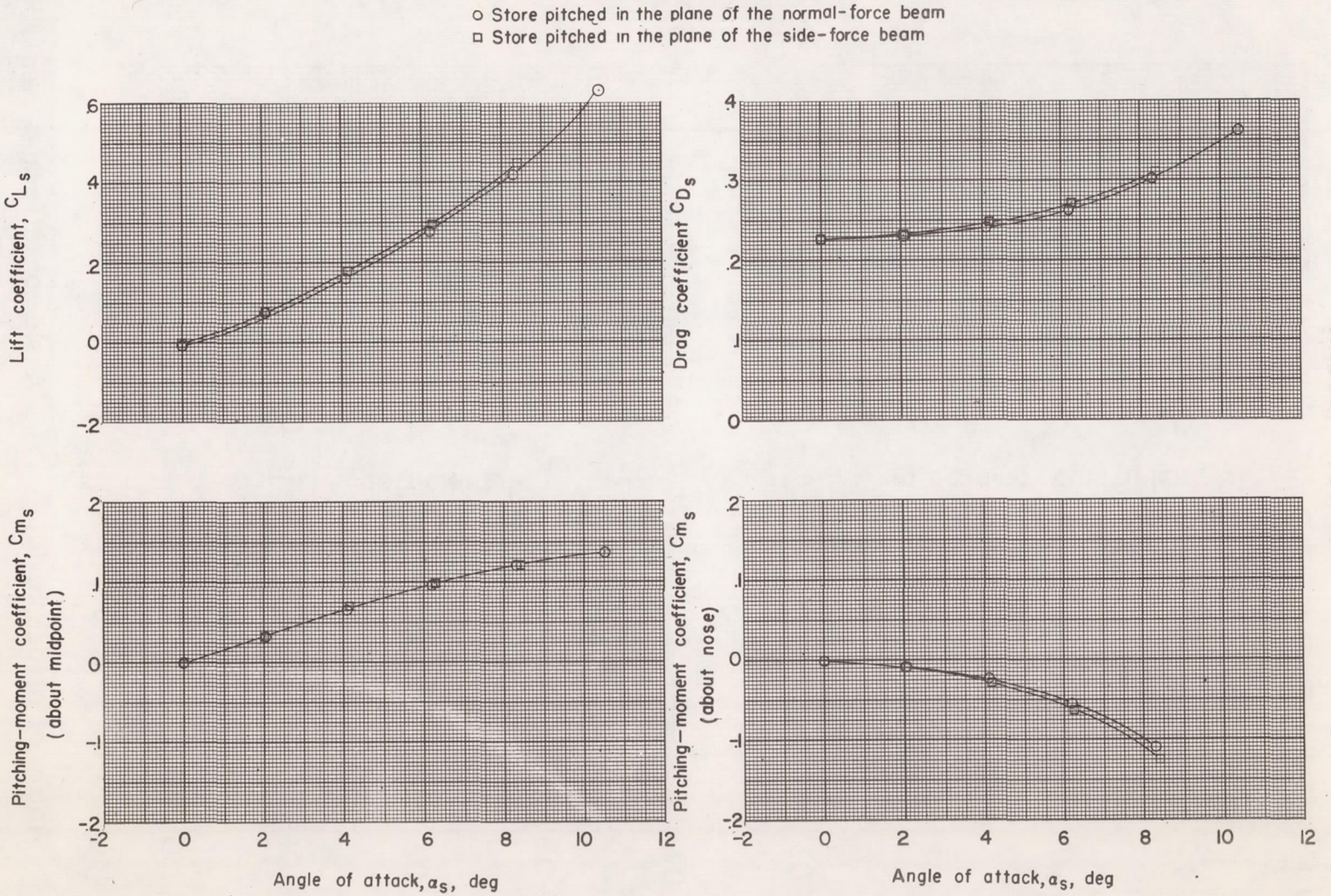


Figure 3.- Aerodynamic characteristics of the isolated store.

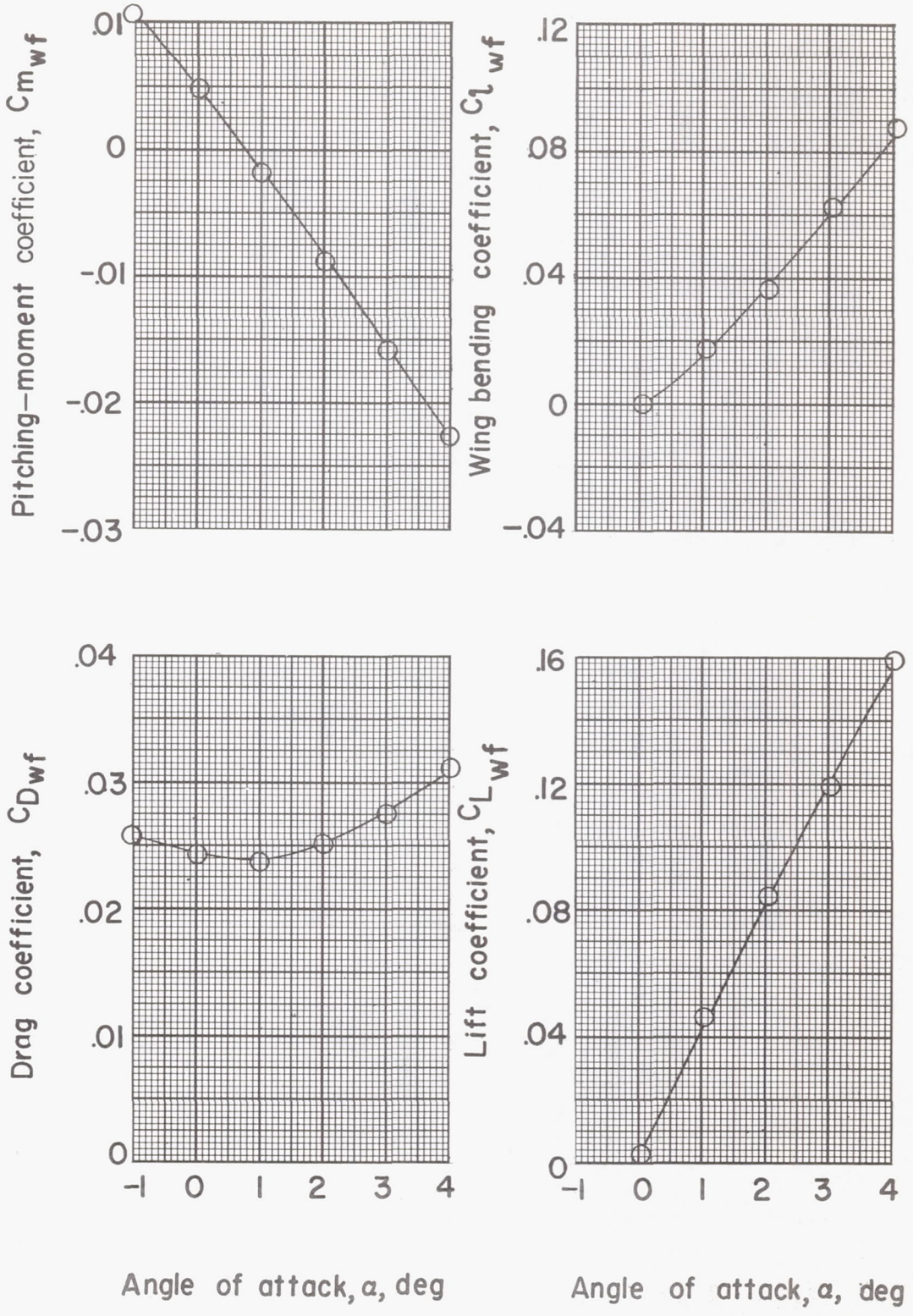
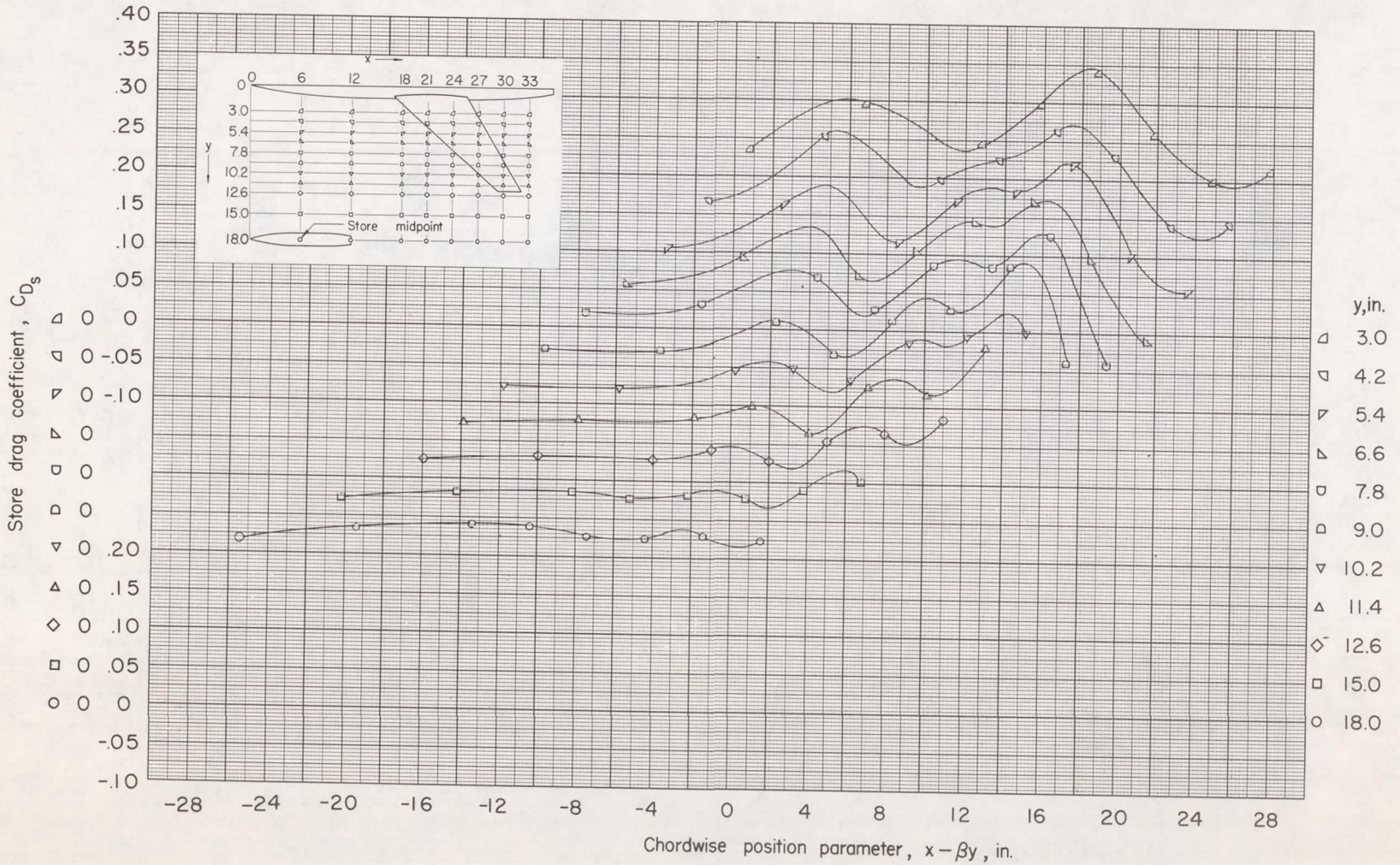
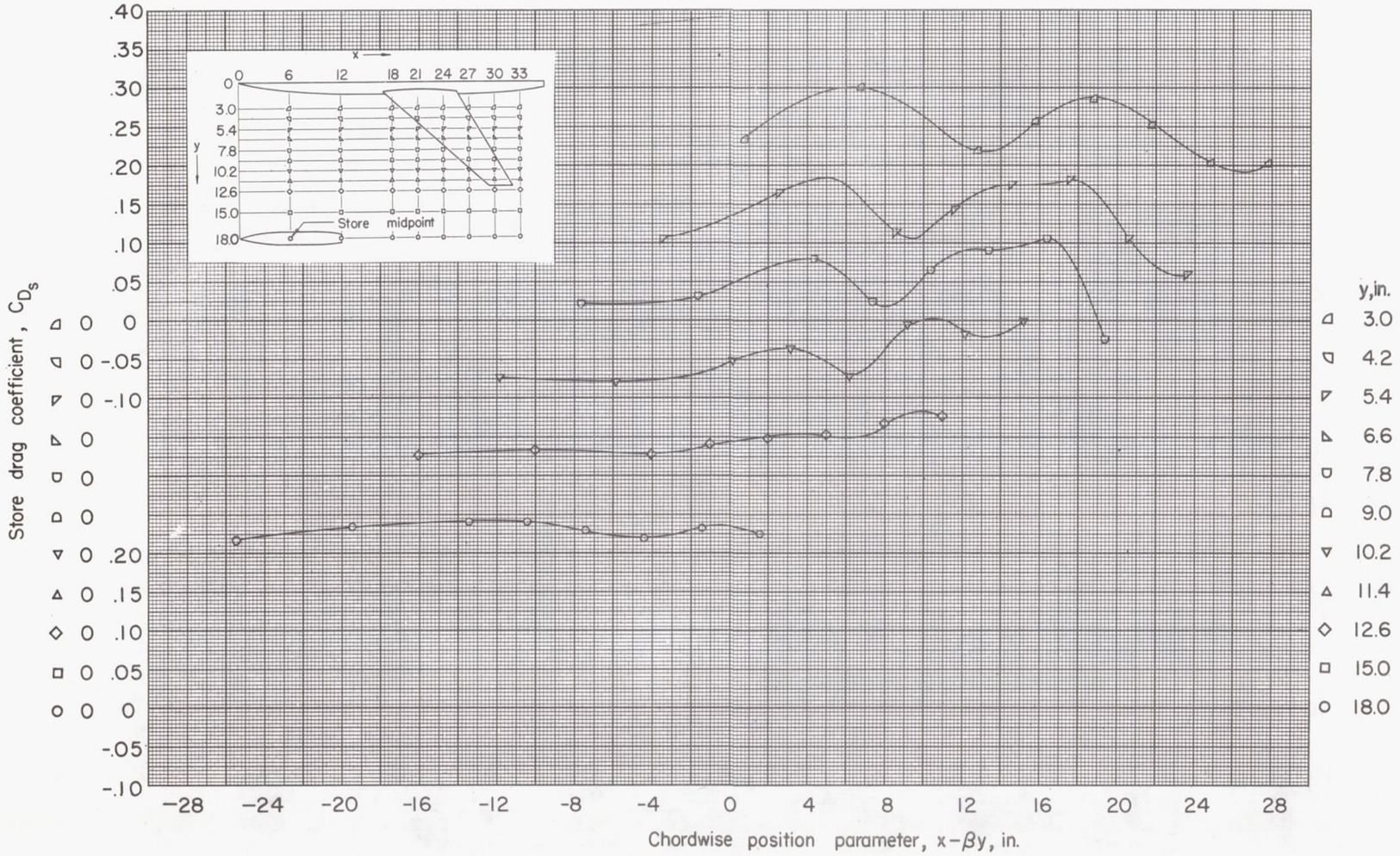


Figure 4.- Aerodynamic characteristics of the isolated wing-fuselage combination.



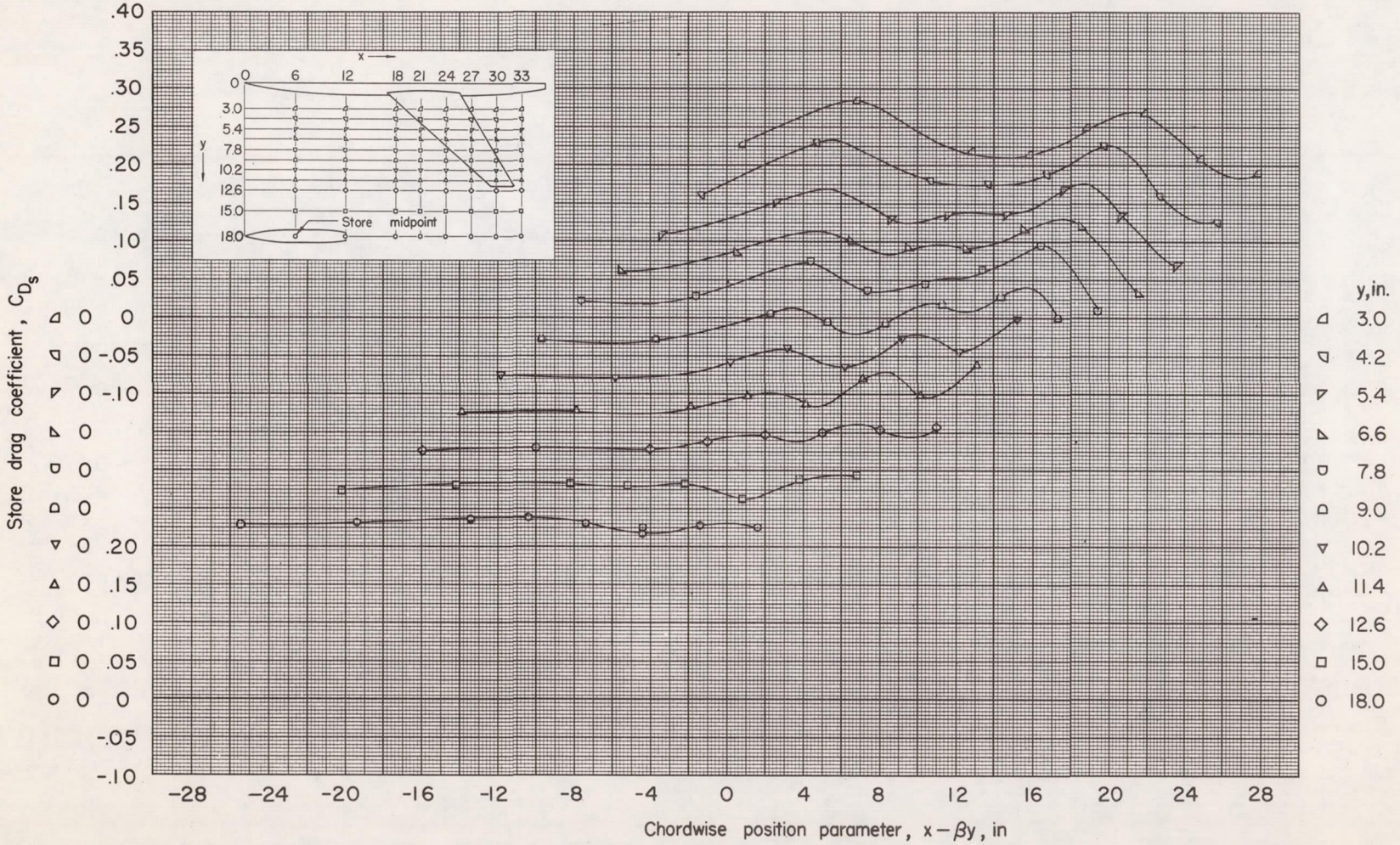
(a) z = 1.15 inches; $\alpha = 0^{\circ}$.

Figure 5.- Drag of store in presence of wing-fuselage combination.



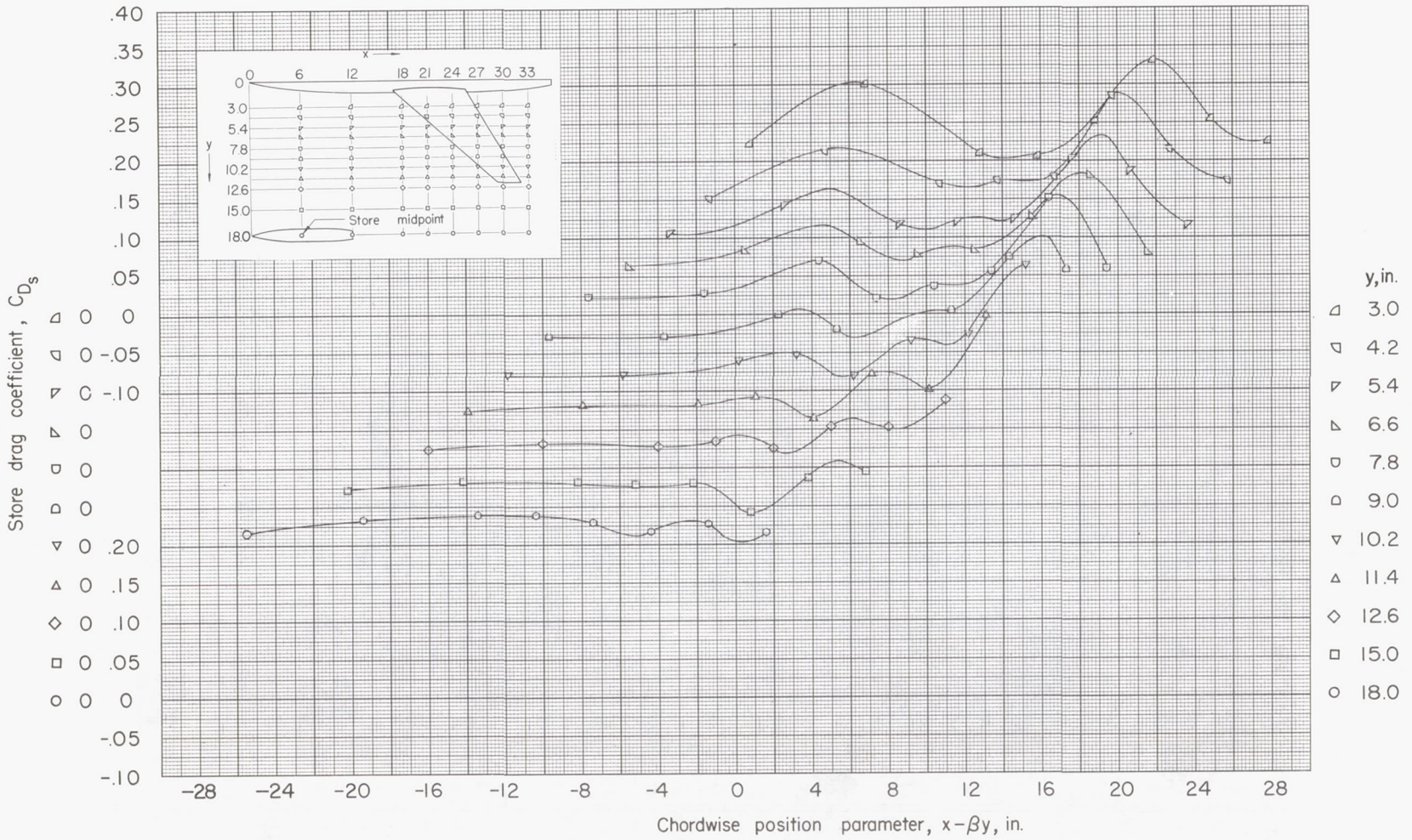
(b) z = 1.67 inches; $\alpha = 0^{\circ}$.

Figure 5.- Continued.



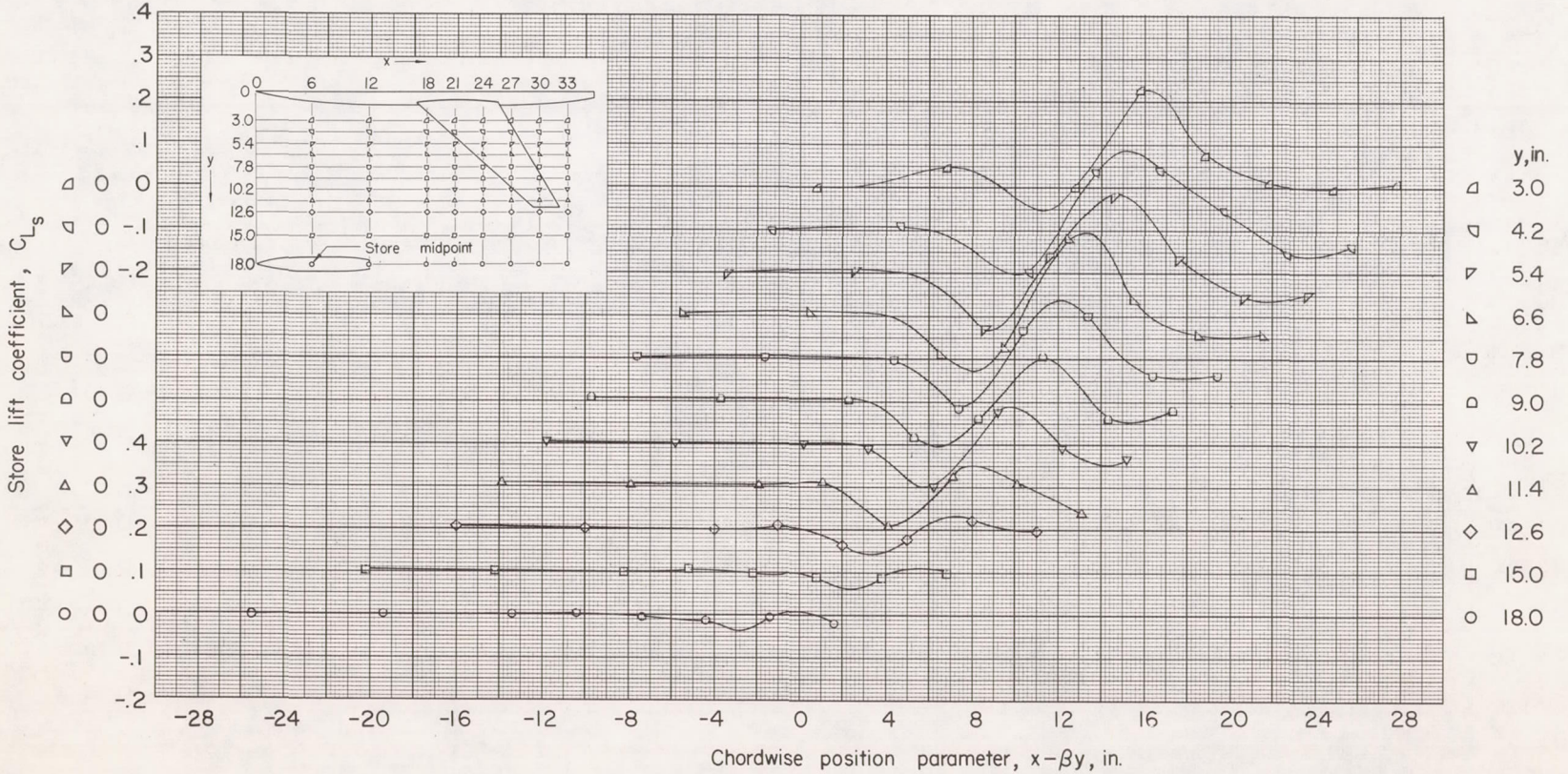
(c) z = 2.09 inches; $\alpha = 0^{\circ}$.

Figure 5.- Continued.



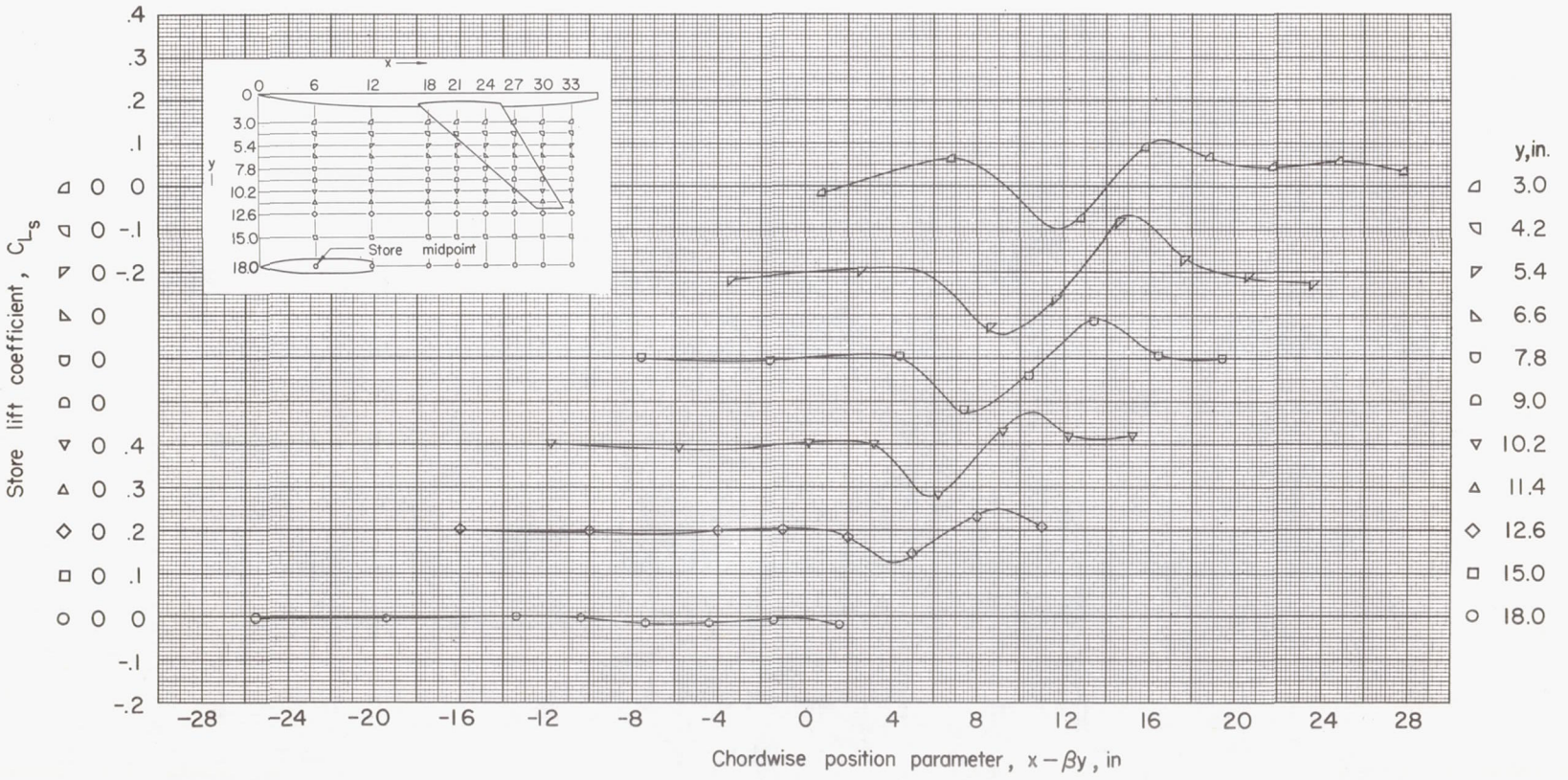
(d) z = 2.09 inches; $\alpha = 4^{\circ}$.

Figure 5.- Concluded.



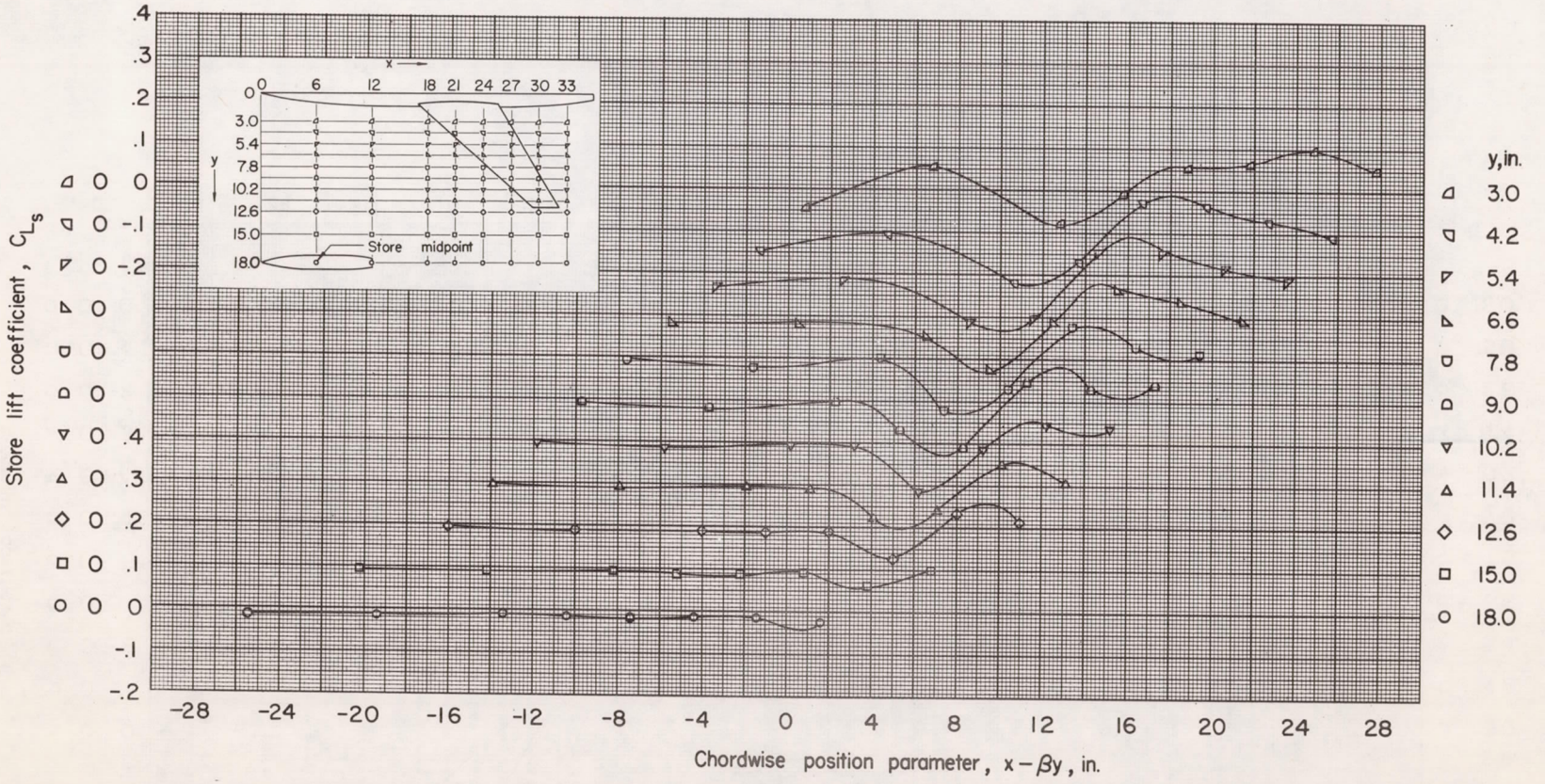
(a) z = 1.15 inches; $\alpha = 0^{\circ}$.

Figure 6.- Lift of store in presence of wing-fuselage combination.



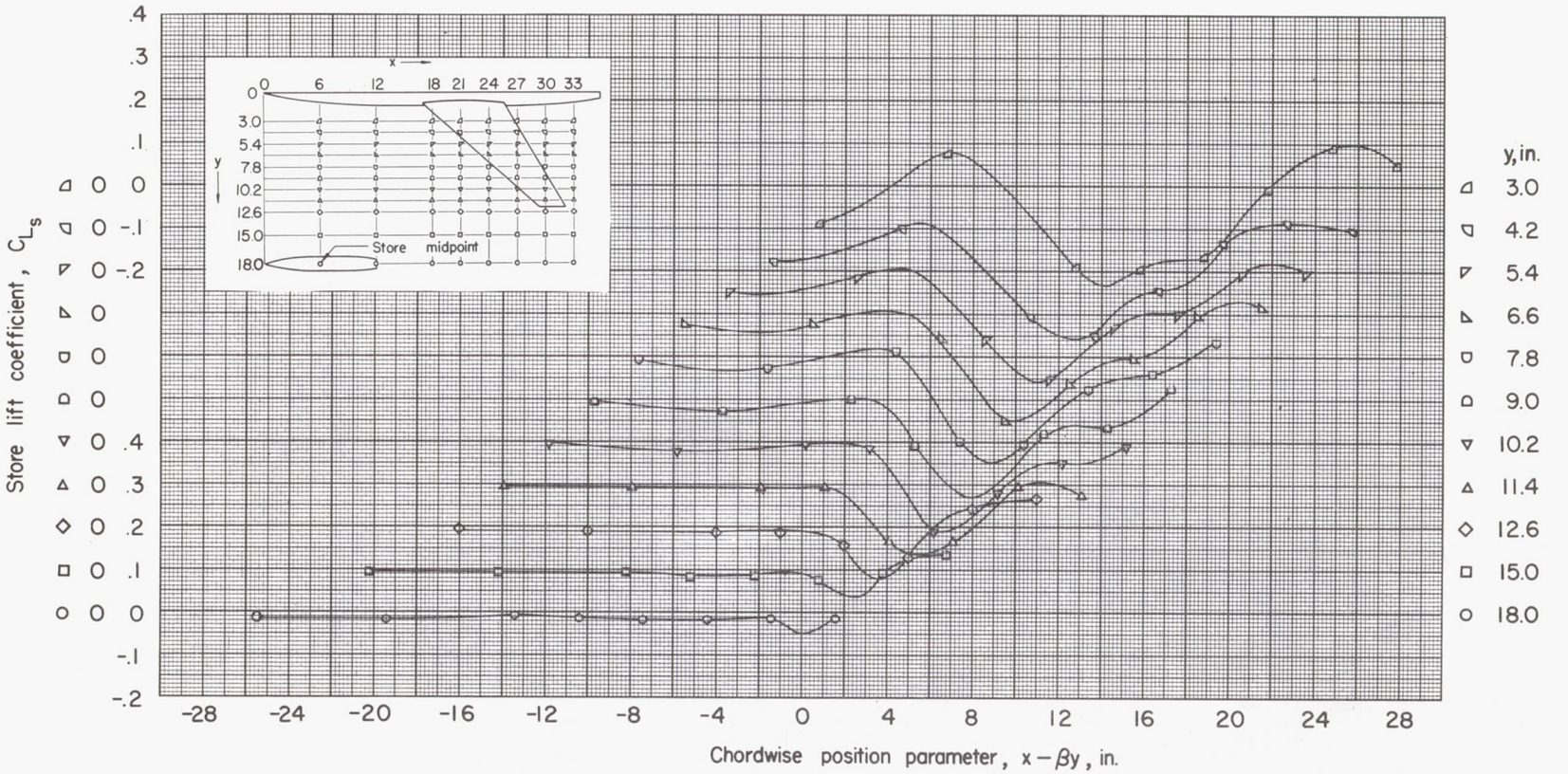
(b) $z = 1.67$ inches; $\alpha = 0^{\circ}$.

Figure 6.- Continued.



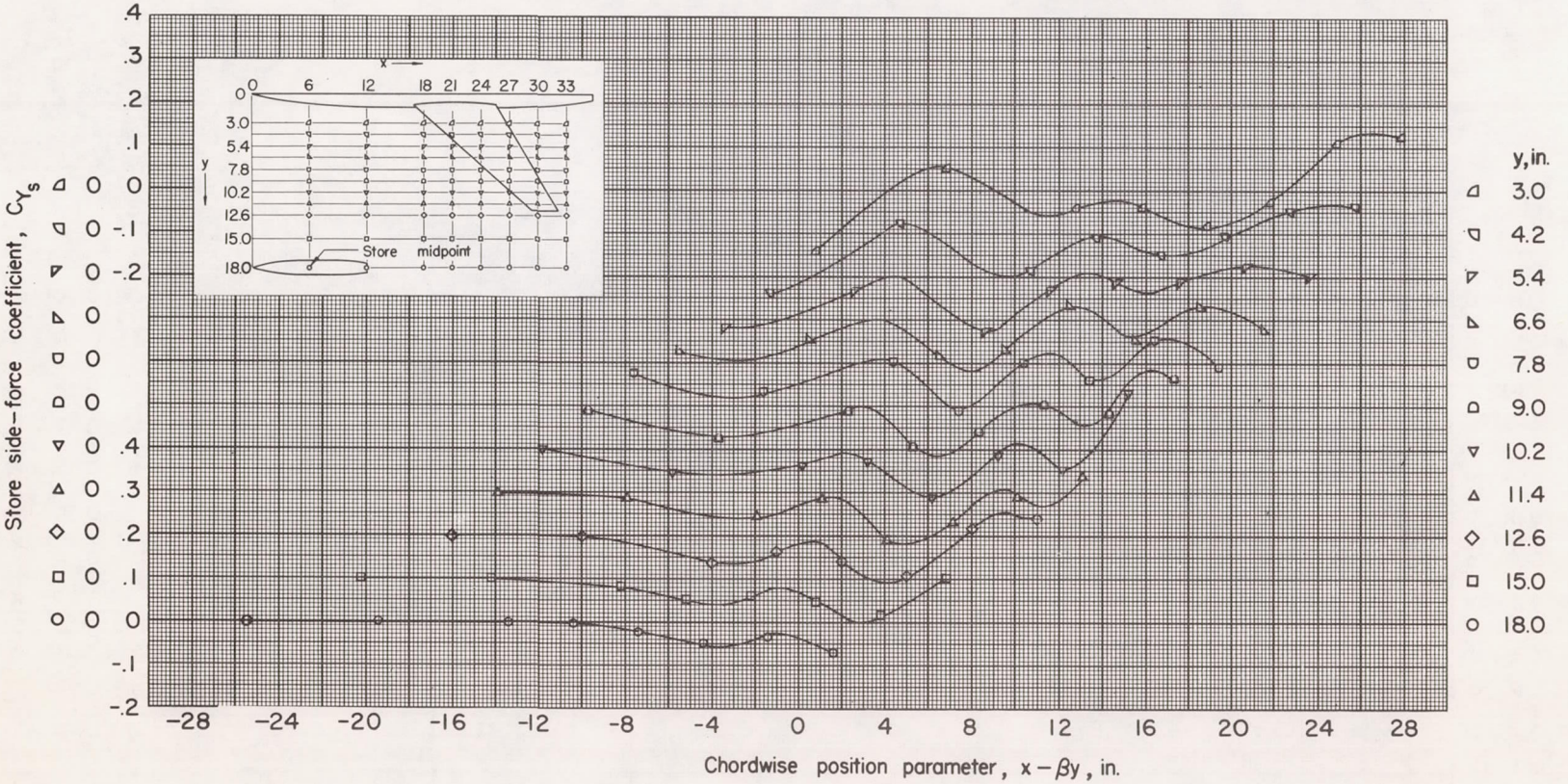
(c) z = 2.09 inches; $\alpha = 0^{\circ}$.

Figure 6.- Continued.



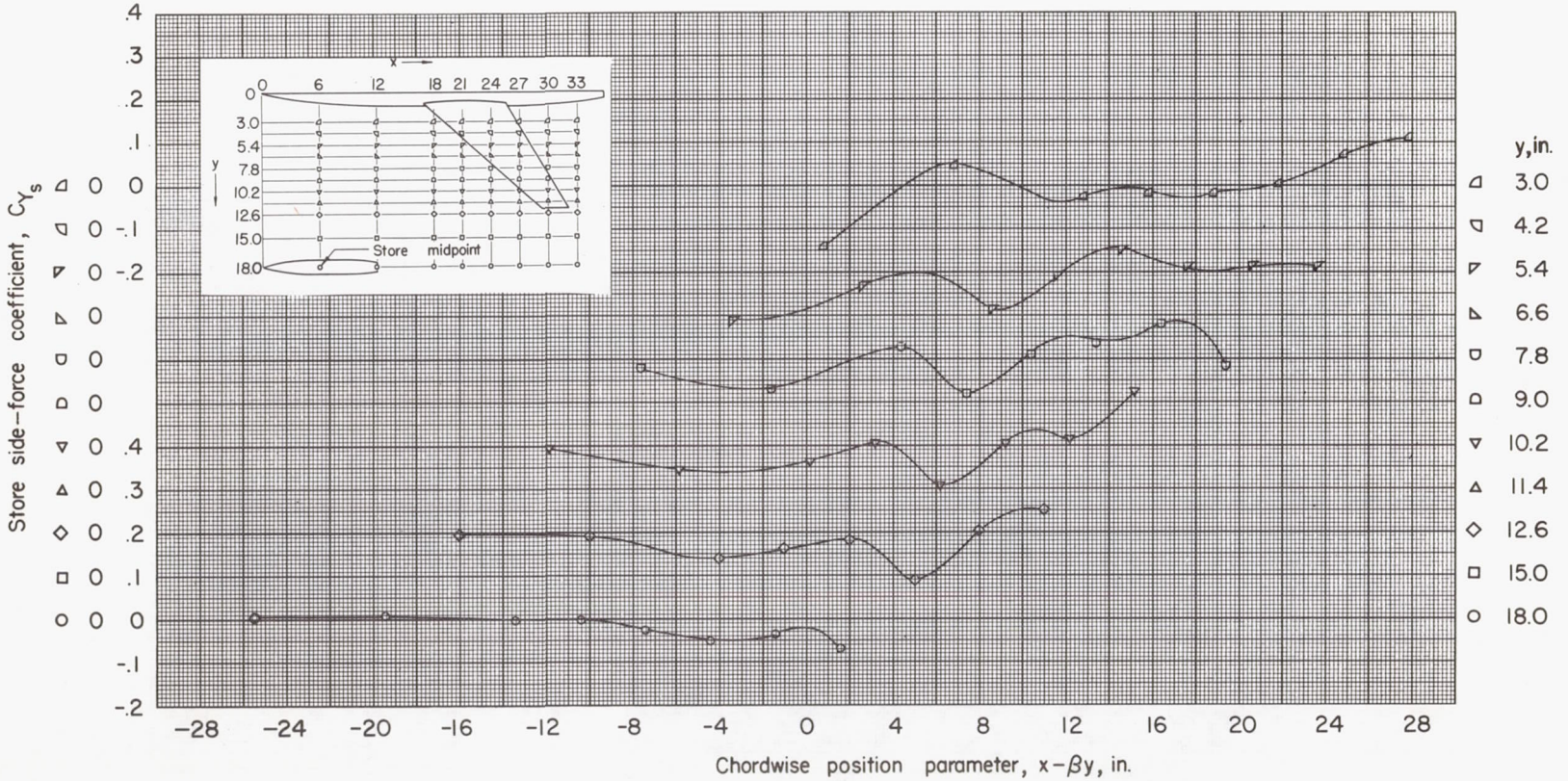
(d) z = 2.09 inches; $\alpha = 4^\circ$.

Figure 6.- Concluded.



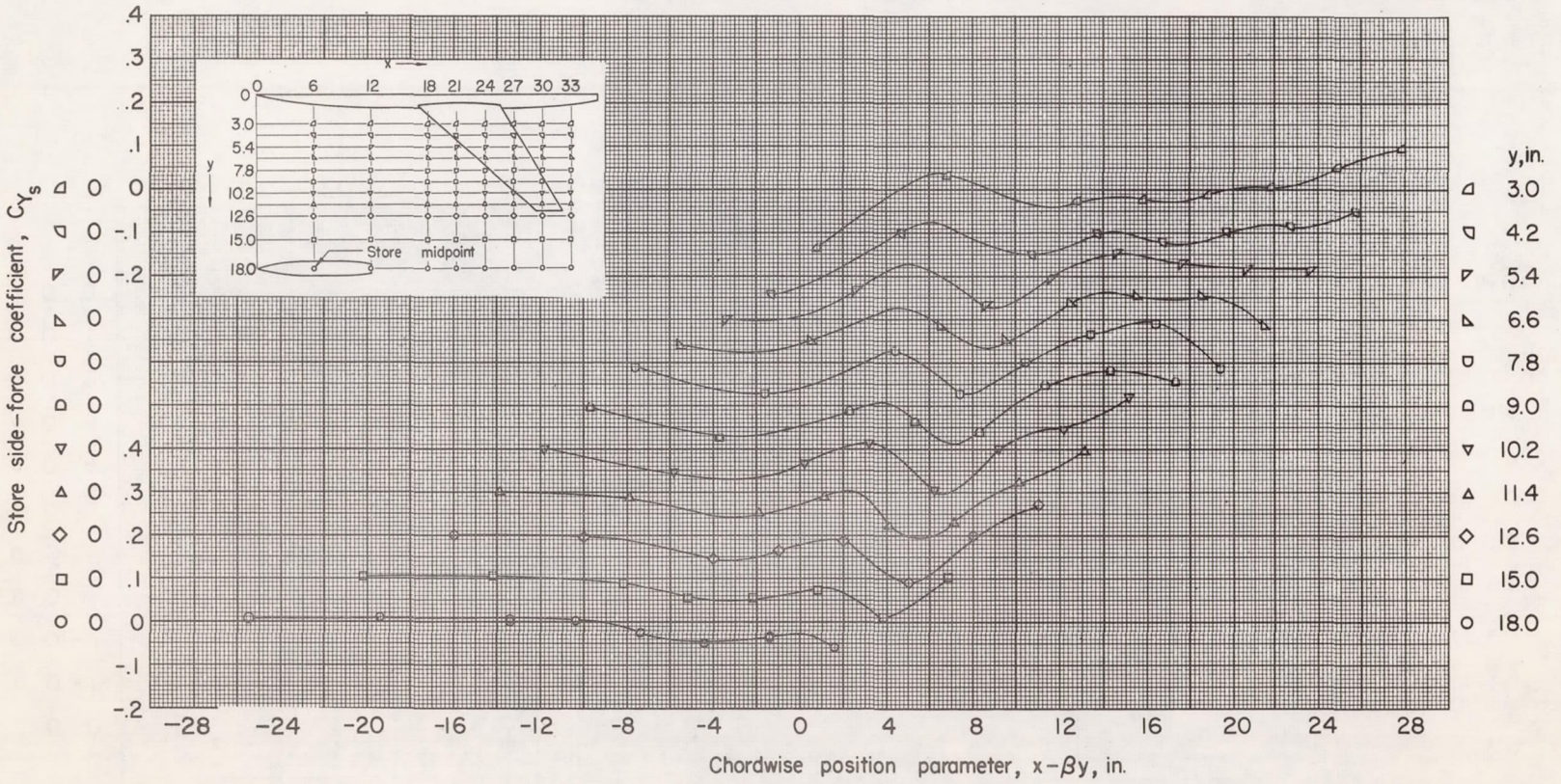
(a) $z = 1.15$ inches; $\alpha = 0^{\circ}$.

Figure 7.- Side force of store in presence of wing-fuselage combination.



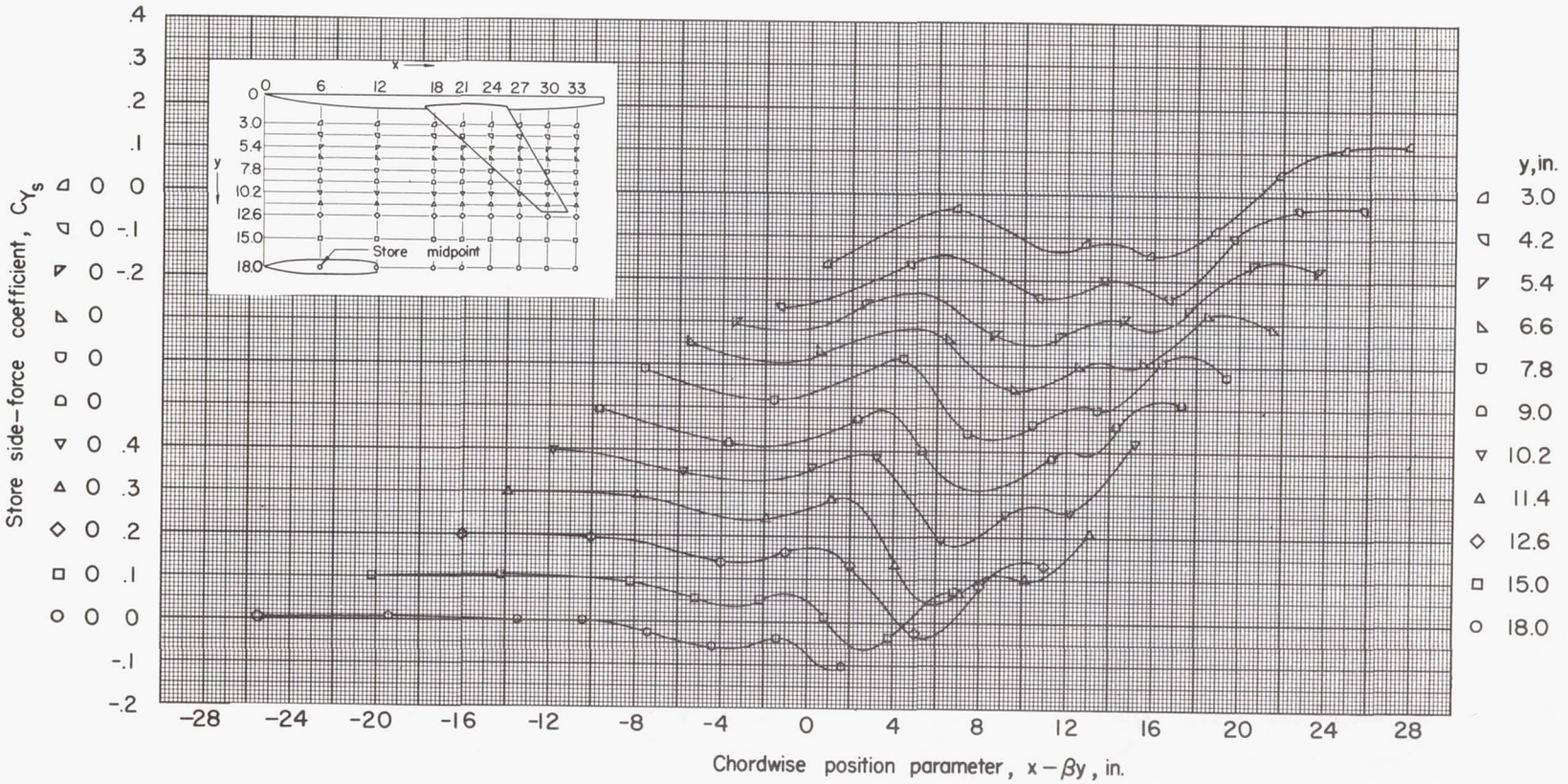
(b) z = 1.67 inches; $\alpha = 0^{\circ}$.

Figure 7.- Continued.



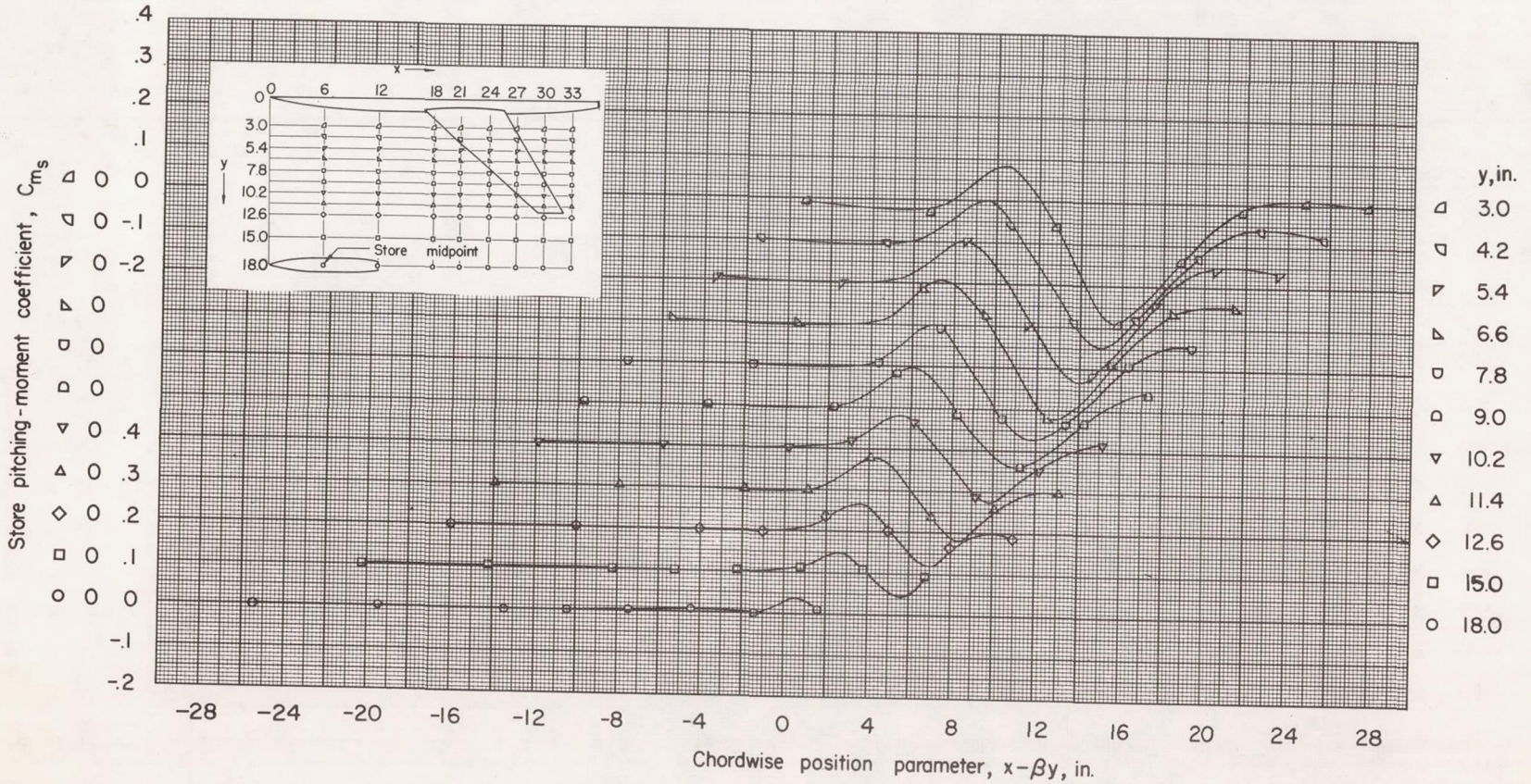
(c) z = 2.09 inches; $\alpha = 0^{\circ}$.

Figure 7.- Continued.



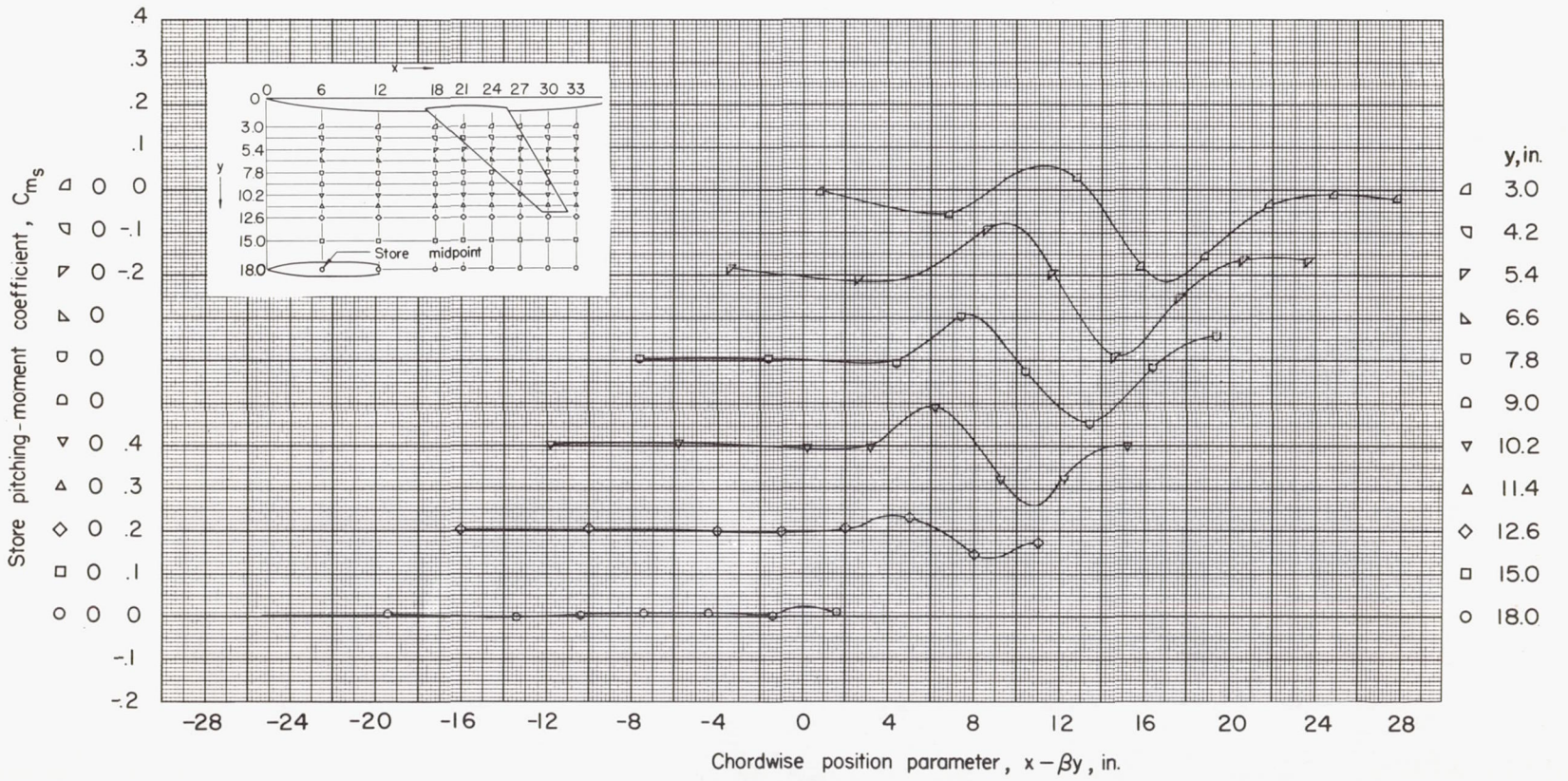
(d) z = 2.09 inches; $\alpha = 4^{\circ}$.

Figure 7.- Concluded.



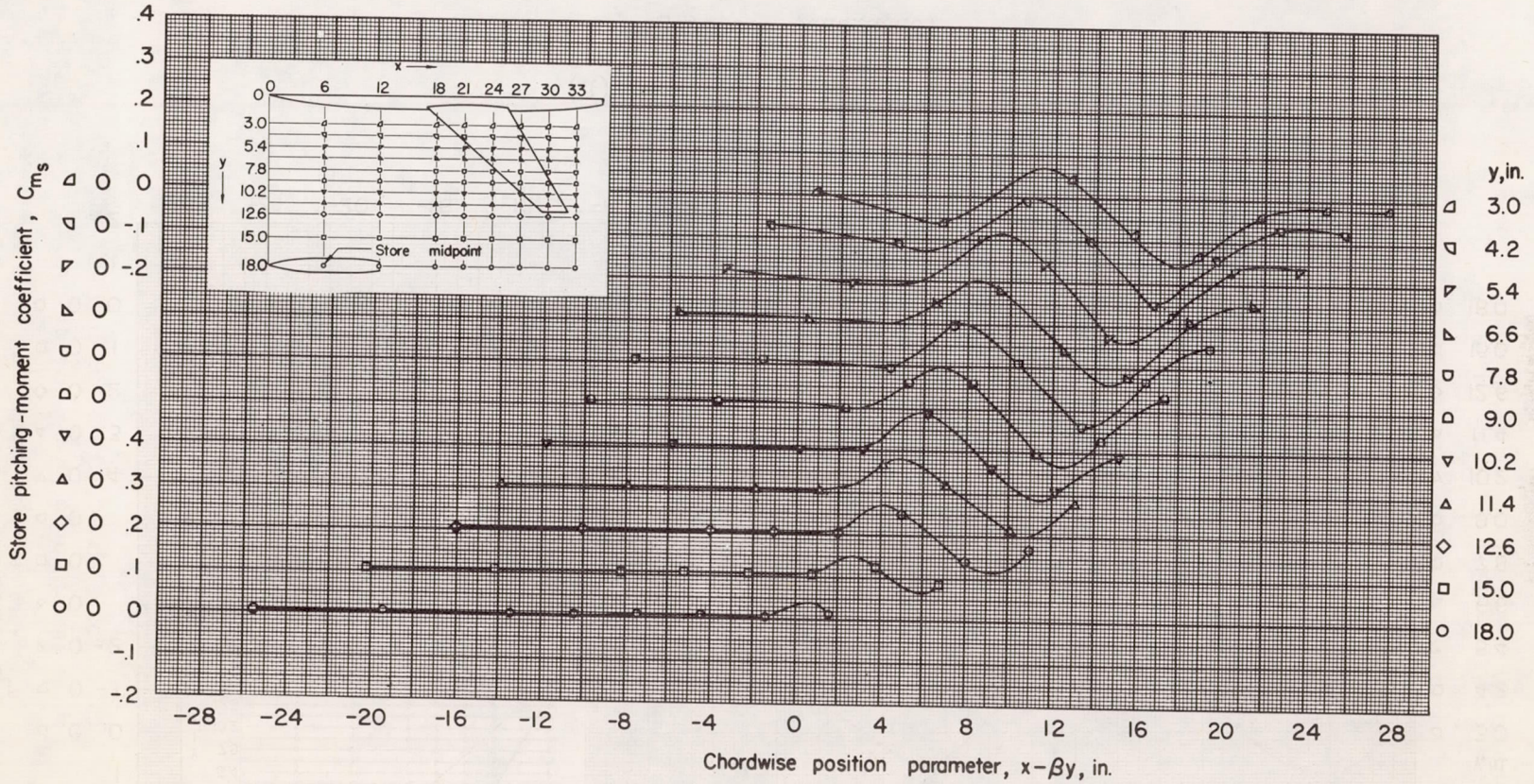
(a) z = 1.15 inches; $\alpha = 0^\circ$.

Figure 8.- Pitching moment of store in presence of wing-fuselage combination.



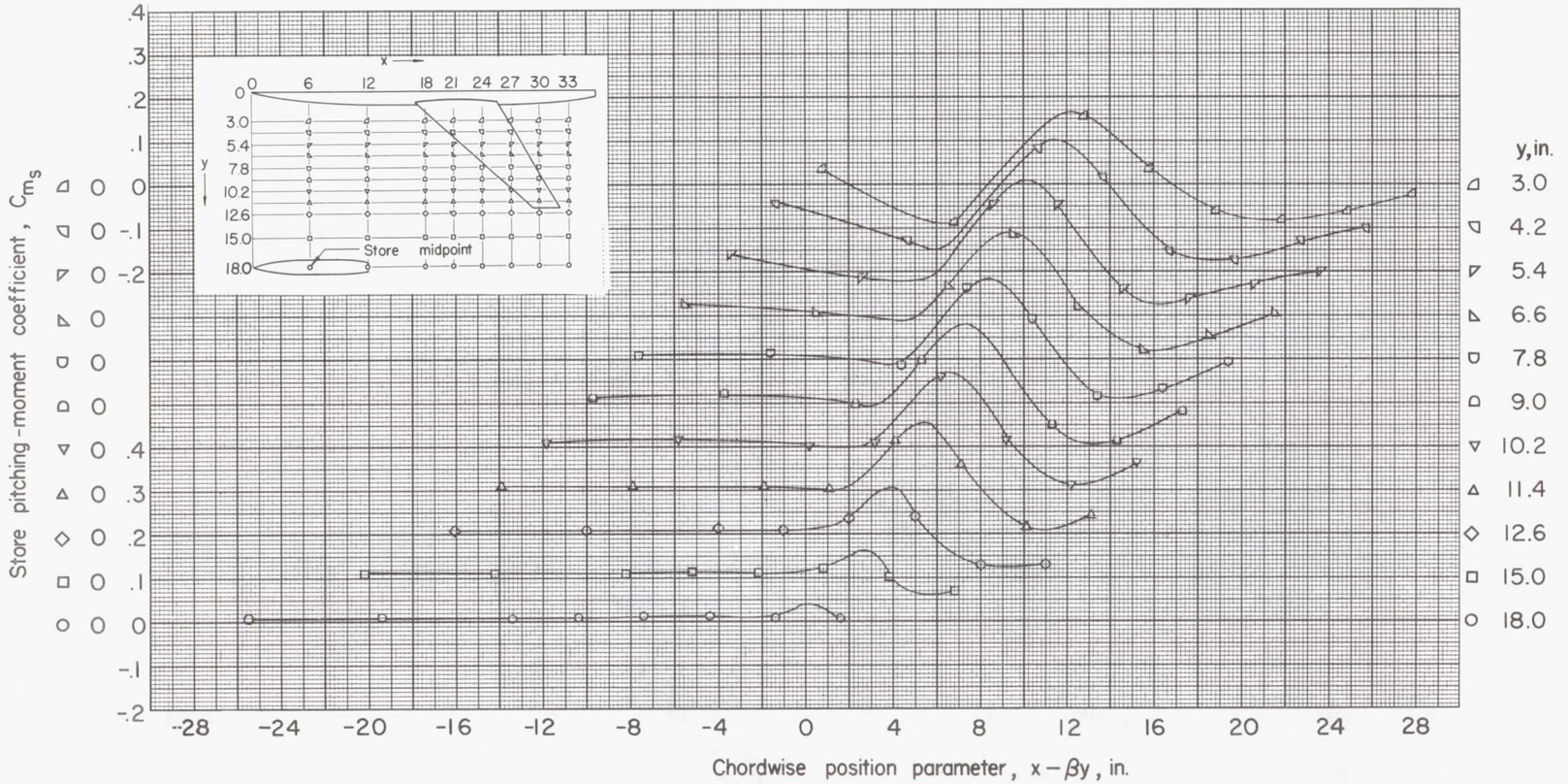
(b) z = 1.67 inches; $\alpha = 0^{\circ}$.

Figure 8.- Continued.



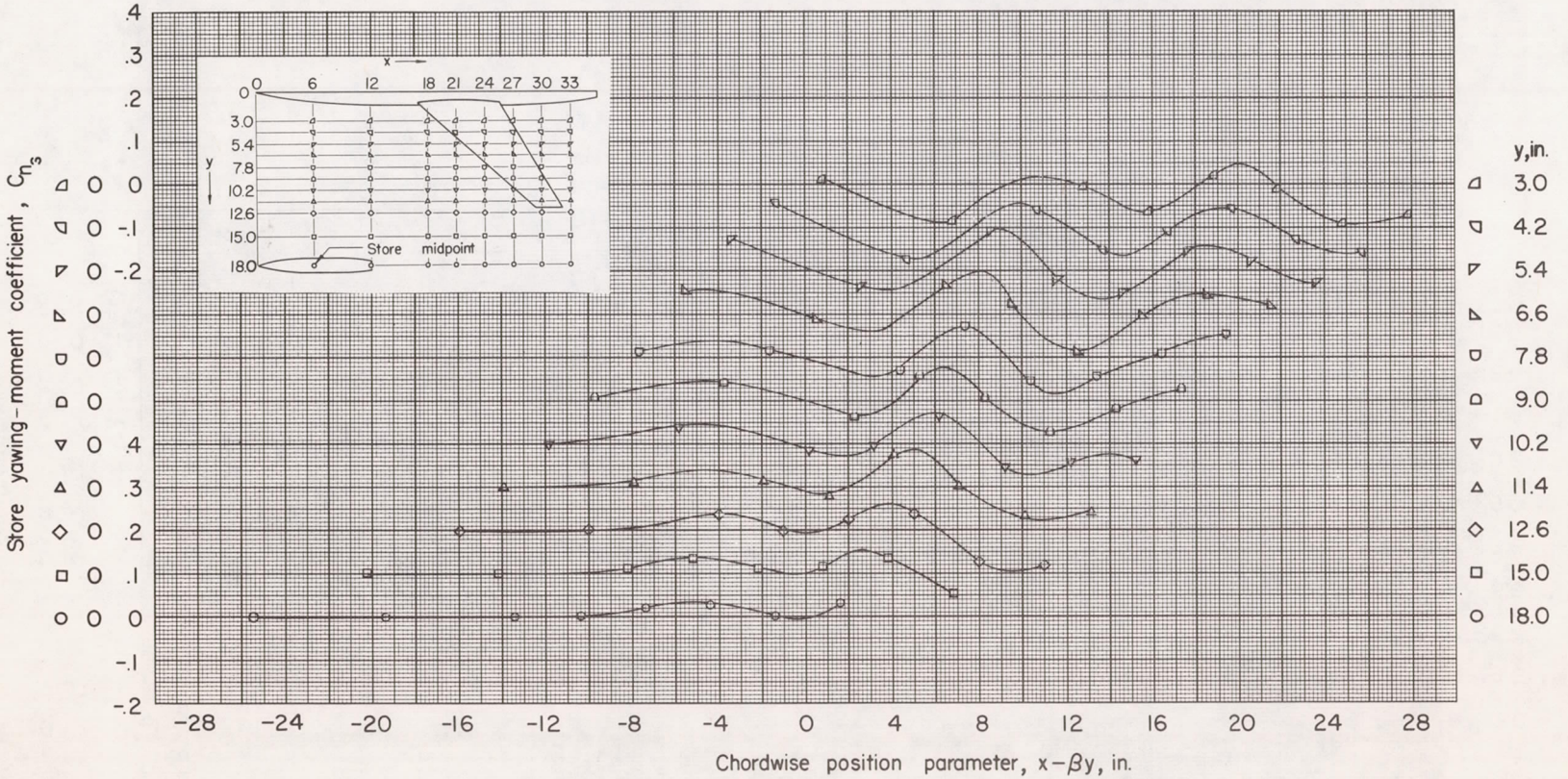
(c) z = 2.09 inches; $\alpha = 0^\circ$.

Figure 8.- Continued.



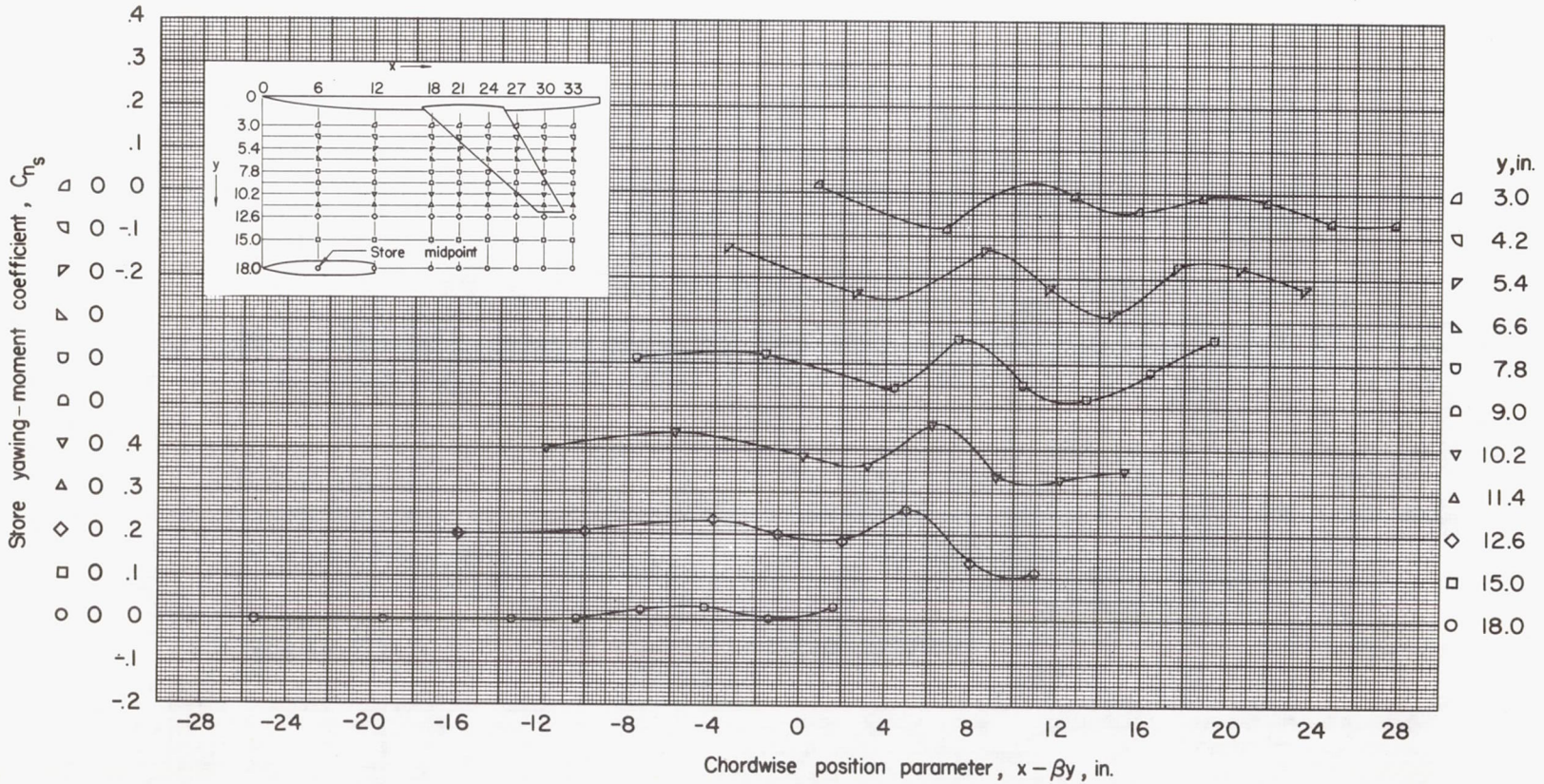
(d) z = 2.09 inches; $\alpha = 4^{\circ}$.

Figure 8.- Concluded.



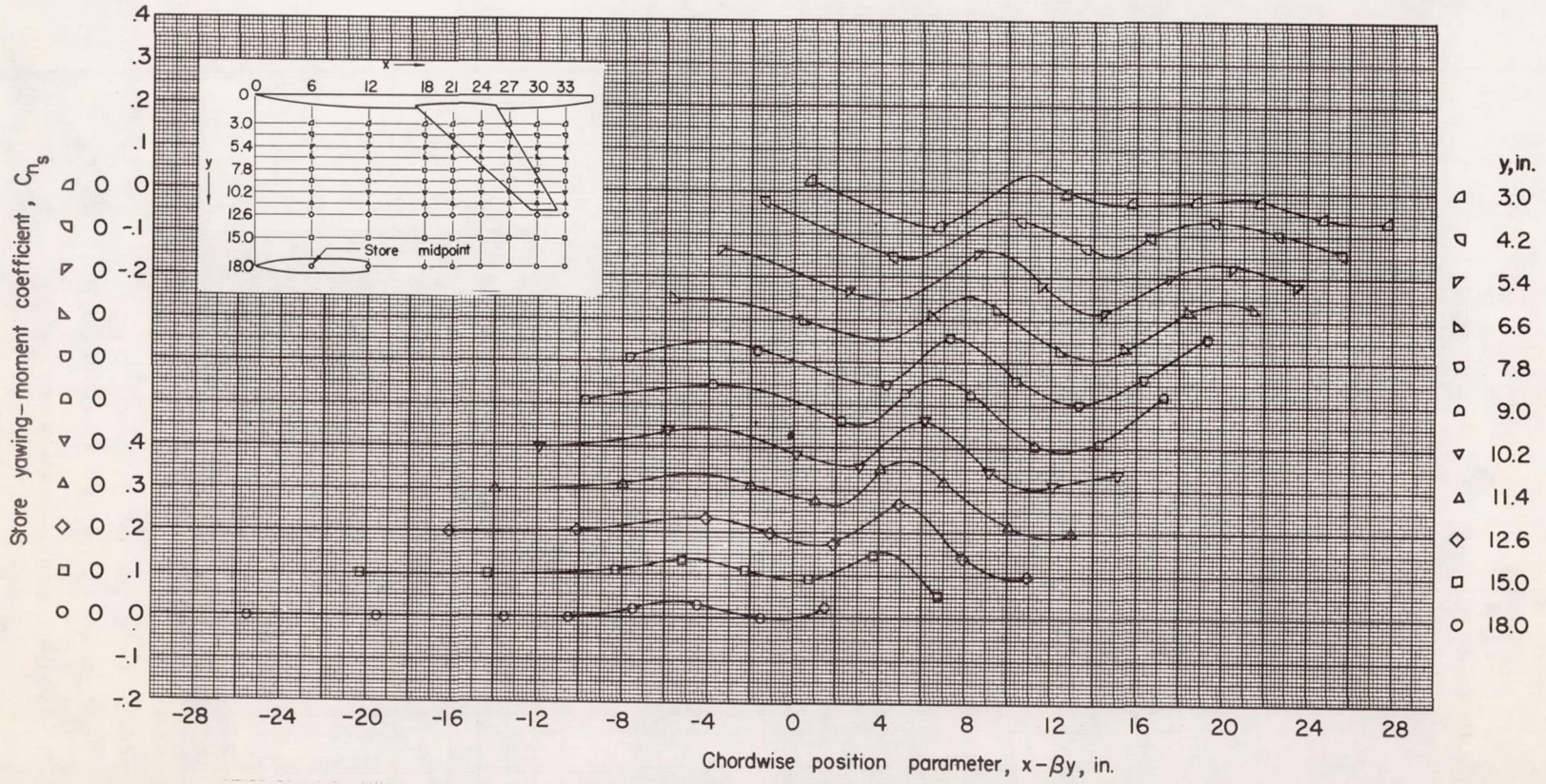
(a) z = 1.15 inches; $\alpha = 0^{\circ}$.

Figure 9.- Yawing moment of store in presence of wing-fuselage combination.



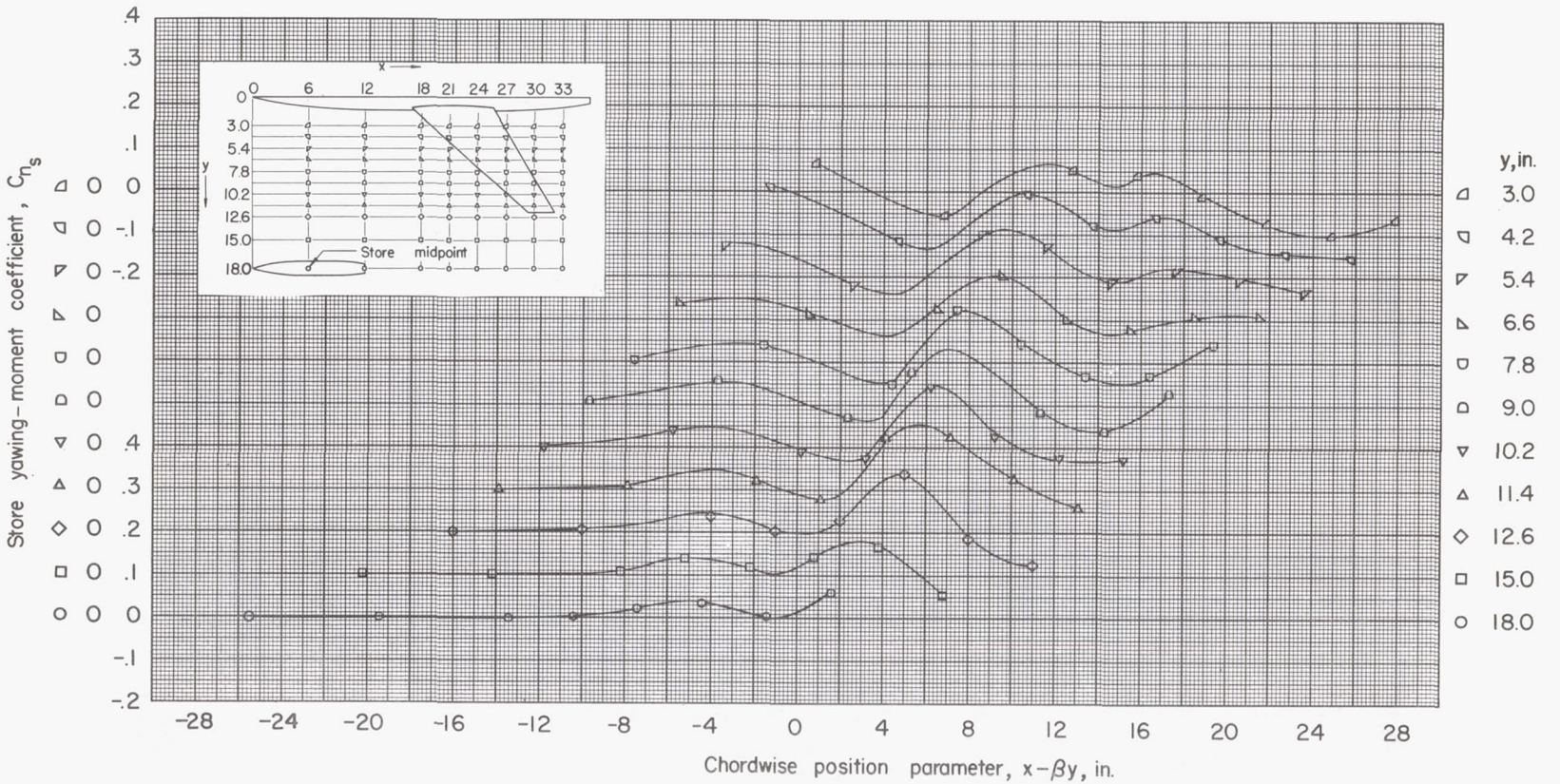
(b) $z = 1.67$ inches; $\alpha = 0^{\circ}$.

Figure 9.- Continued.



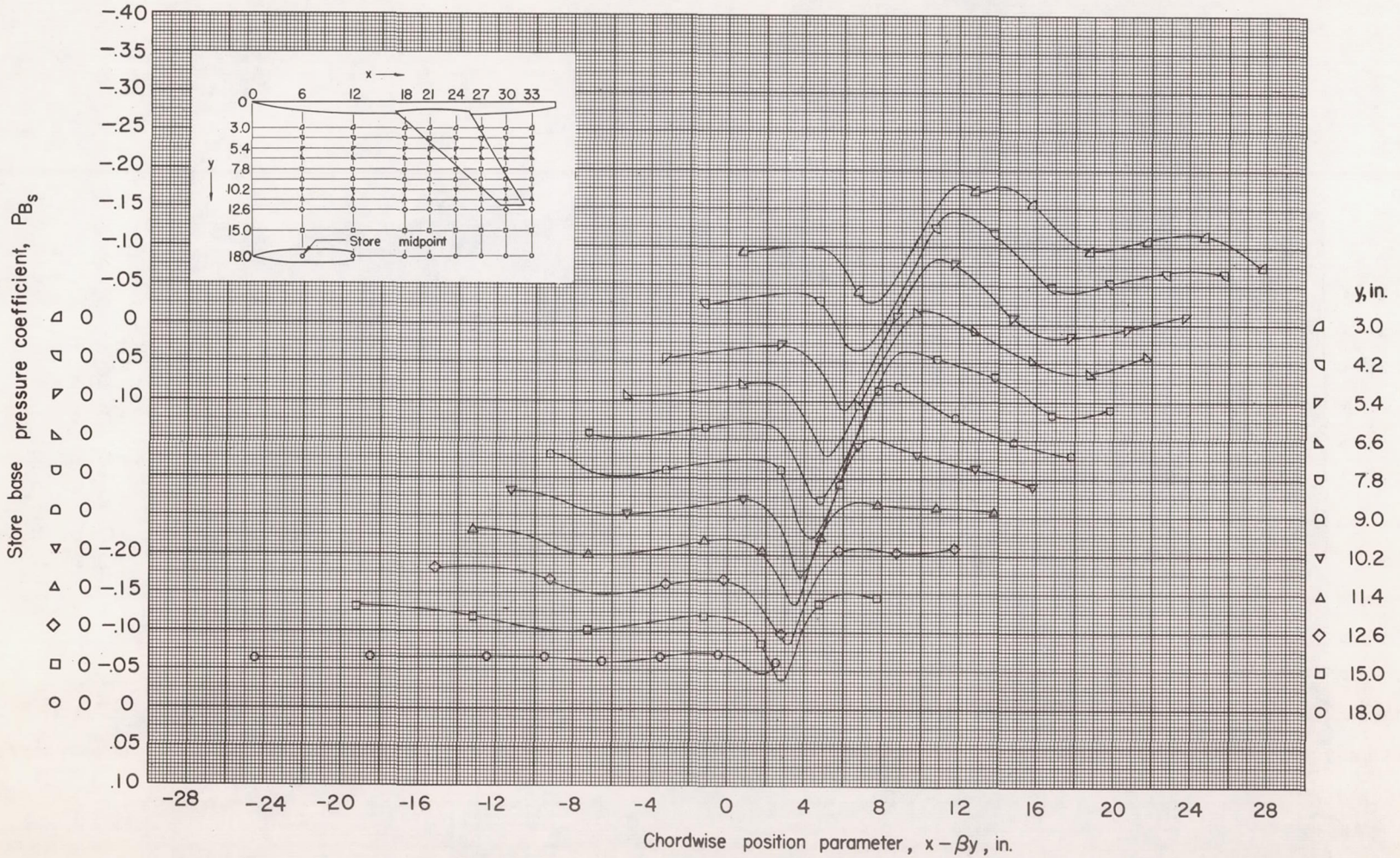
(c) z = 2.09 inches; $\alpha = 0^{\circ}$.

Figure 9.- Continued.



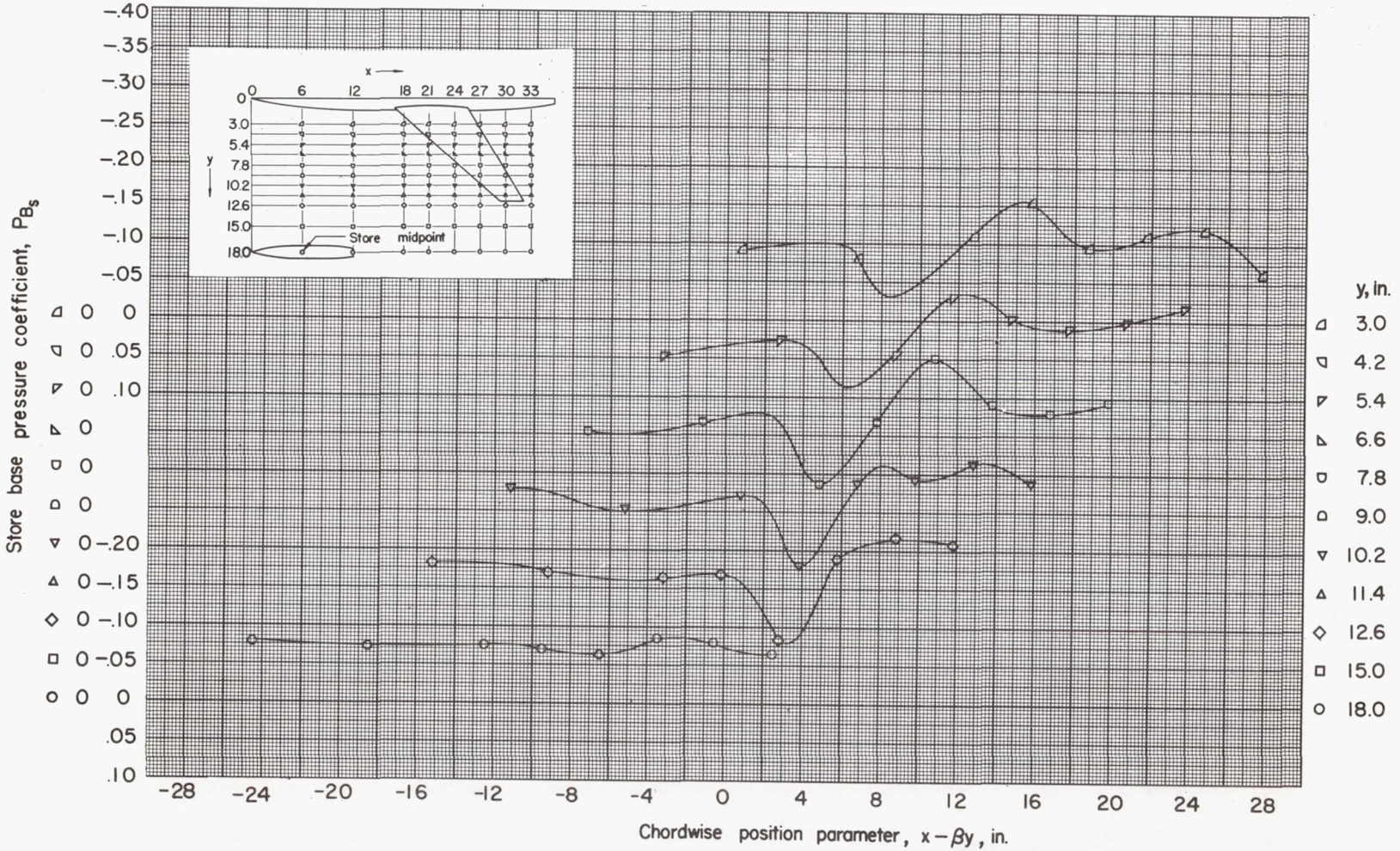
(d) z = 2.09 inches; $\alpha = 4^{\circ}$.

Figure 9.- Concluded.



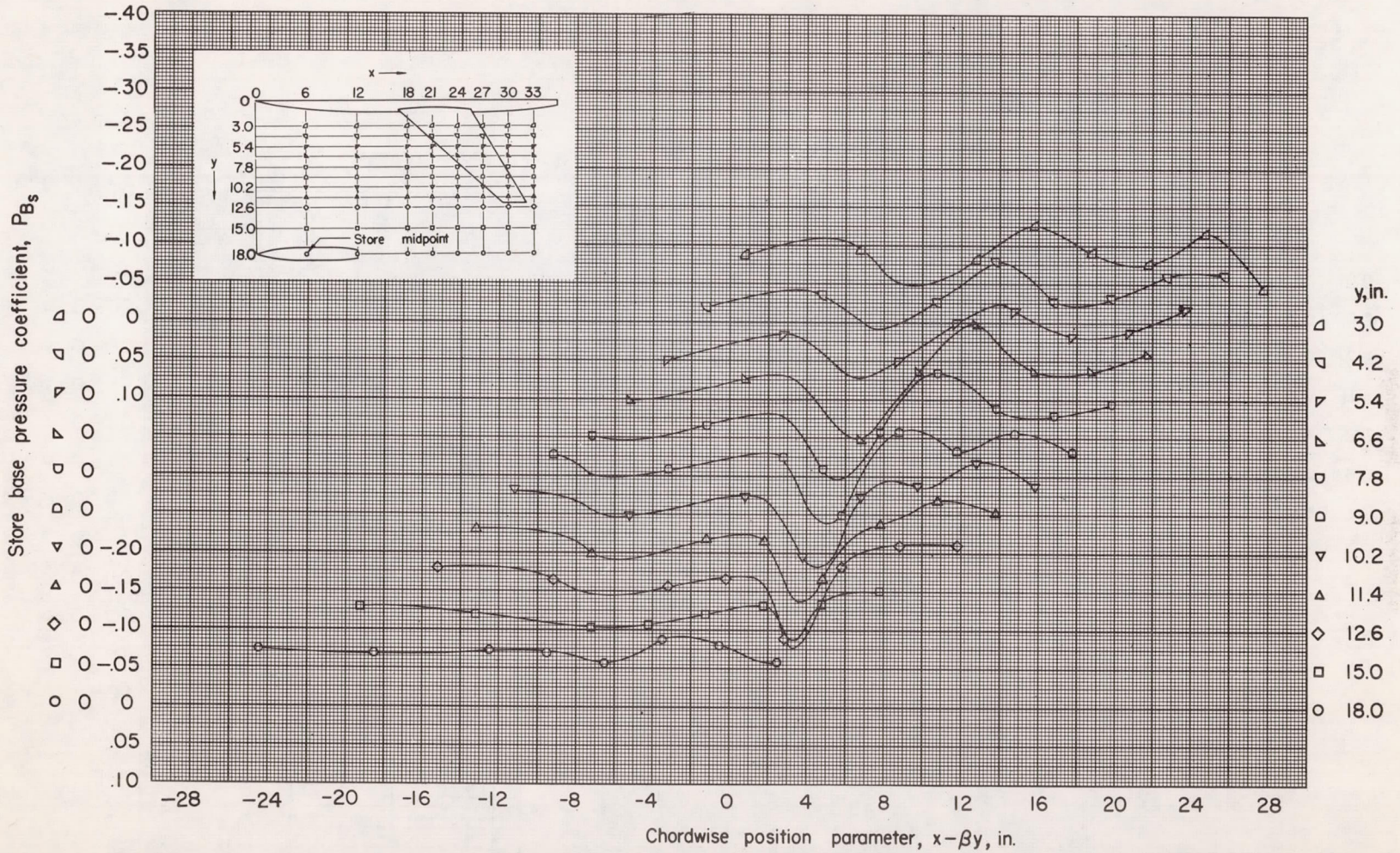
(a) z = 1.15 inches; $\alpha = 0^\circ$.

Figure 10.- Base pressure of store in presence of wing-fuselage combination.



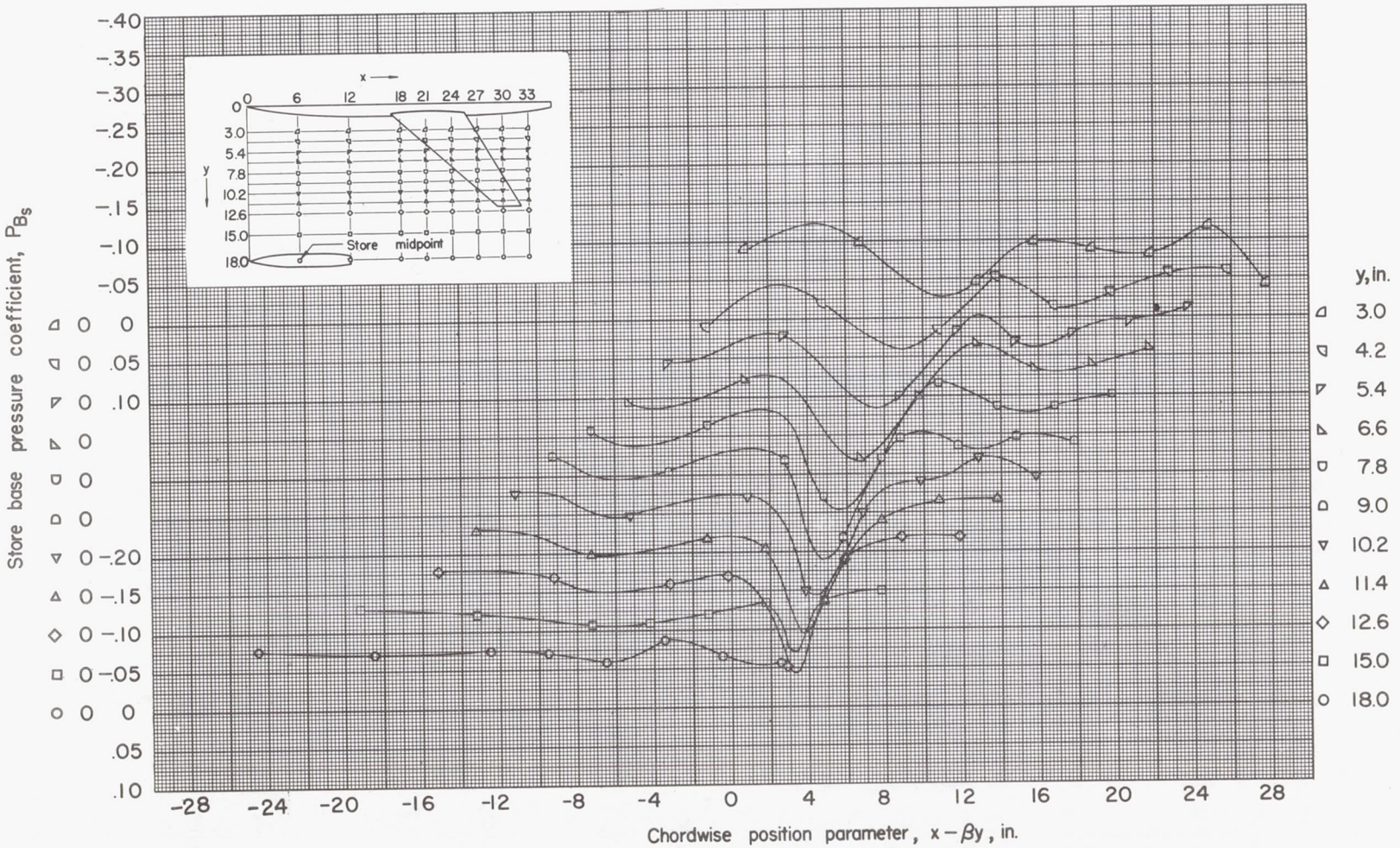
(b) z = 1.67 inches; $\alpha = 0^\circ$.

Figure 10.- Continued.



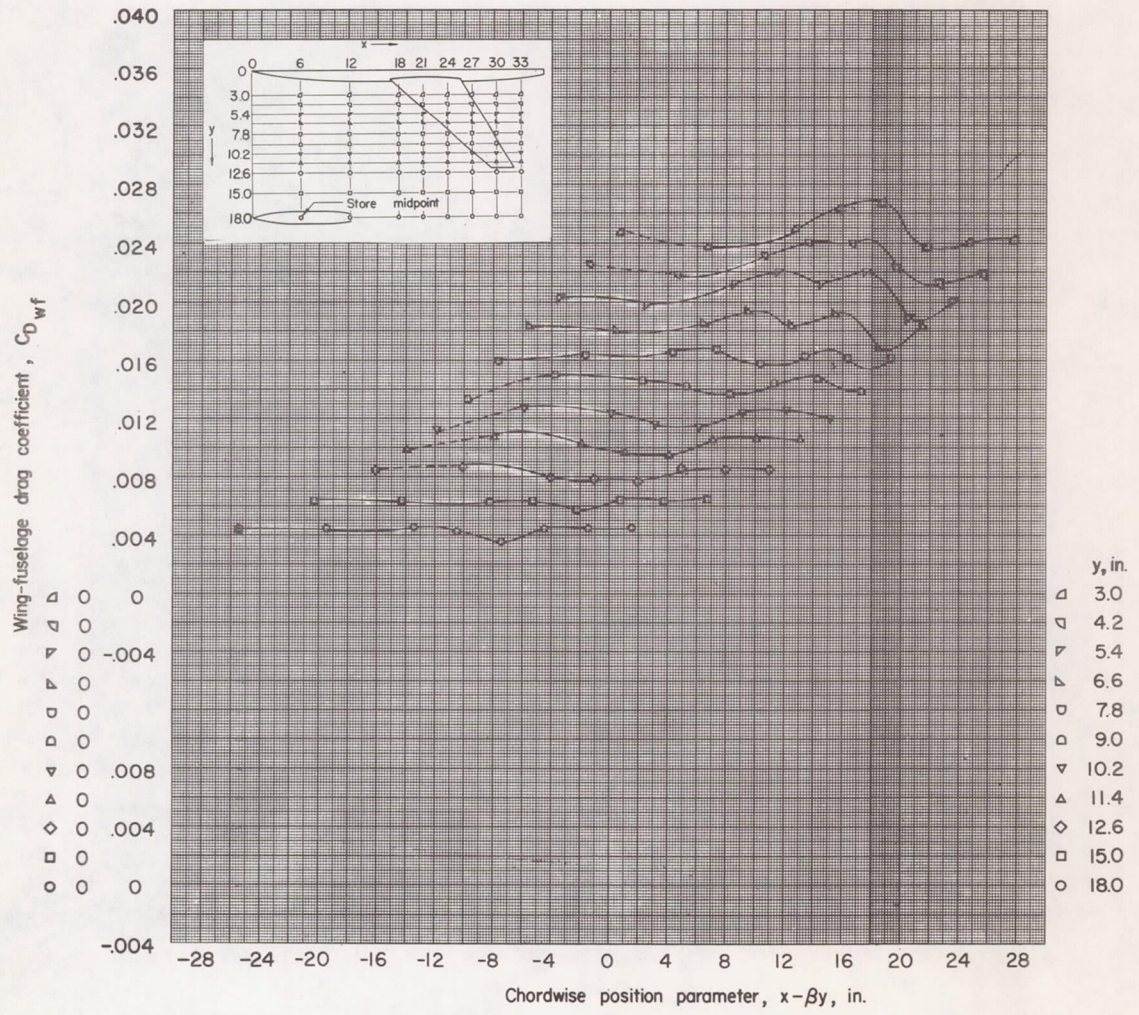
(c) z = 2.09 inches; $\alpha = 0^{\circ}$.

Figure 10.- Continued.



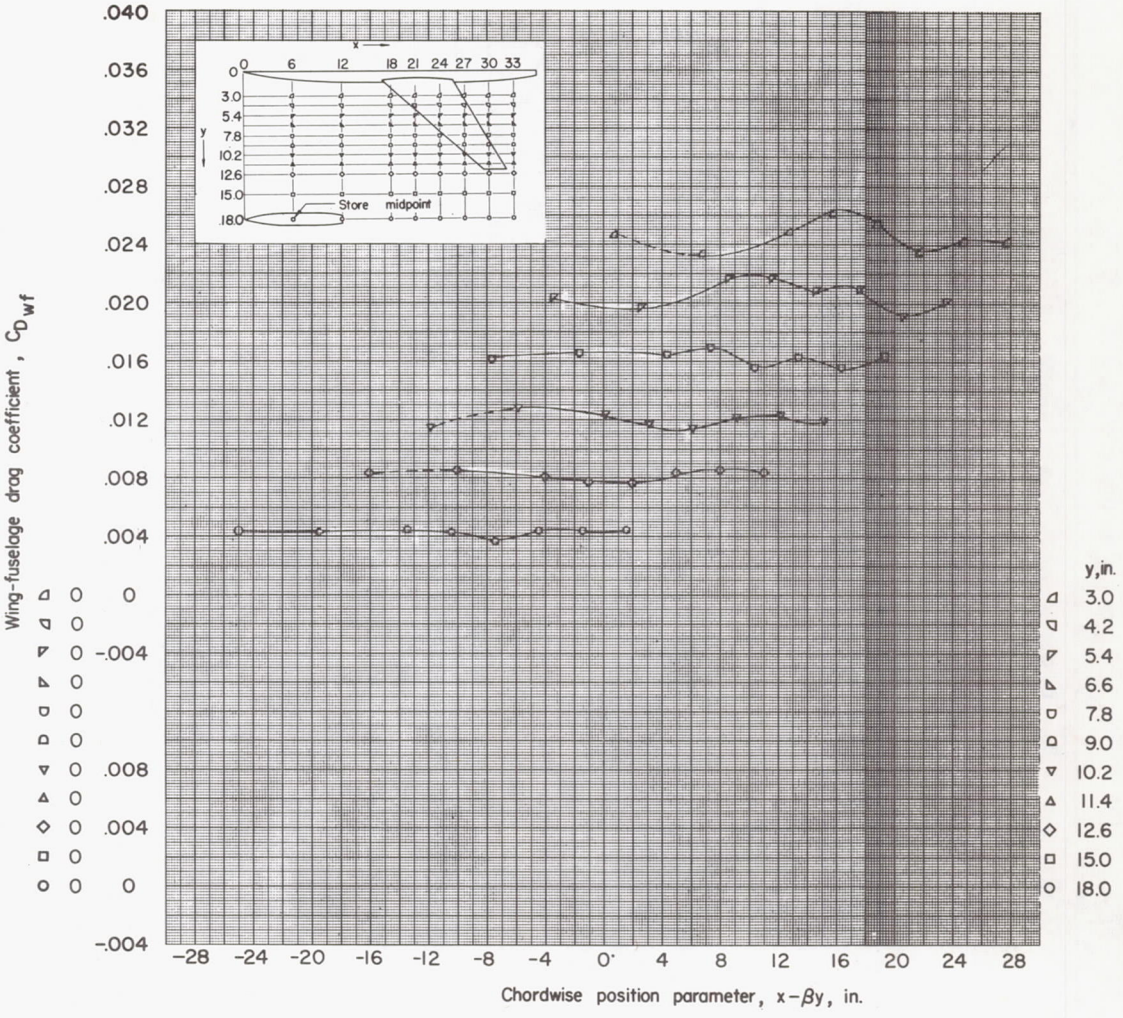
(d) z = 2.09 inches; $\alpha = 4^{\circ}$.

Figure 10.- Concluded.



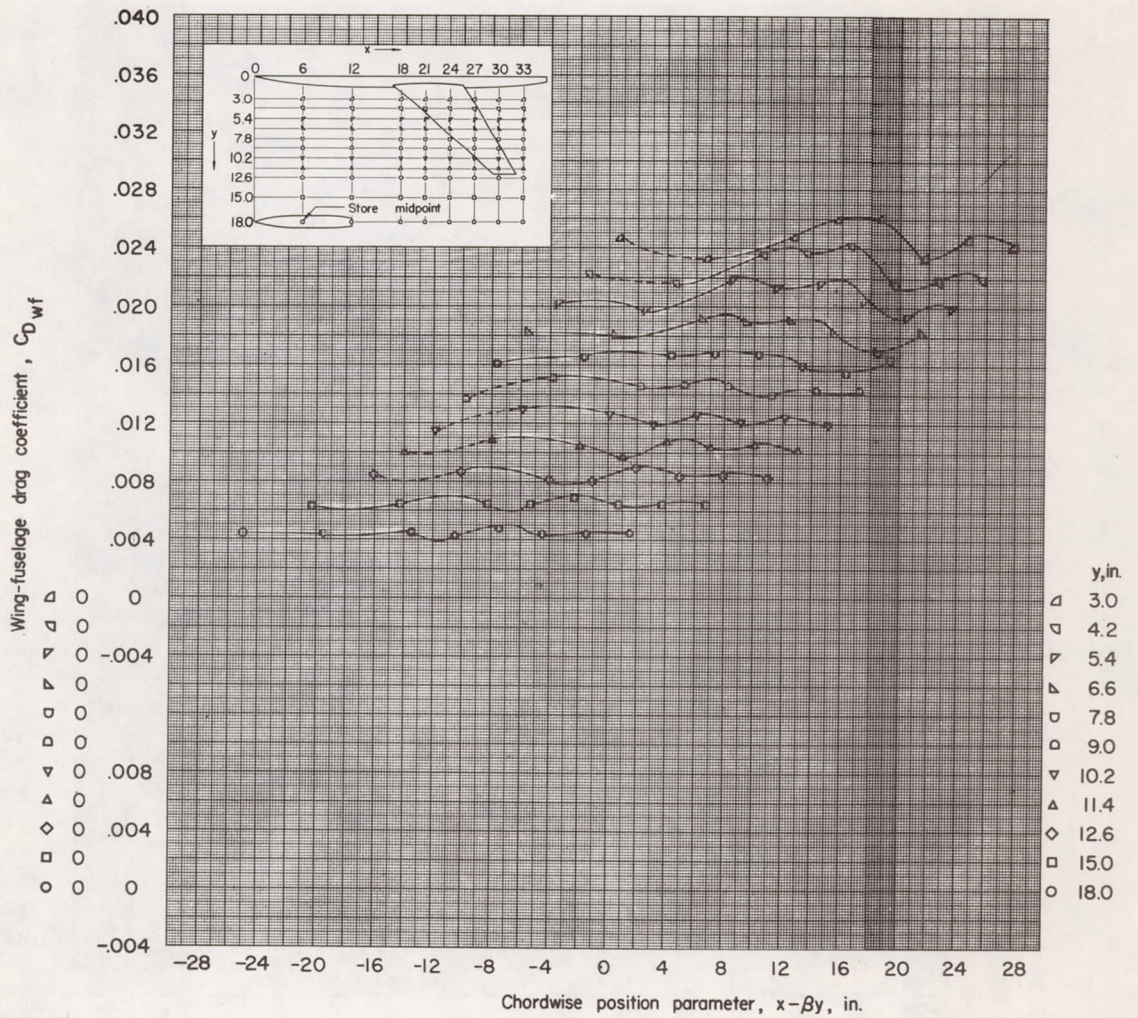
(a) $z = 1.15$ inches; $\alpha = 0^{\circ}$.

Figure 11.- Drag of the wing-fuselage combination in presence of store.



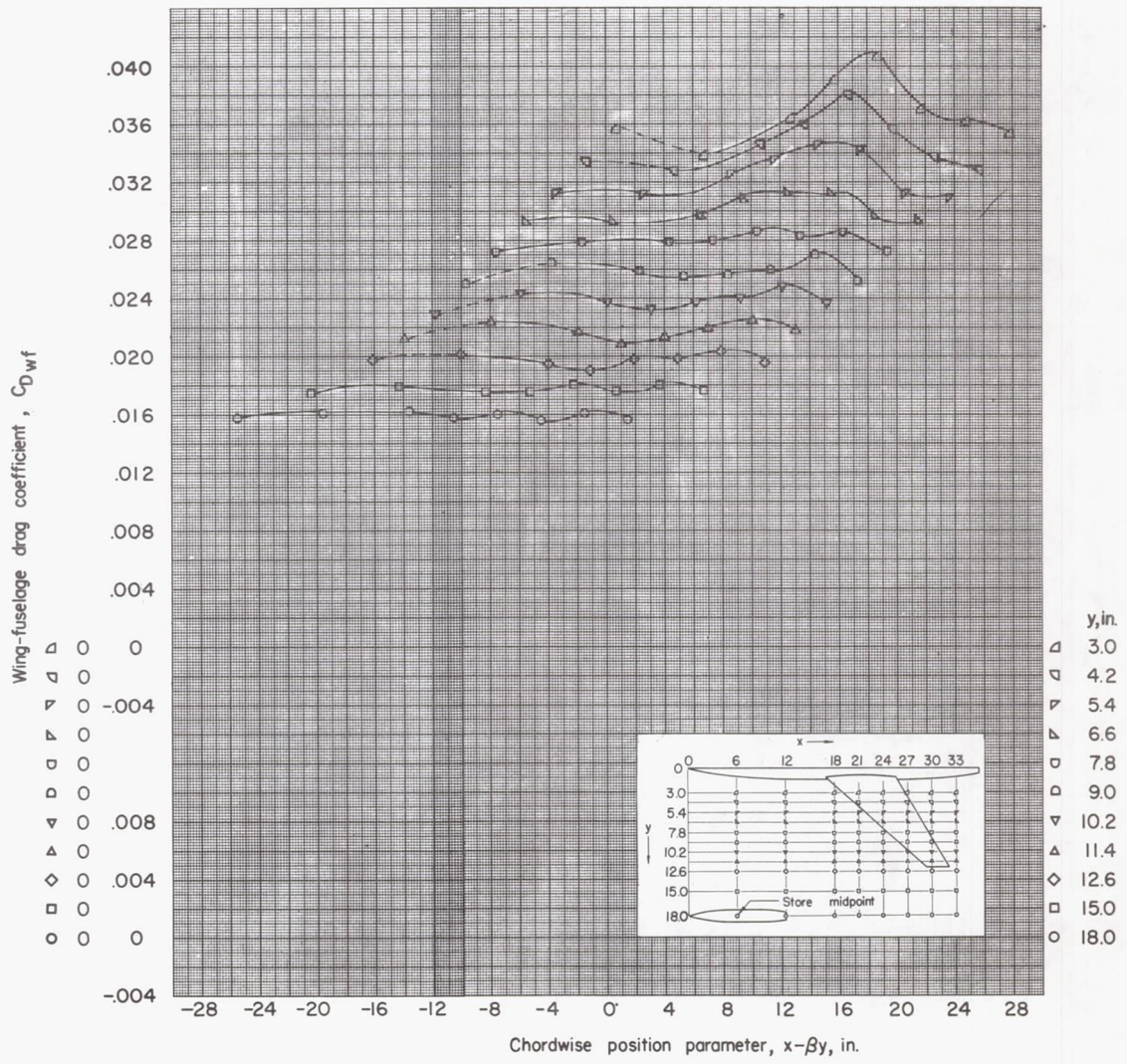
(b) z = 1.67 inches; $\alpha = 0^{\circ}$.

Figure 11.- Continued.



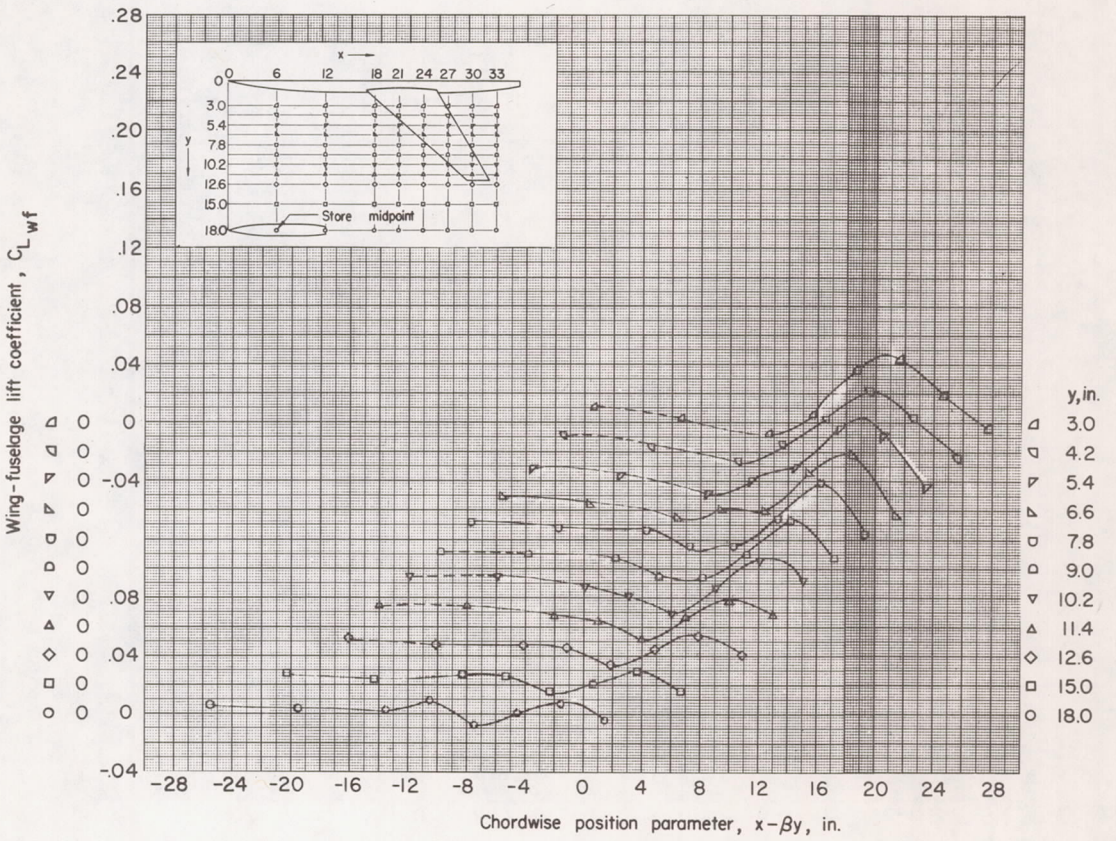
(c) z = 2.09 inches; $\alpha = 0^{\circ}$.

Figure 11.- Continued.



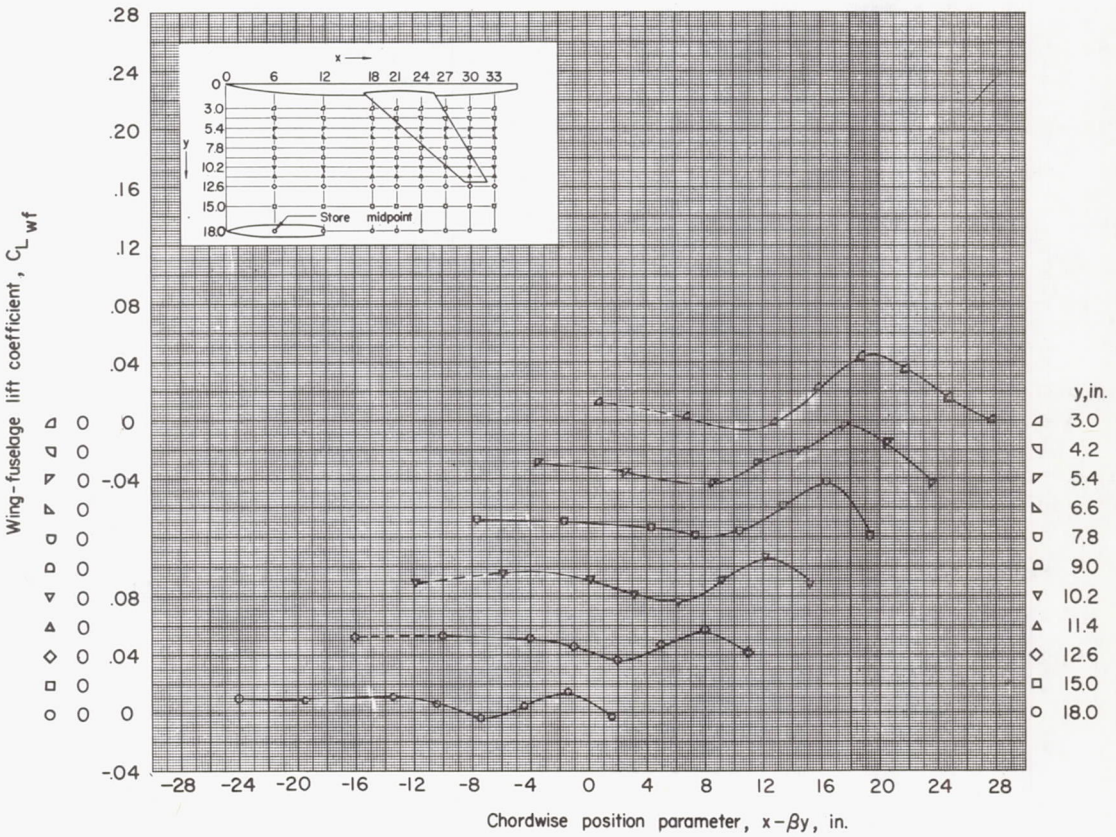
(d) z = 2.09 inches; $\alpha = 4^{\circ}$.

Figure 11.- Concluded.



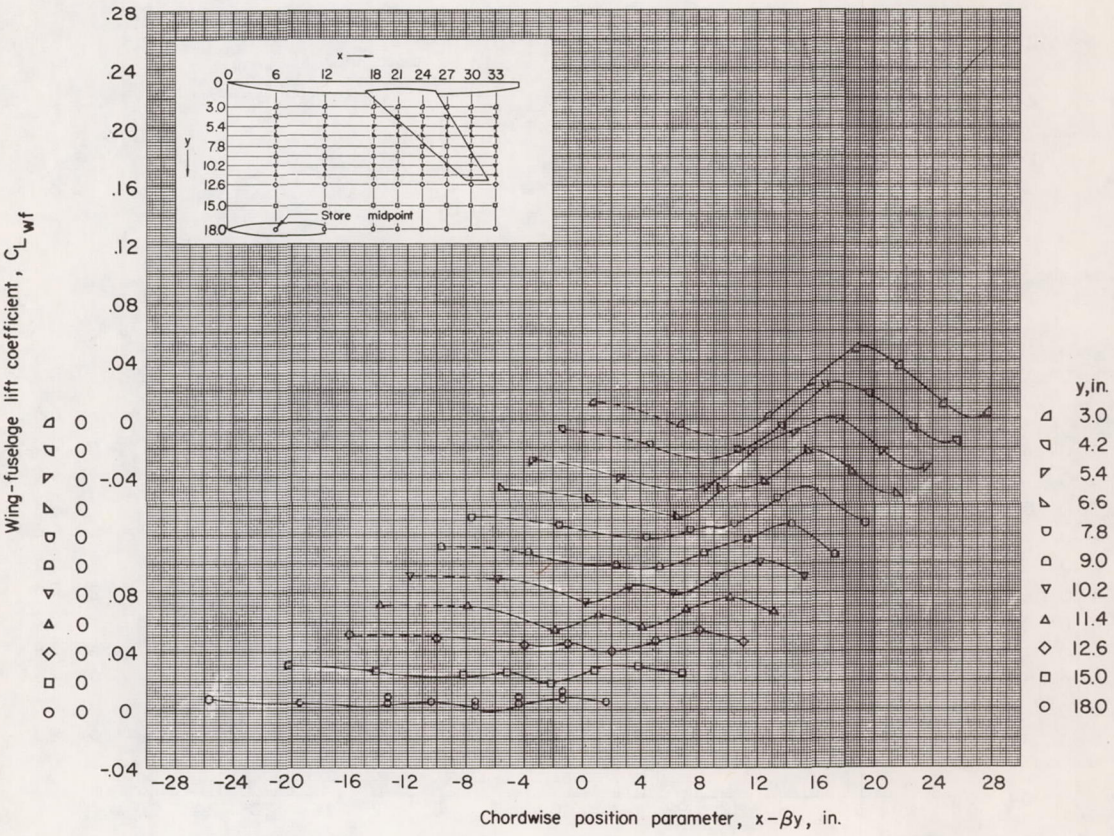
(a) $z = 1.15$ inches; $\alpha = 0^{\circ}$.

Figure 12.- Lift of the wing-fuselage combination in presence of store.



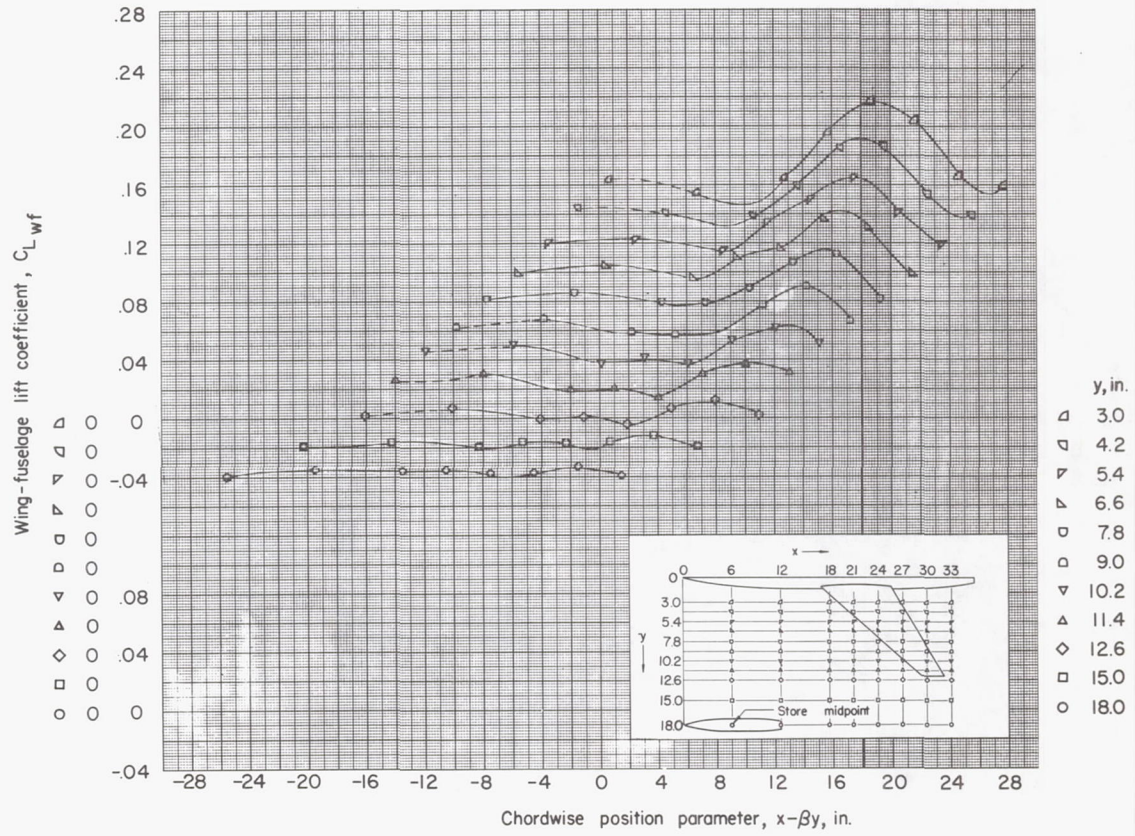
(b) z = 1.67 inches; $\alpha = 0^{\circ}$.

Figure 12.- Continued.



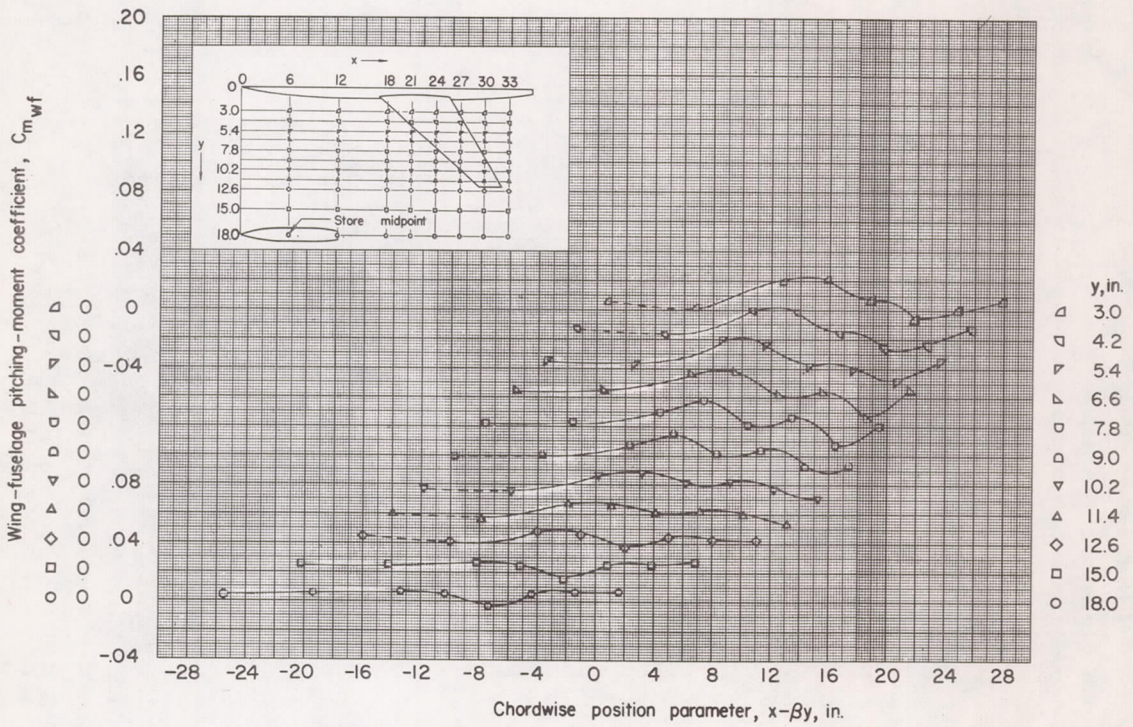
(c) z = 2.09 inches; $\alpha = 0^{\circ}$.

Figure 12.- Continued.



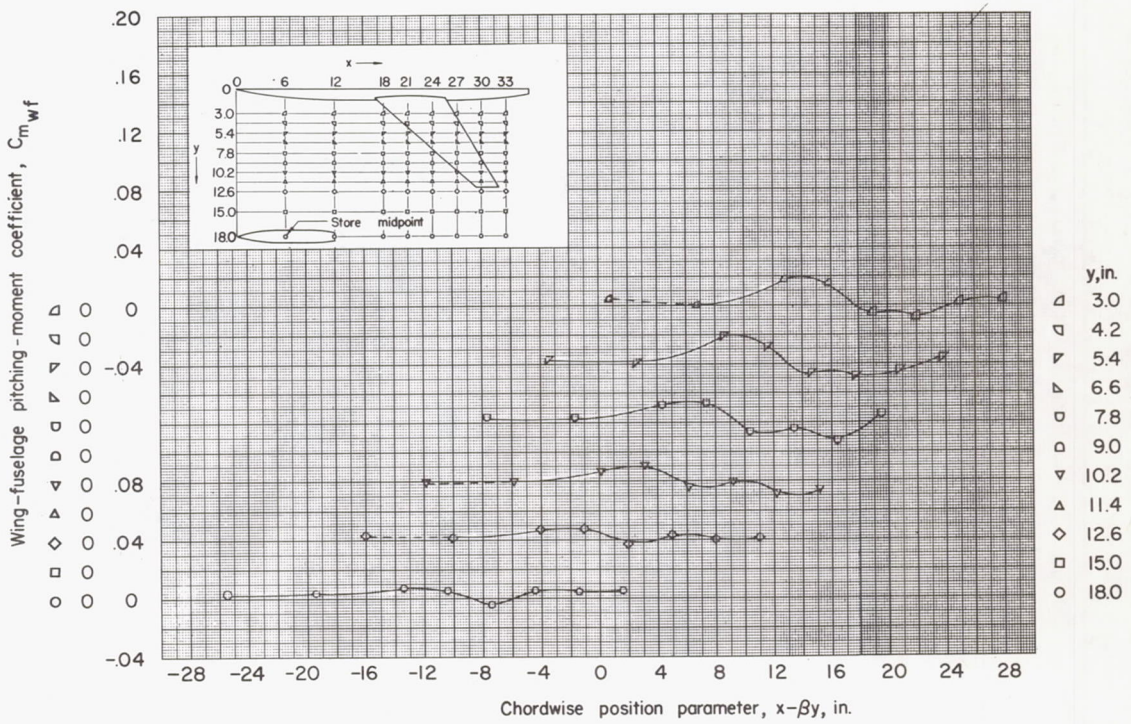
(d) z = 2.09 inches; $\alpha = 4^{\circ}$.

Figure 12.- Concluded.



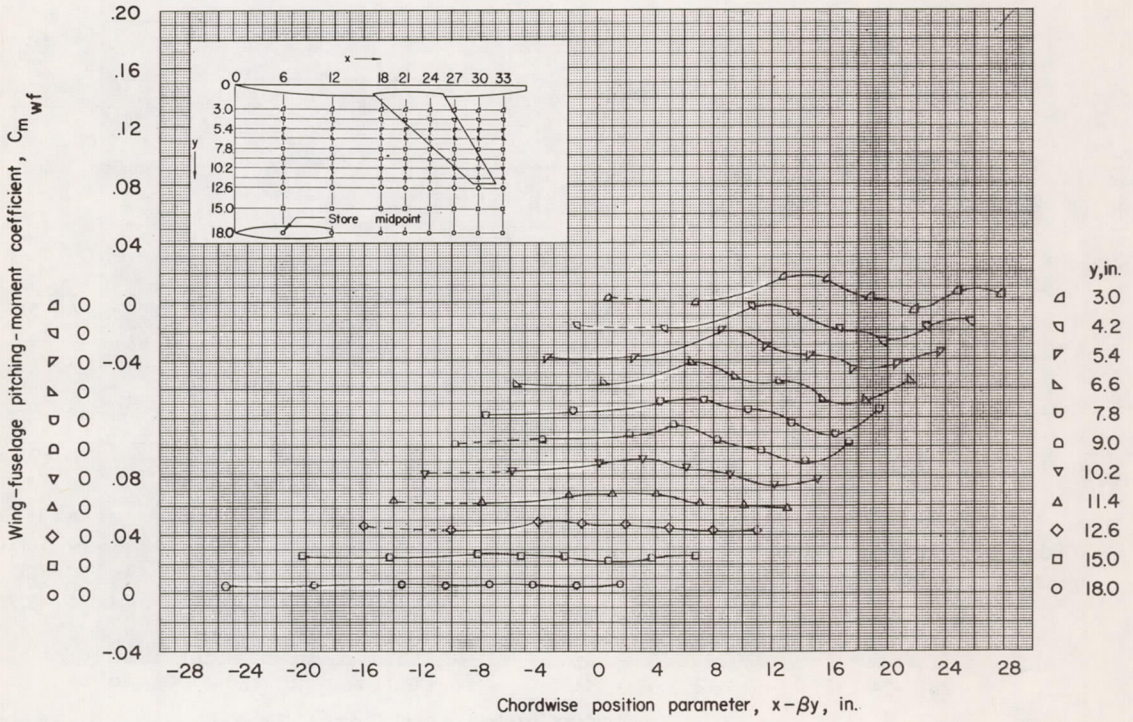
(a) z = 1.15 inches; $\alpha = 0^{\circ}$.

Figure 13.- Pitching moment of the wing-fuselage combination in presence of store.



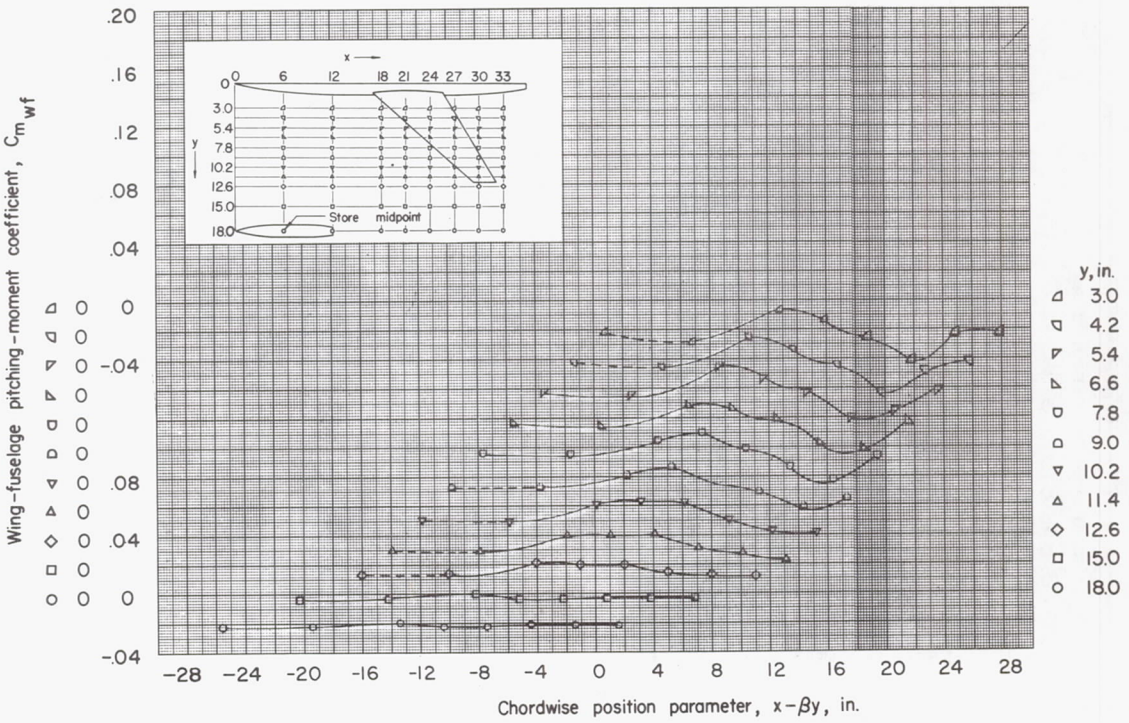
(b) z = 1.67 inches; $\alpha = 0^{\circ}$.

Figure 13.- Continued.



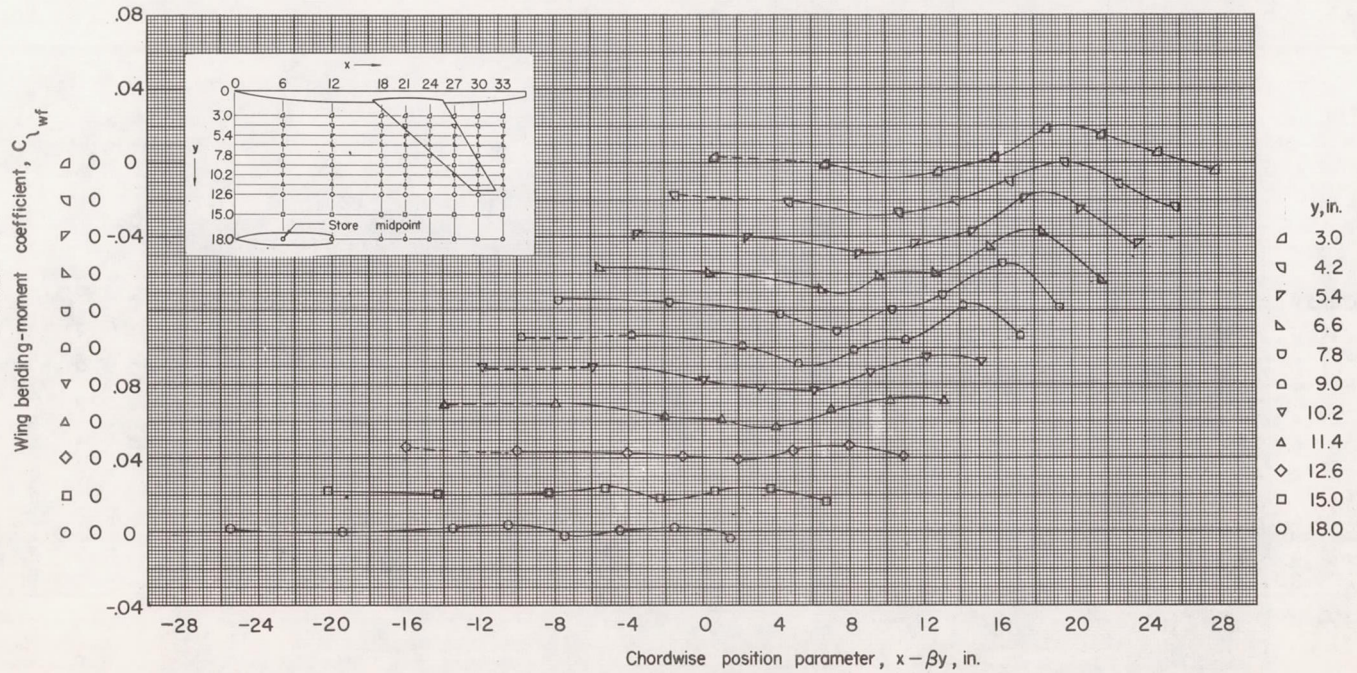
(c) z = 2.09 inches; $\alpha = 0^{\circ}$.

Figure 13.- Continued.



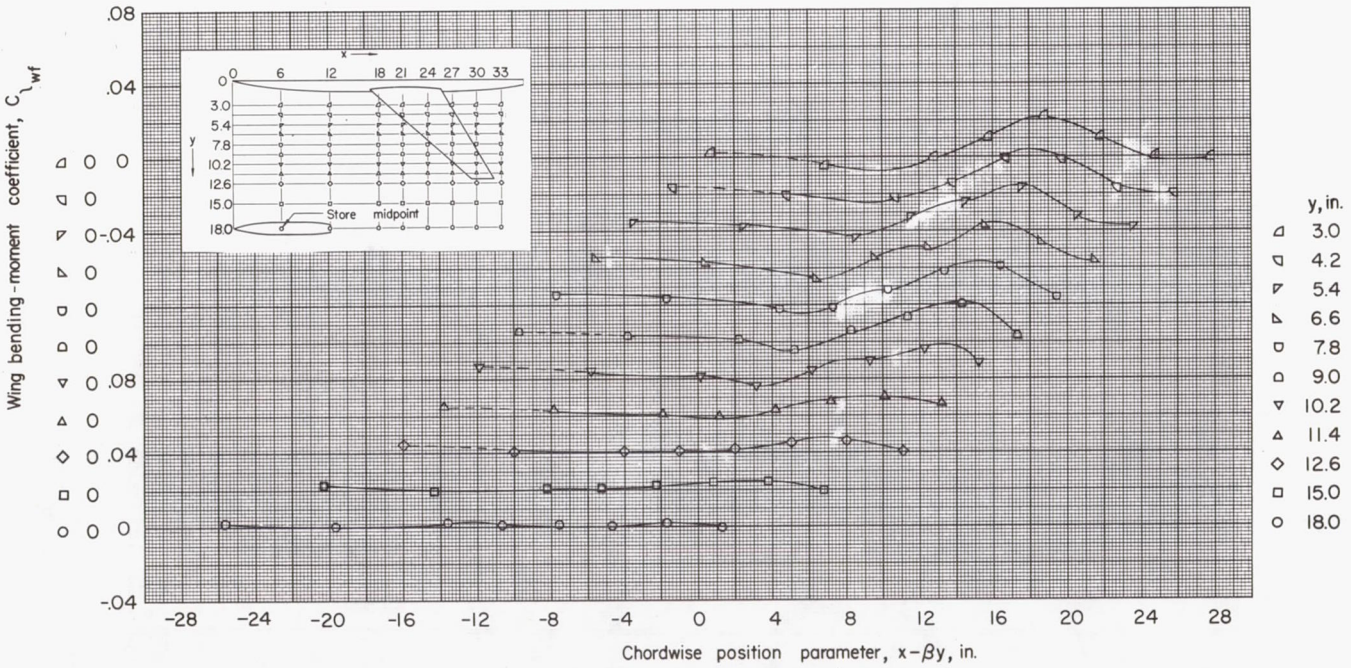
(d) $z = 2.09$ inches; $\alpha = 4^{\circ}$.

Figure 13.- Concluded.



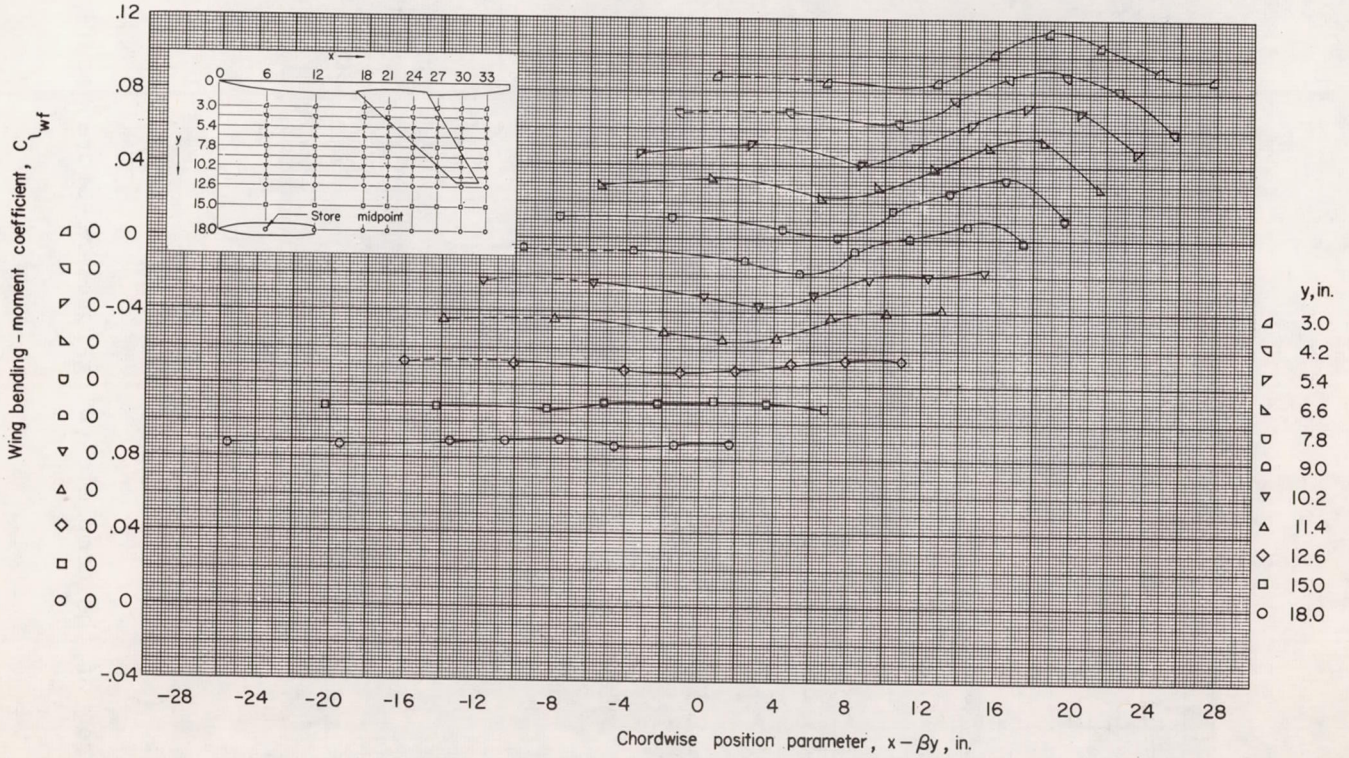
(a) $z = 1.15$ inches; $\alpha = 0^{\circ}$.

Figure 14.- Wing bending moment of the wing-fuselage combination in presence of store.



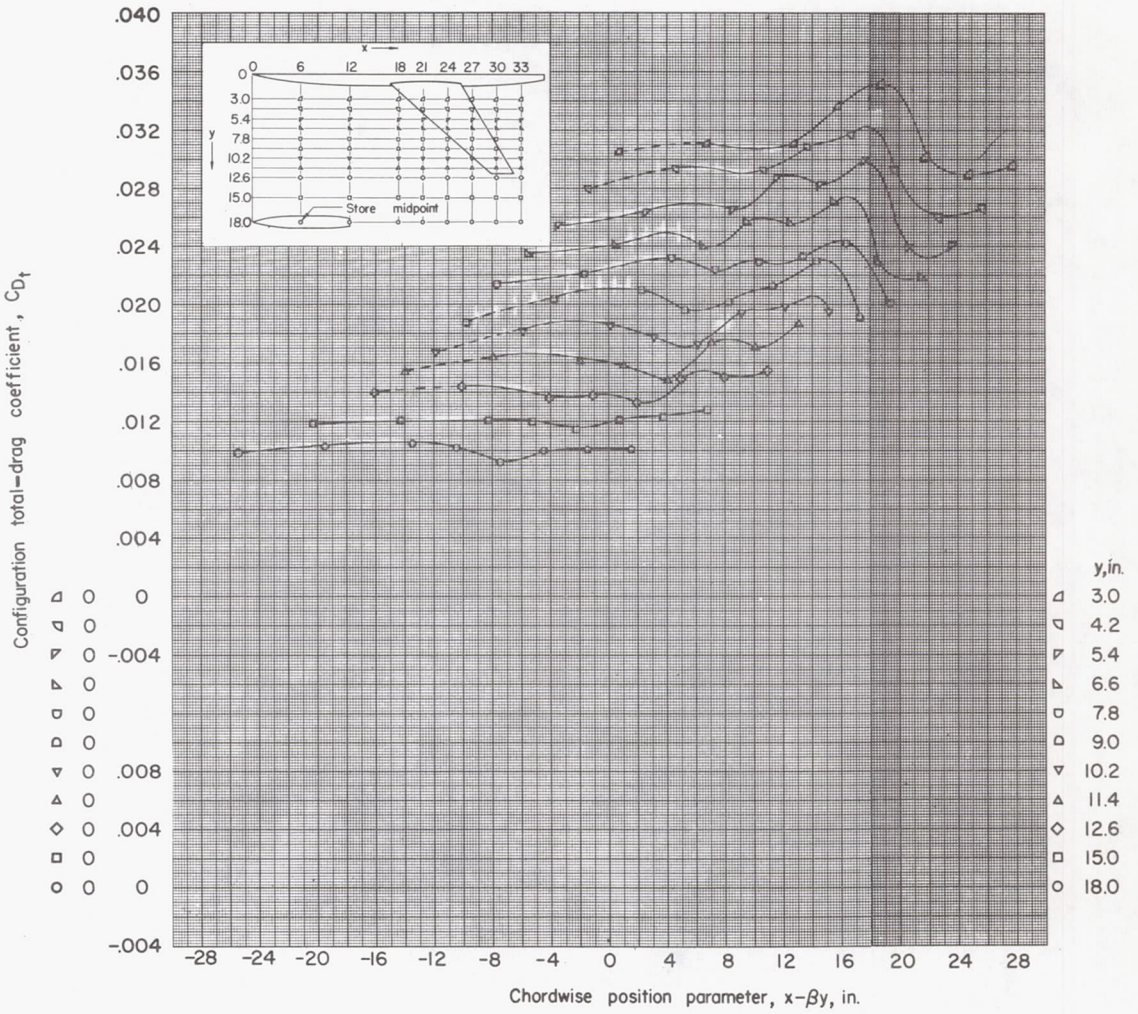
(b) z = 2.09 inches; $\alpha = 0^{\circ}$.

Figure 14.- Continued.



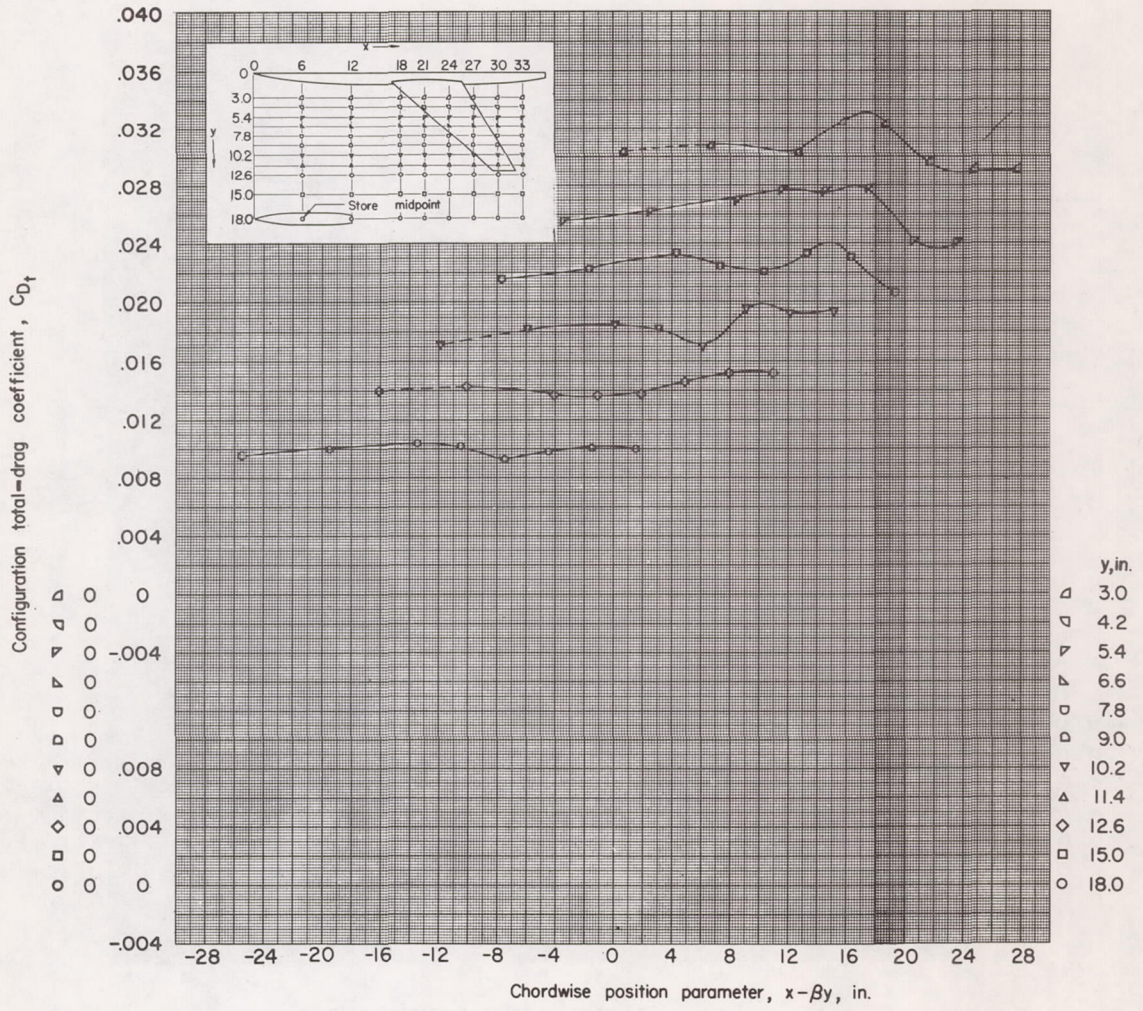
(c) z = 2.09 inches; $\alpha = 4^{\circ}$.

Figure 14.- Concluded.



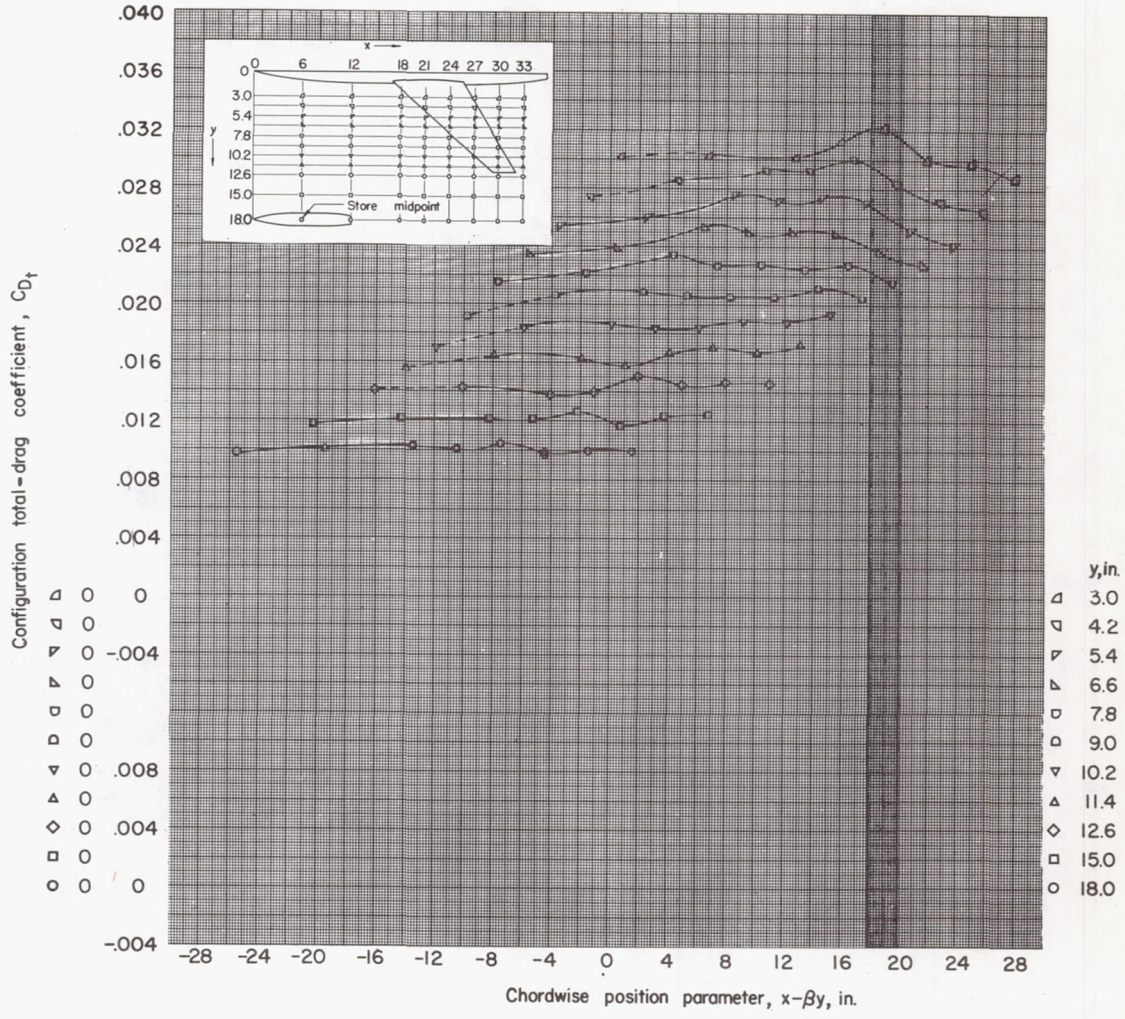
(a) z = 1.15 inches; $\alpha = 0^{\circ}$.

Figure 15.- Total drag of the complete (wing-fuselage-store) configuration.



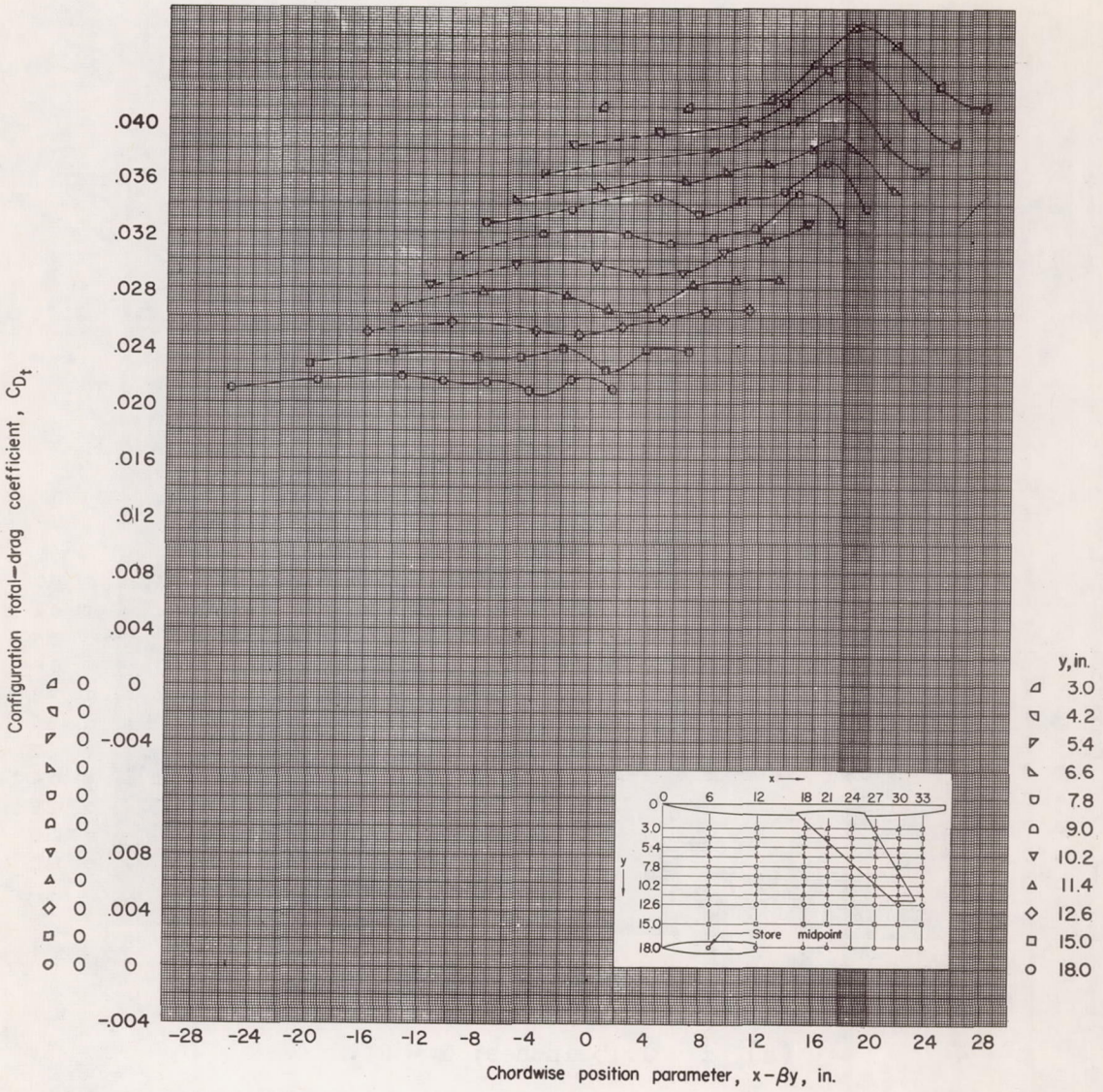
(b) z = 1.67 inches; $\alpha = 0^{\circ}$.

Figure 15.- Continued.



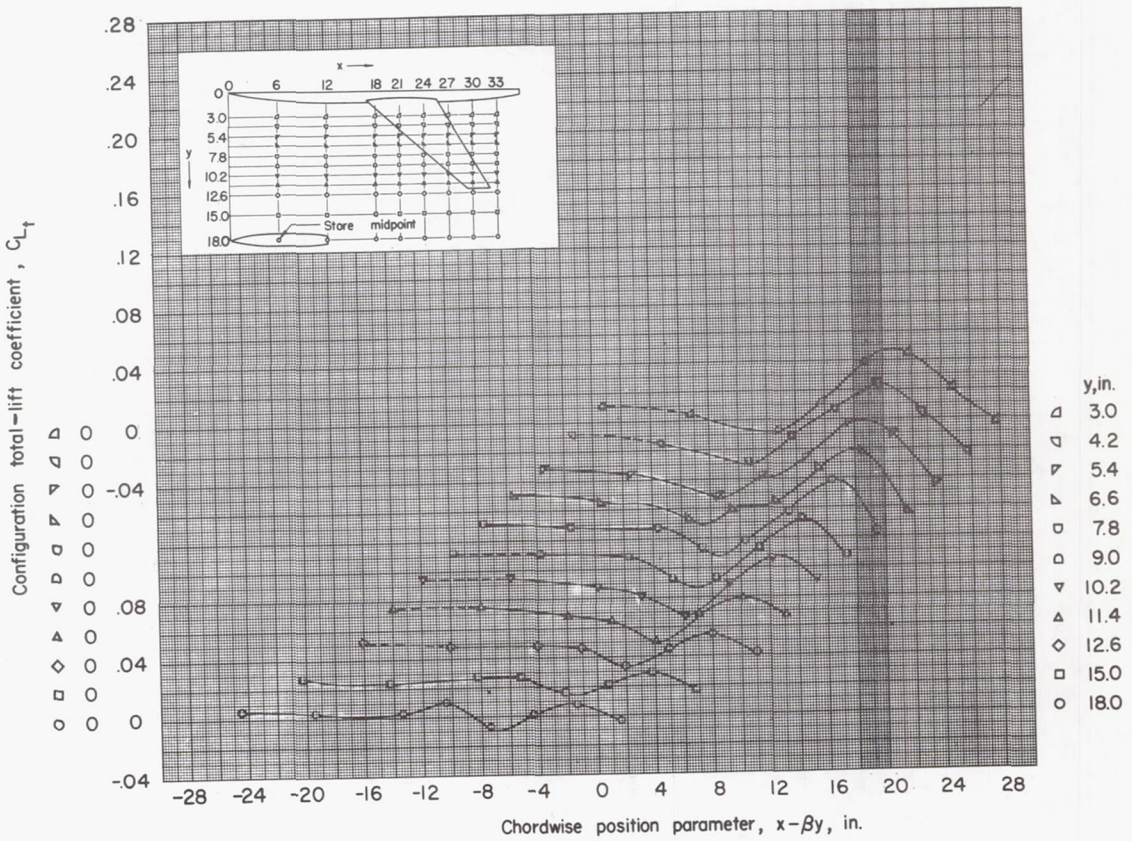
(c) z = 2.09 inches; $\alpha = 0^{\circ}$.

Figure 15.- Continued.



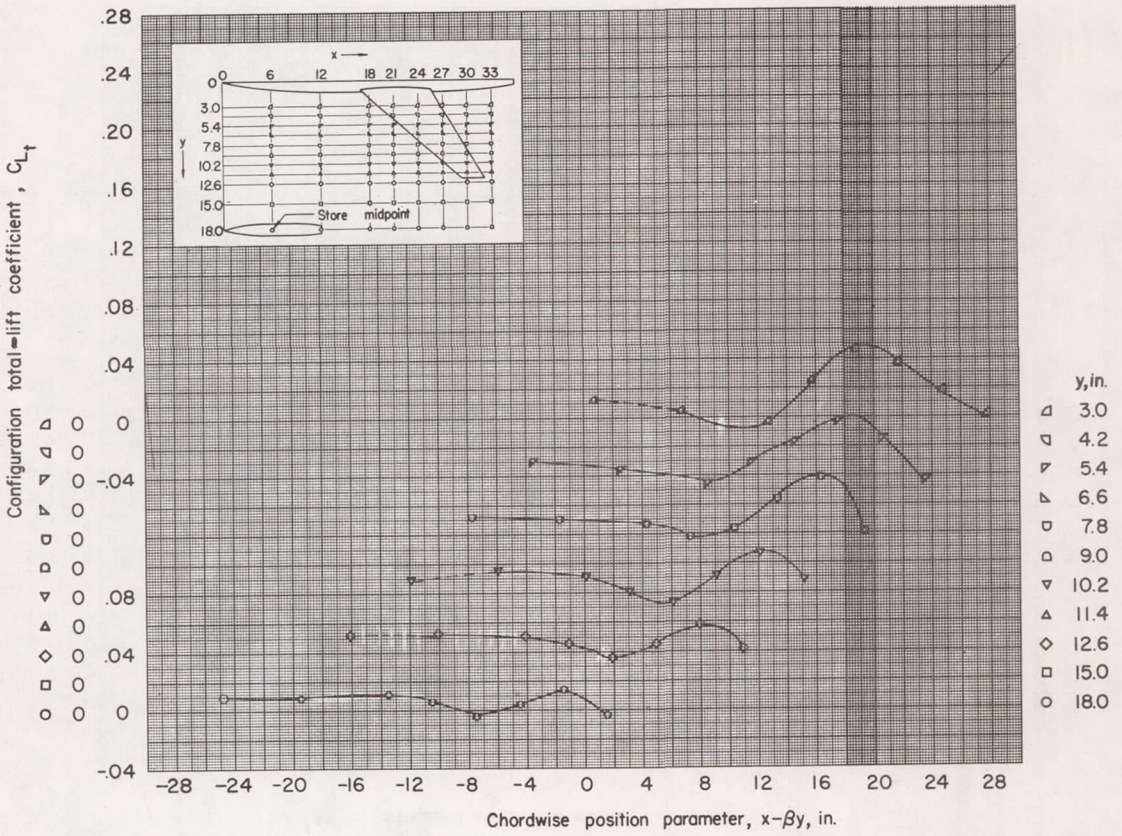
(d) z = 2.09 inches; $\alpha = 4^{\circ}$.

Figure 15.- Concluded.



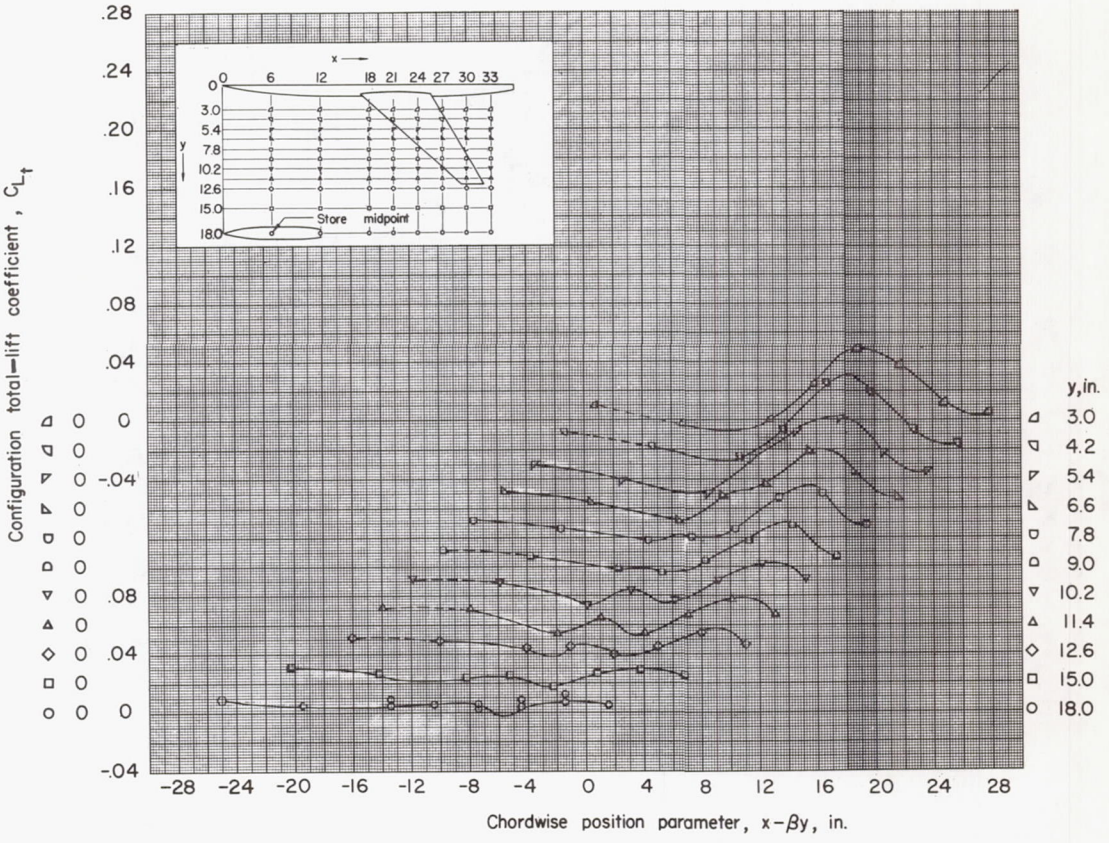
(a) z = 1.15 inches; $\alpha = 0^{\circ}$.

Figure 16.- Total lift of complete (wing-fuselage-store) configuration.



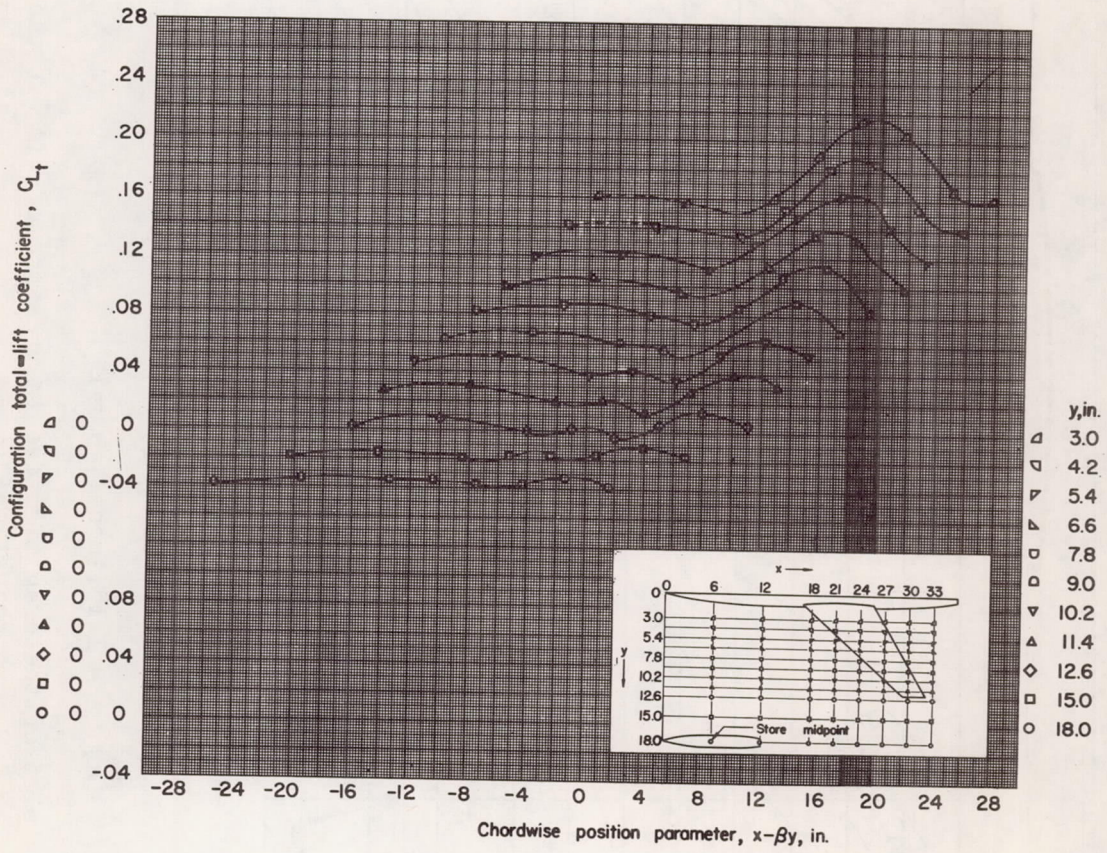
(b) z = 1.67 inches; $\alpha = 0^{\circ}$.

Figure 16.- Continued.



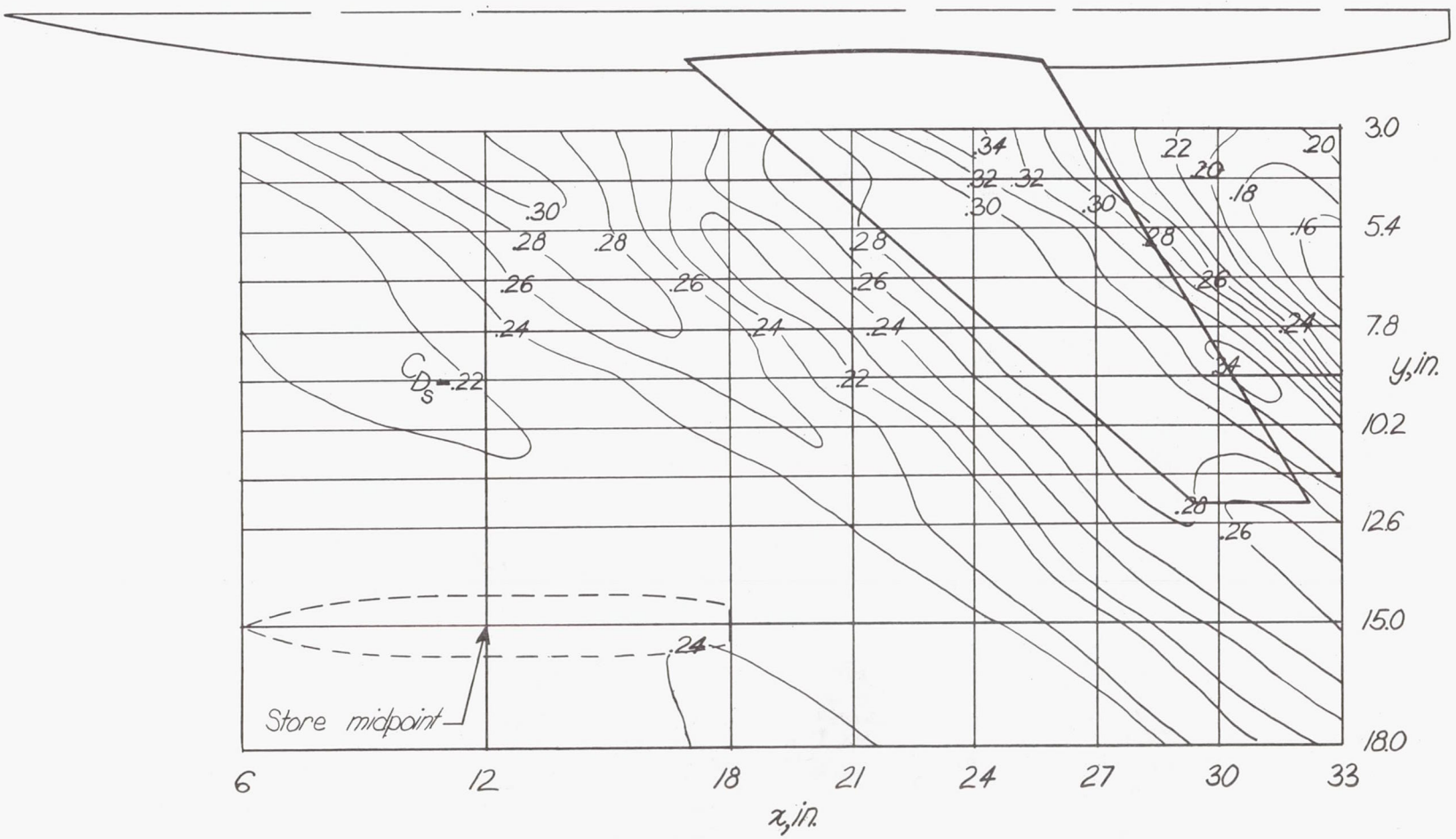
(c) z = 2.09 inches; $\alpha = 0^{\circ}$.

Figure 16.- Continued.



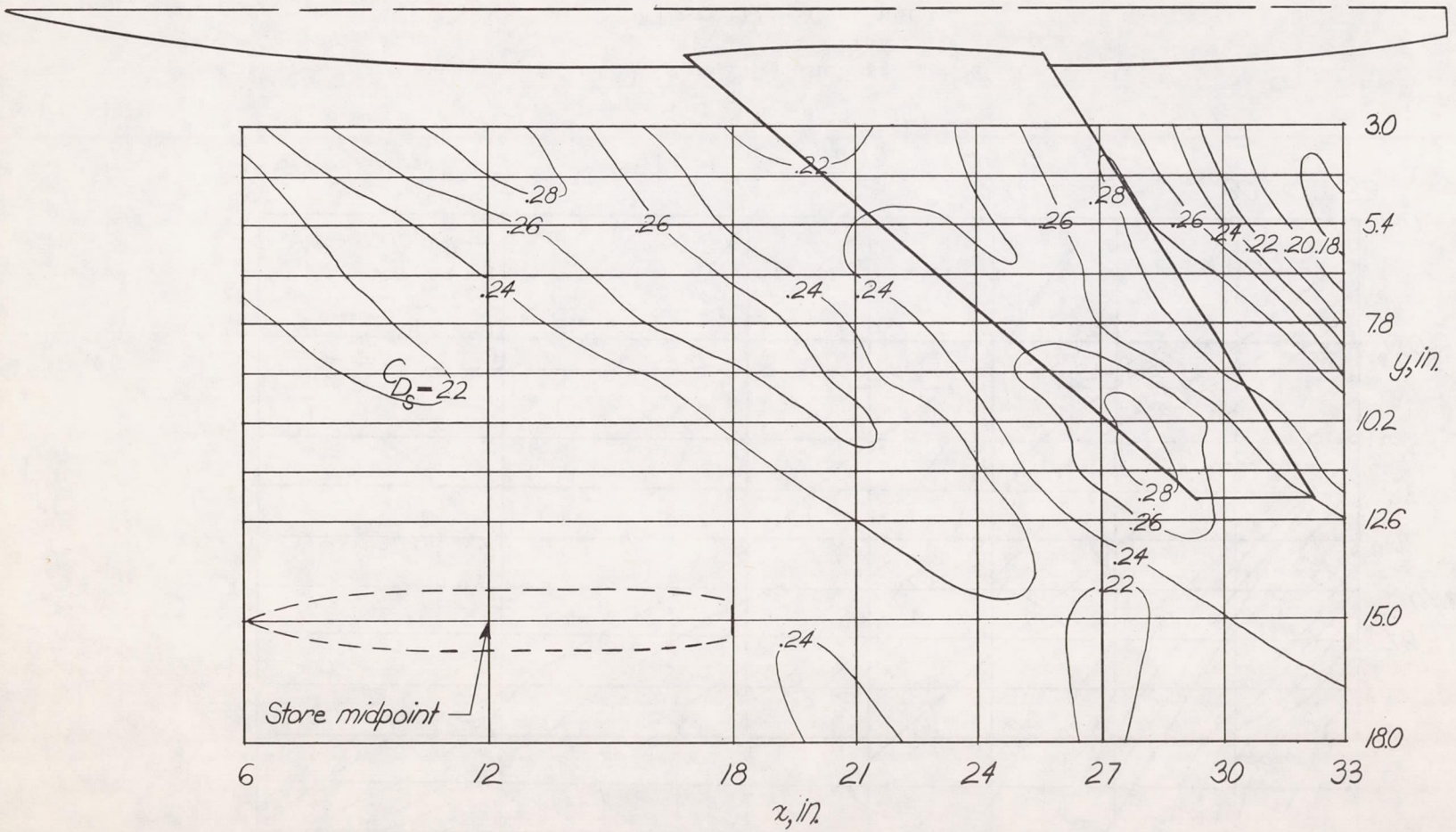
(d) z = 2.09 inches; $\alpha = 4^\circ$.

Figure 16.- Concluded.



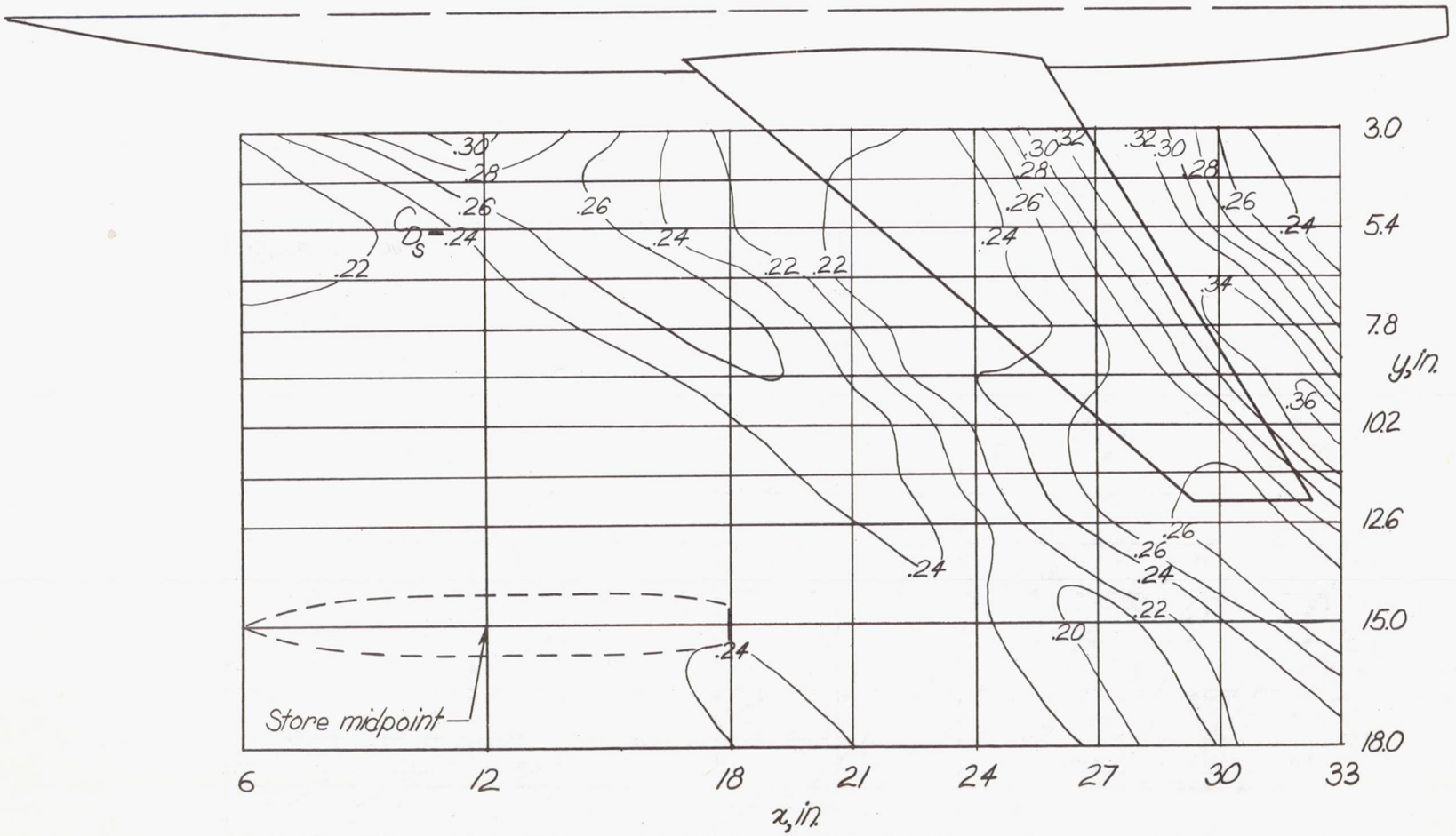
(a) z = 1.15, inches; $\alpha = 0^{\circ}$.

Figure 17.- Contour plot of the drag of store in presence of wing-fuselage combination.



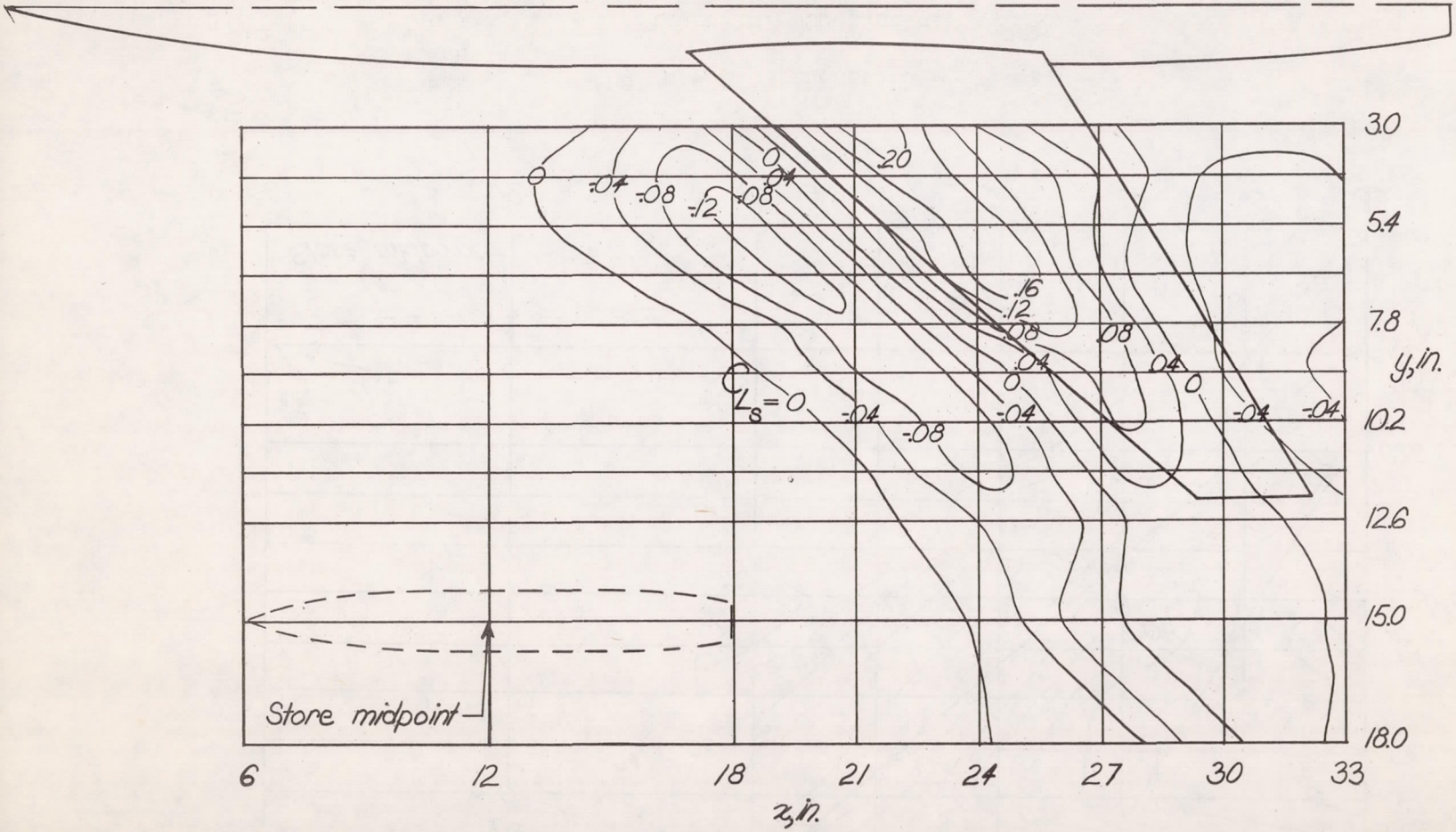
(b) z = 2.09 inches; $\alpha = 0^{\circ}$.

Figure 17.- Continued.



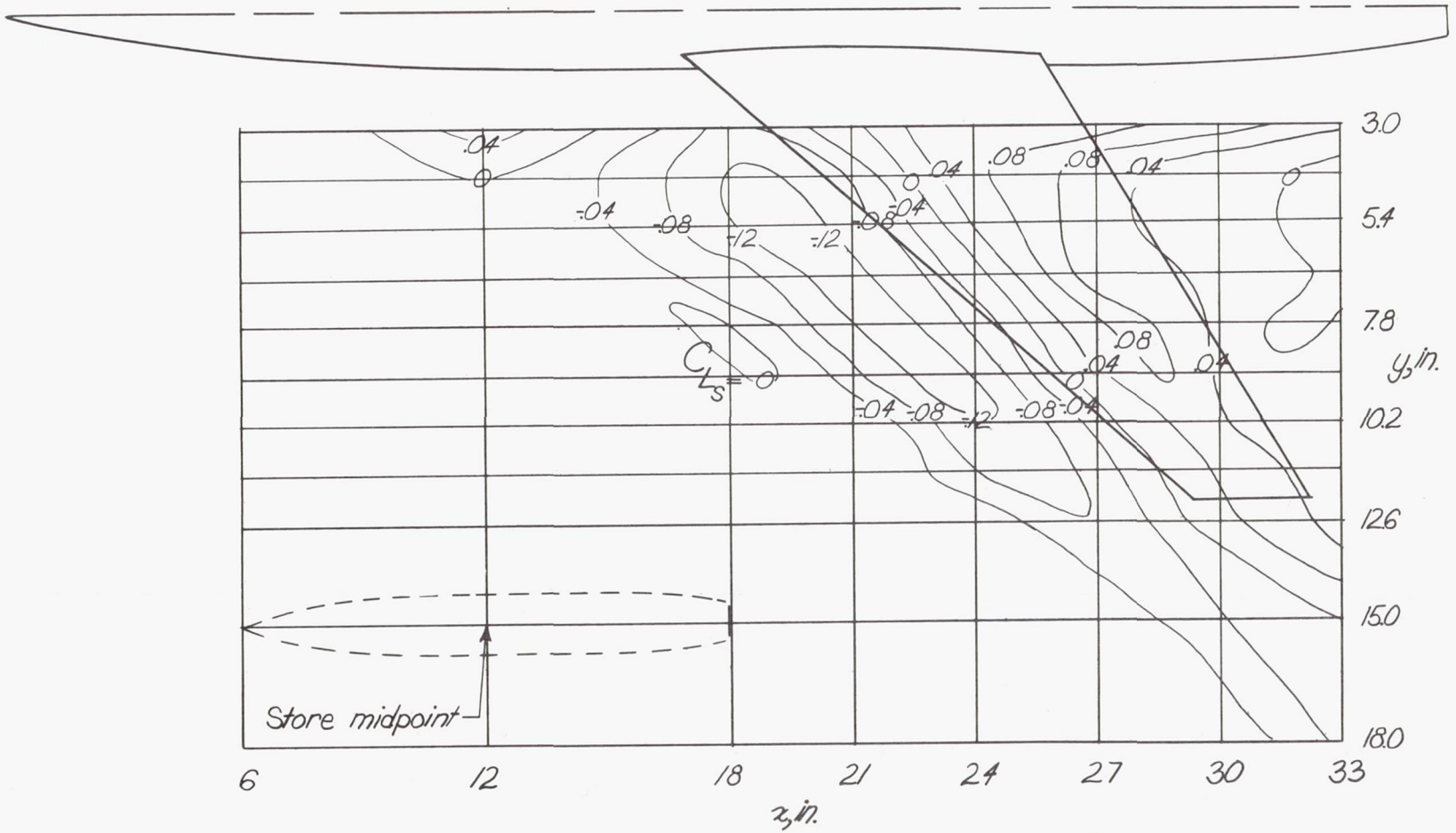
(c) z = 2.09 inches; $\alpha = 4^{\circ}$.

Figure 17.- Concluded.



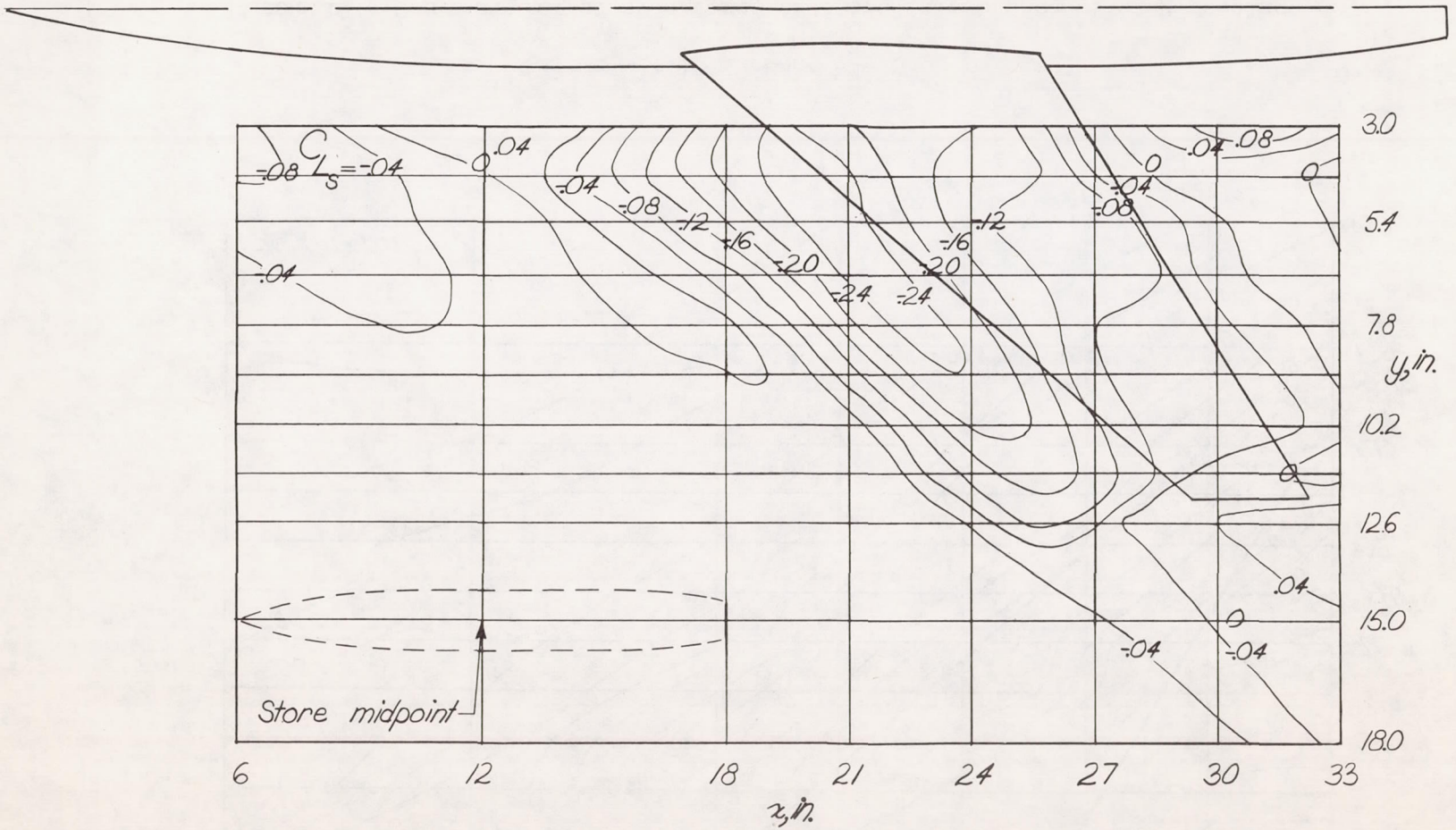
(a) z = 1.15 inches; $\alpha = 0^\circ$.

Figure 18.- Contour plot of lift of store in presence of wing-fuselage combination.



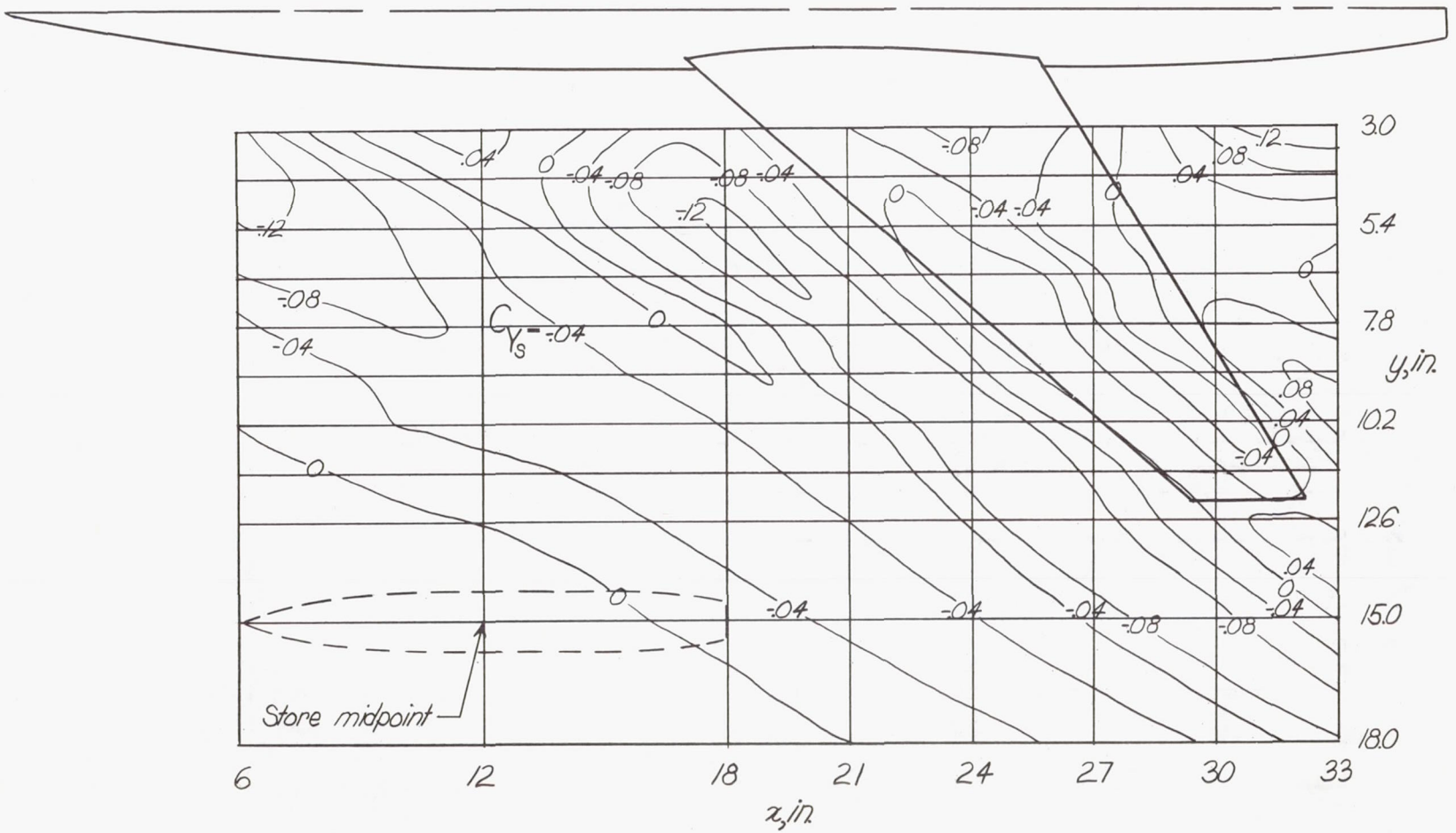
(b) z = 2.09 inches; $\alpha = 0^{\circ}$.

Figure 18.- Continued.



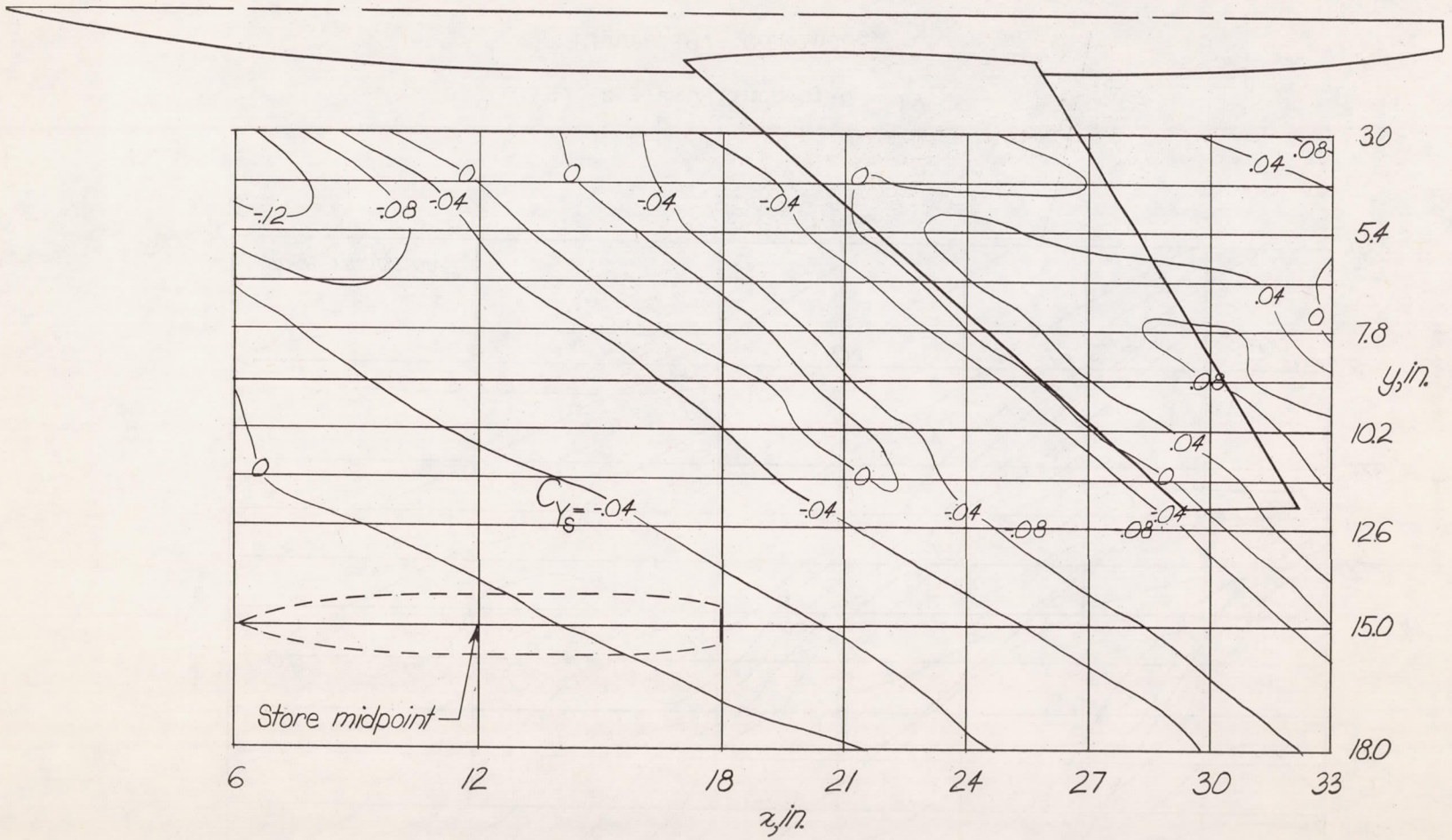
(c) z = 2.09 inches; $\alpha = 4^\circ$.

Figure 18.- Concluded.



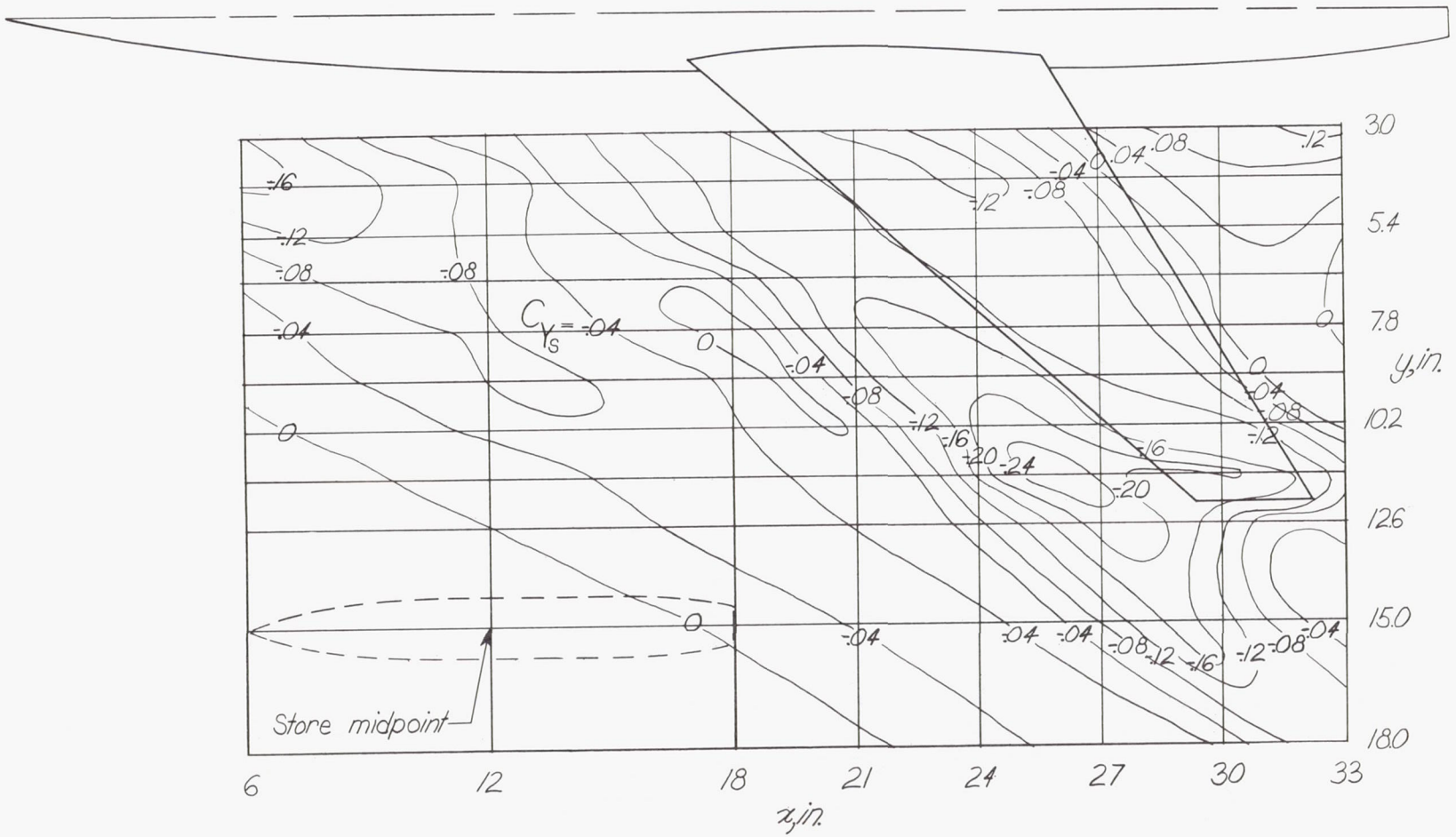
(a) z = 1.15 inches; $\alpha = 0^\circ$.

Figure 19.- Contour plot of side force of store in presence of wing-fuselage combination.



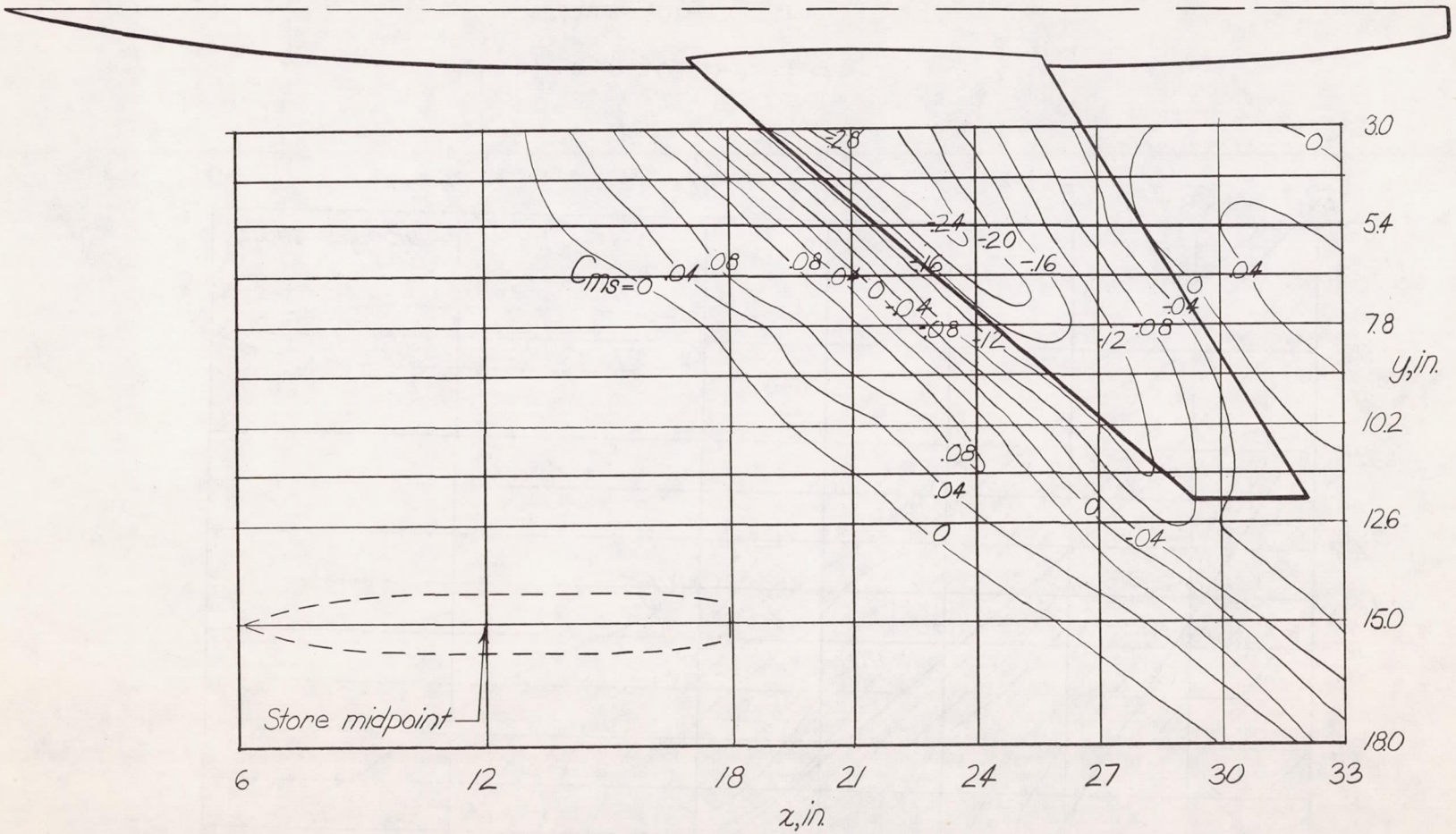
(b) z = 2.09 inches; $\alpha = 0^\circ$.

Figure 19.- Continued.



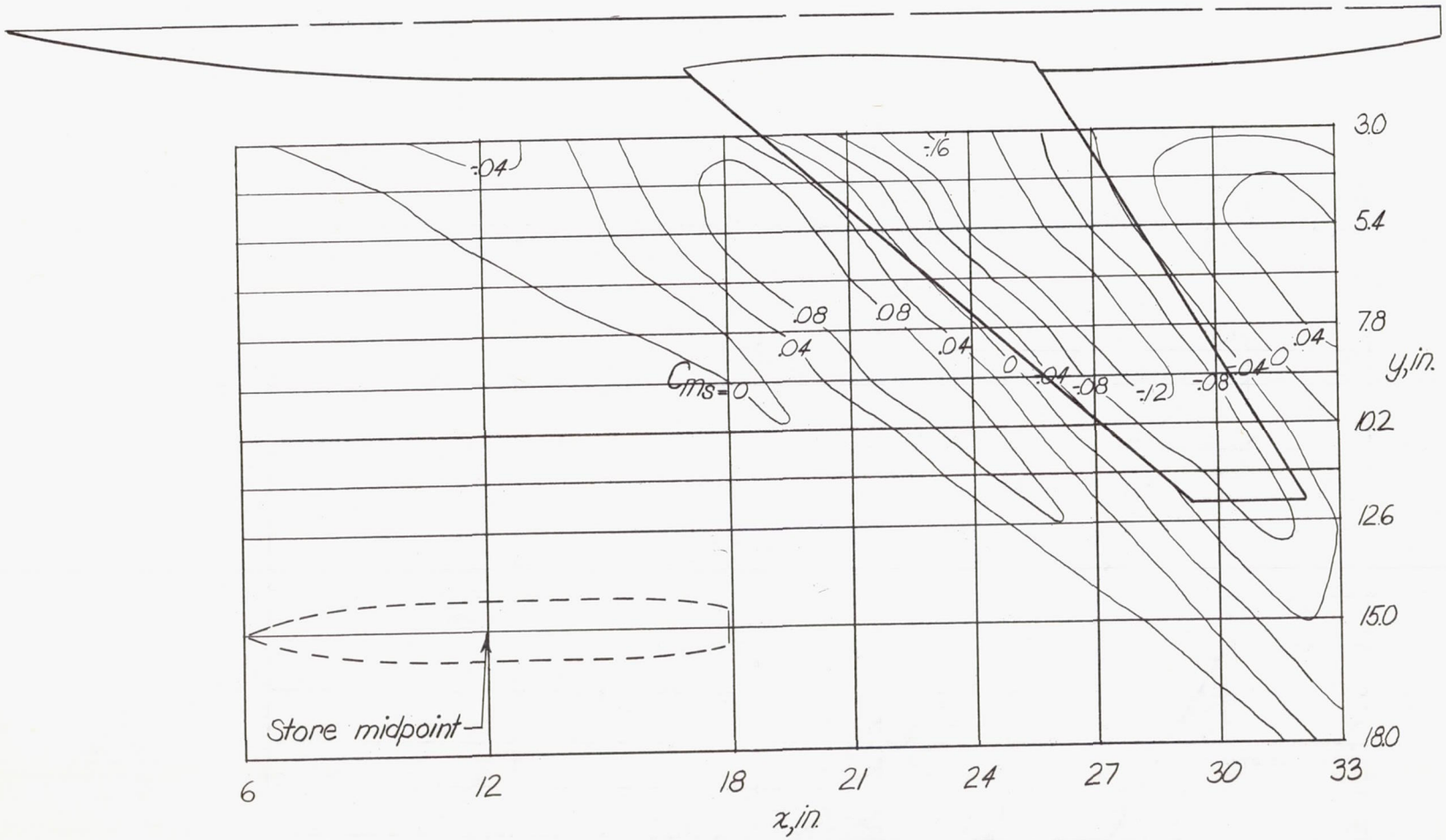
(c) z = 2.09 inches; $\alpha = 4^\circ$.

Figure 19.- Concluded.



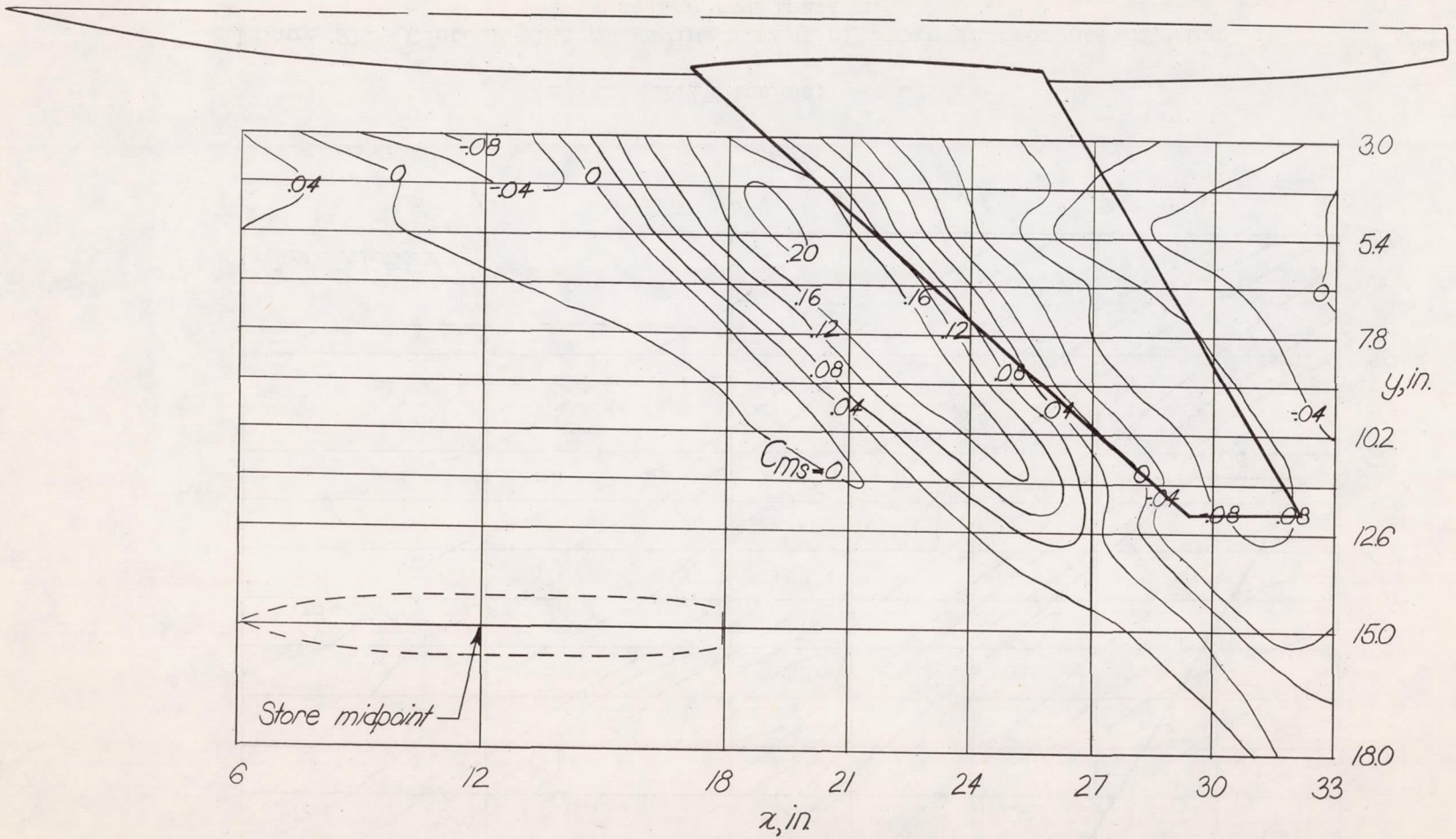
(a) z = 1.15 inches; $\alpha = 0^{\circ}$.

Figure 20.- Contour plot of pitching moment of store in presence of wing-fuselage combination.



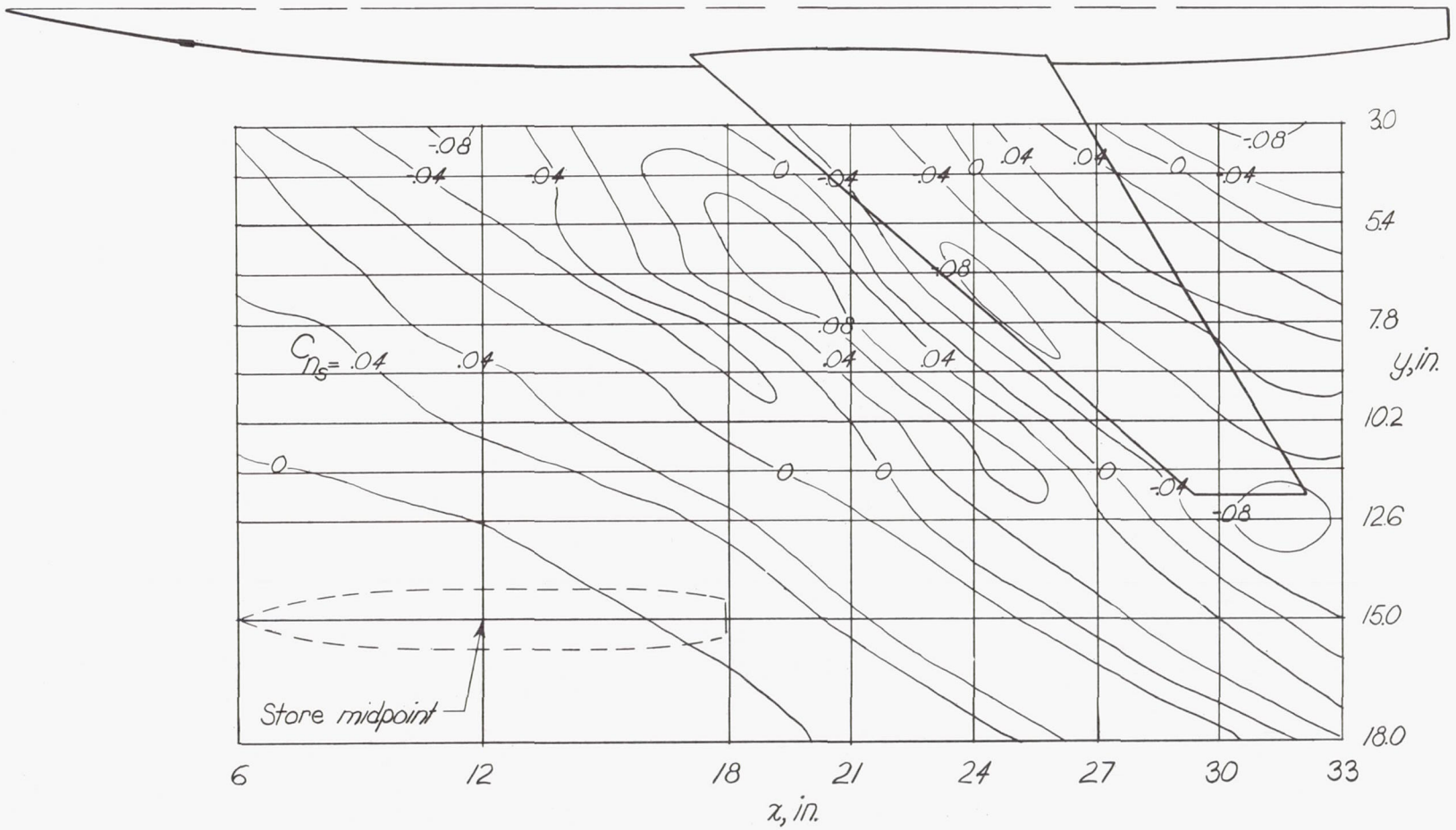
(b) z = 2.09 inches; $\alpha = 0^{\circ}$.

Figure 20.- Continued.



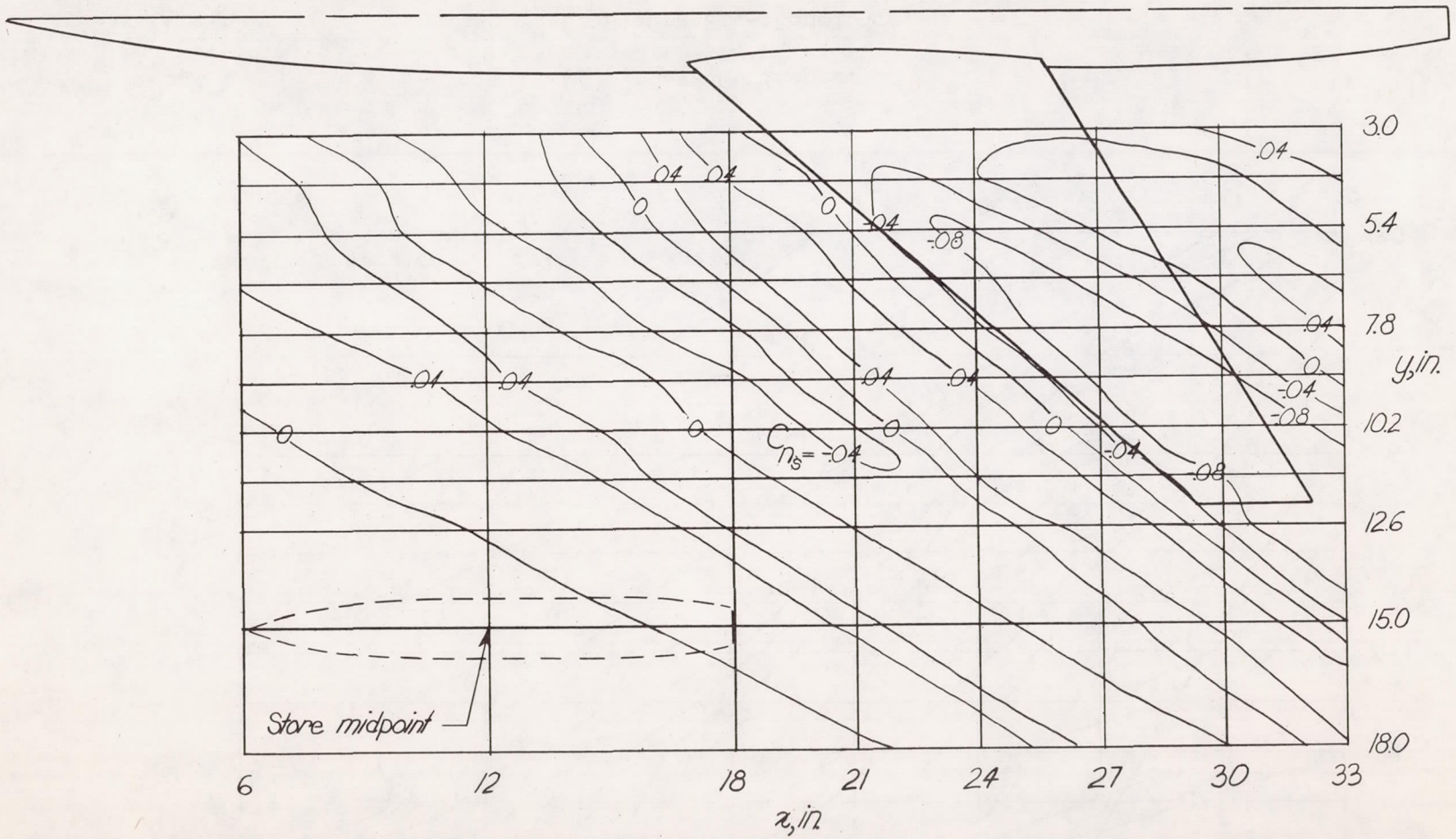
(c) z = 2.09 inches; $\alpha = 4^\circ$.

Figure 20.- Concluded.



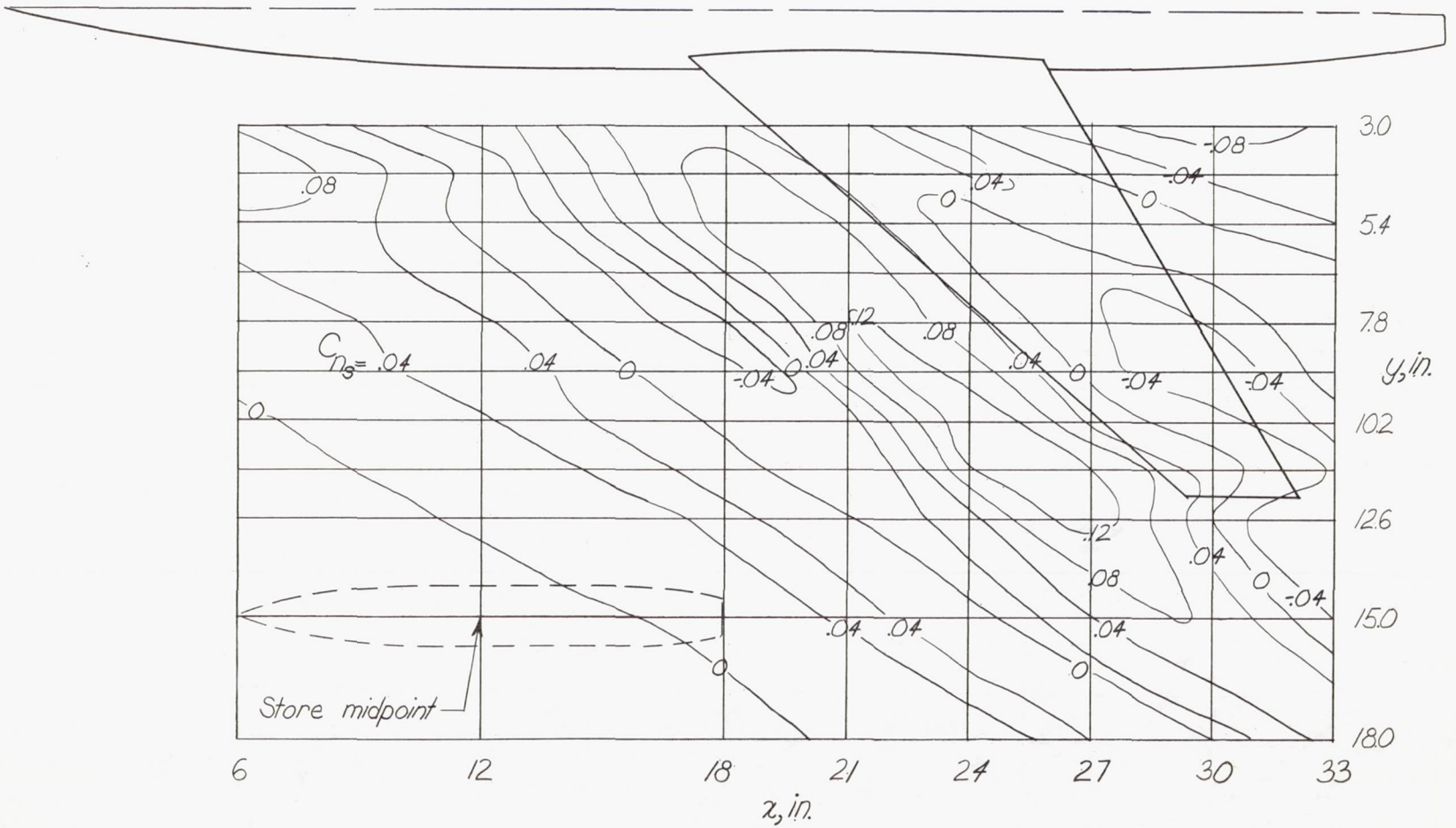
(a) z = 1.15 inches; $\alpha = 0^{\circ}$.

Figure 21.- Contour plot of yawing moment of store in presence of wing-fuselage combination.



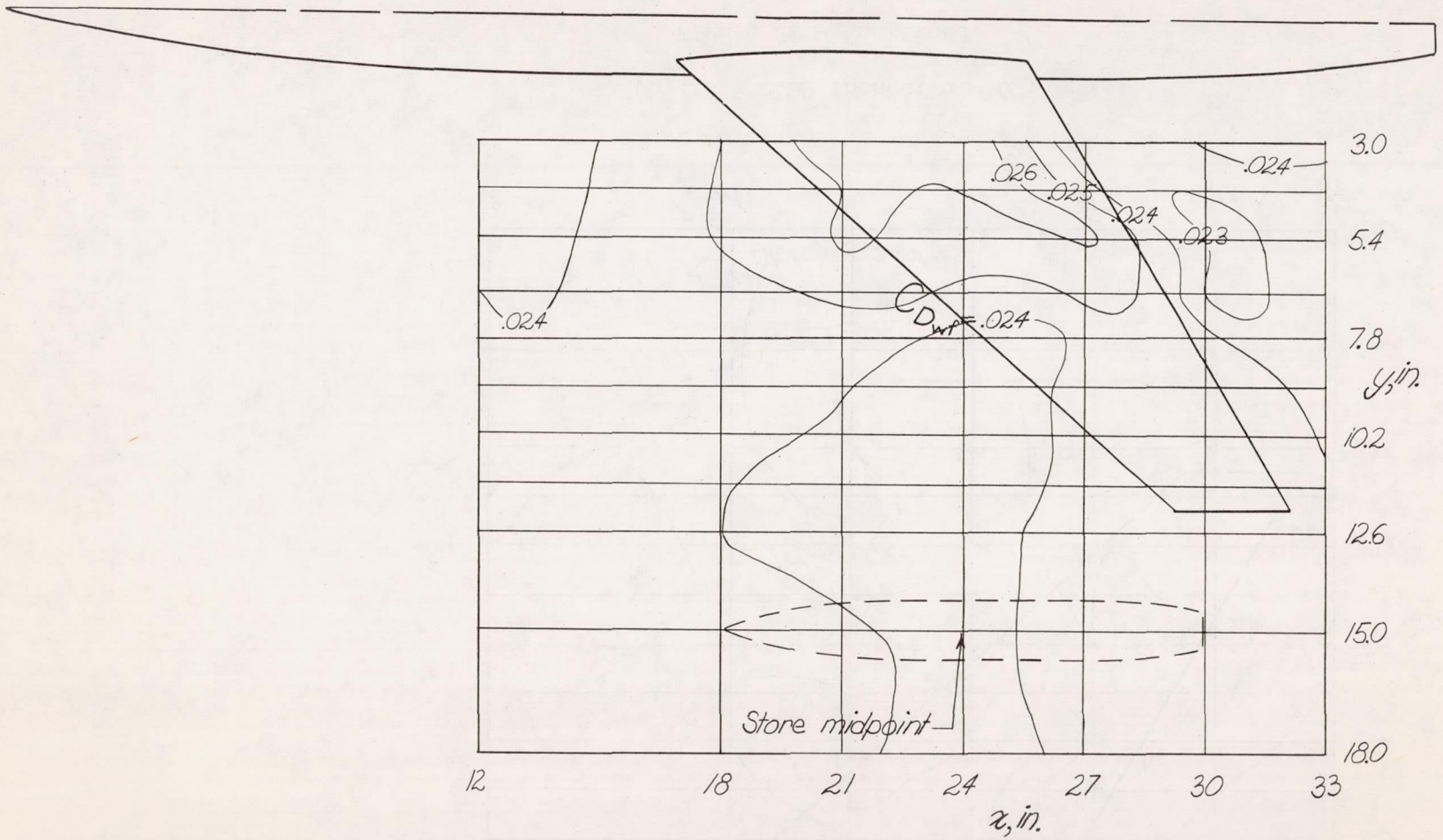
(b) z = 2.09 inches; $\alpha = 0^\circ$.

Figure 21.- Continued.



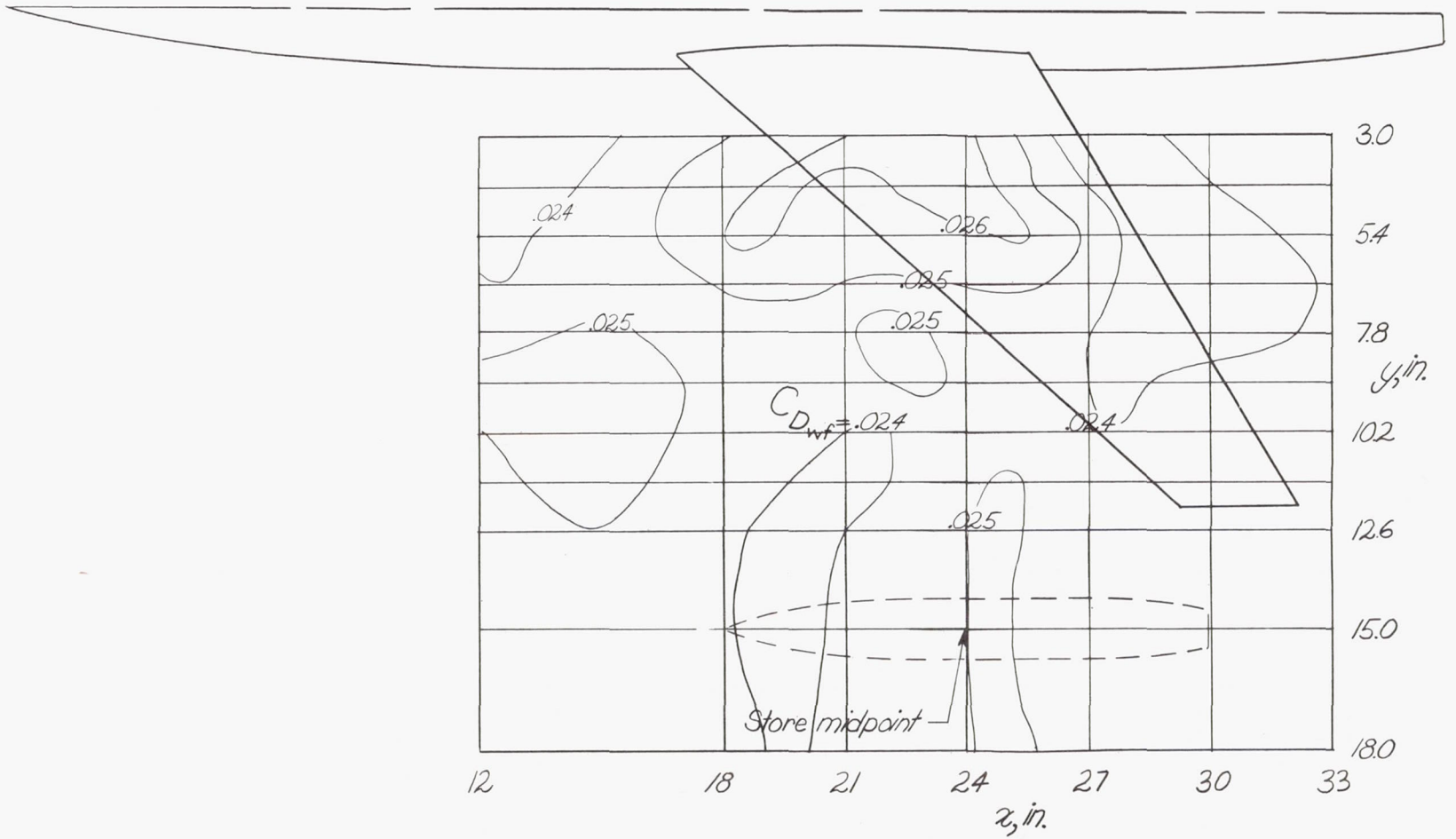
(c) z = 2.09 inches; $\alpha = 4^\circ$.

Figure 21.- Concluded.



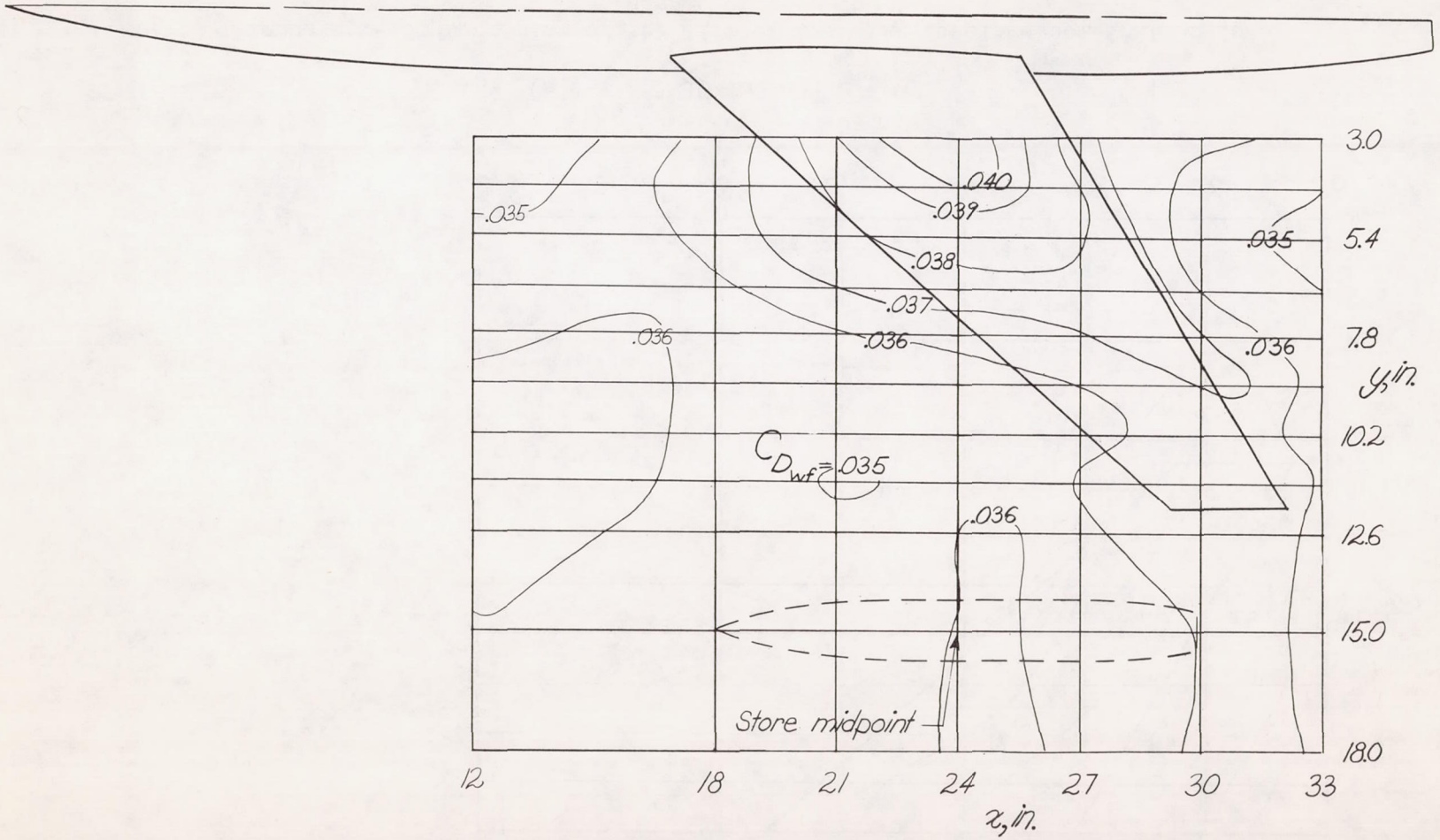
(a) z = 1.15 inches; $\alpha = 0^{\circ}$.

Figure 22.- Contour plot of the drag of the wing-fuselage combination in presence of store.



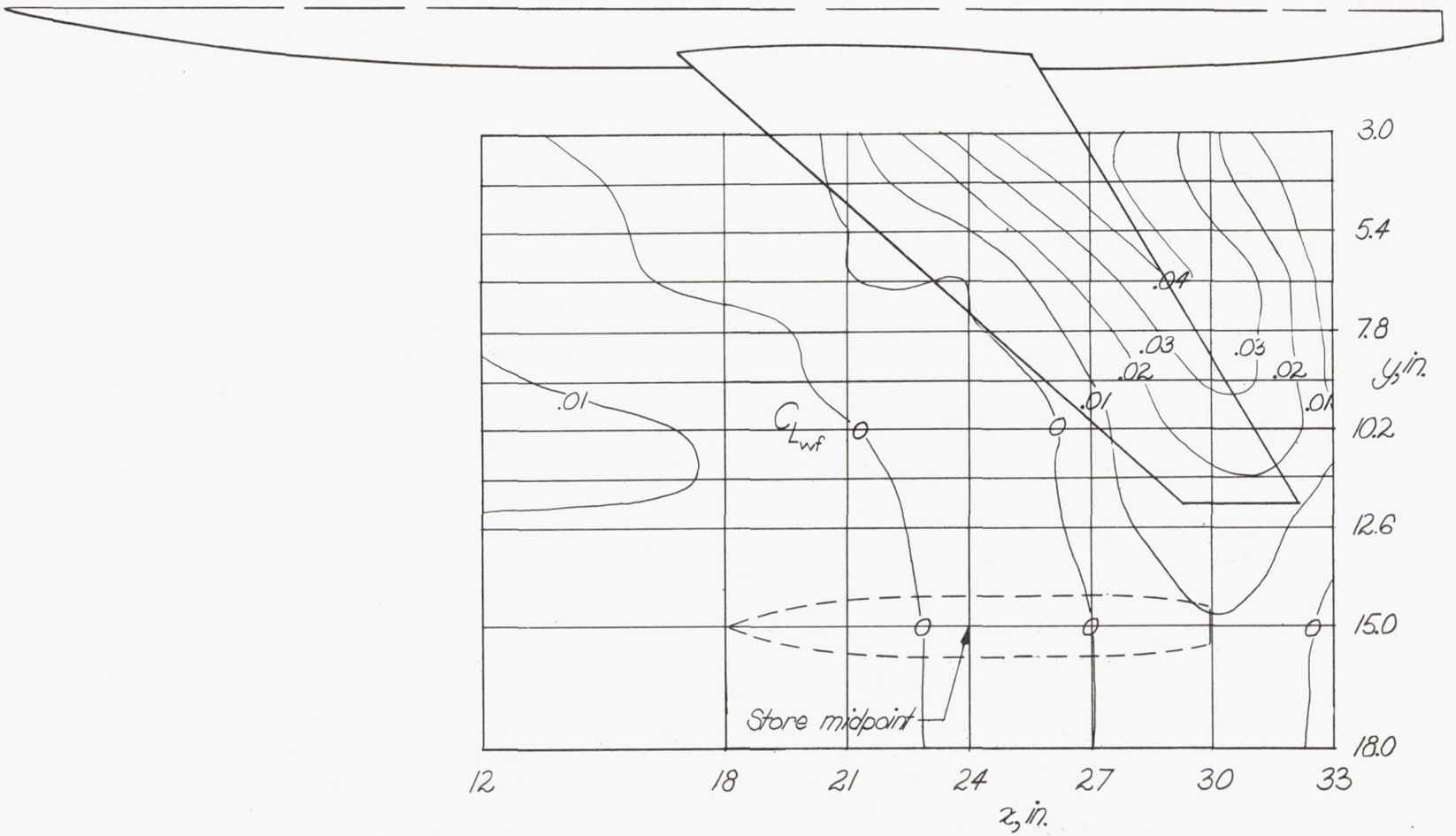
(b) z = 2.09 inches; $\alpha = 0^{\circ}$.

Figure 22.- Continued.



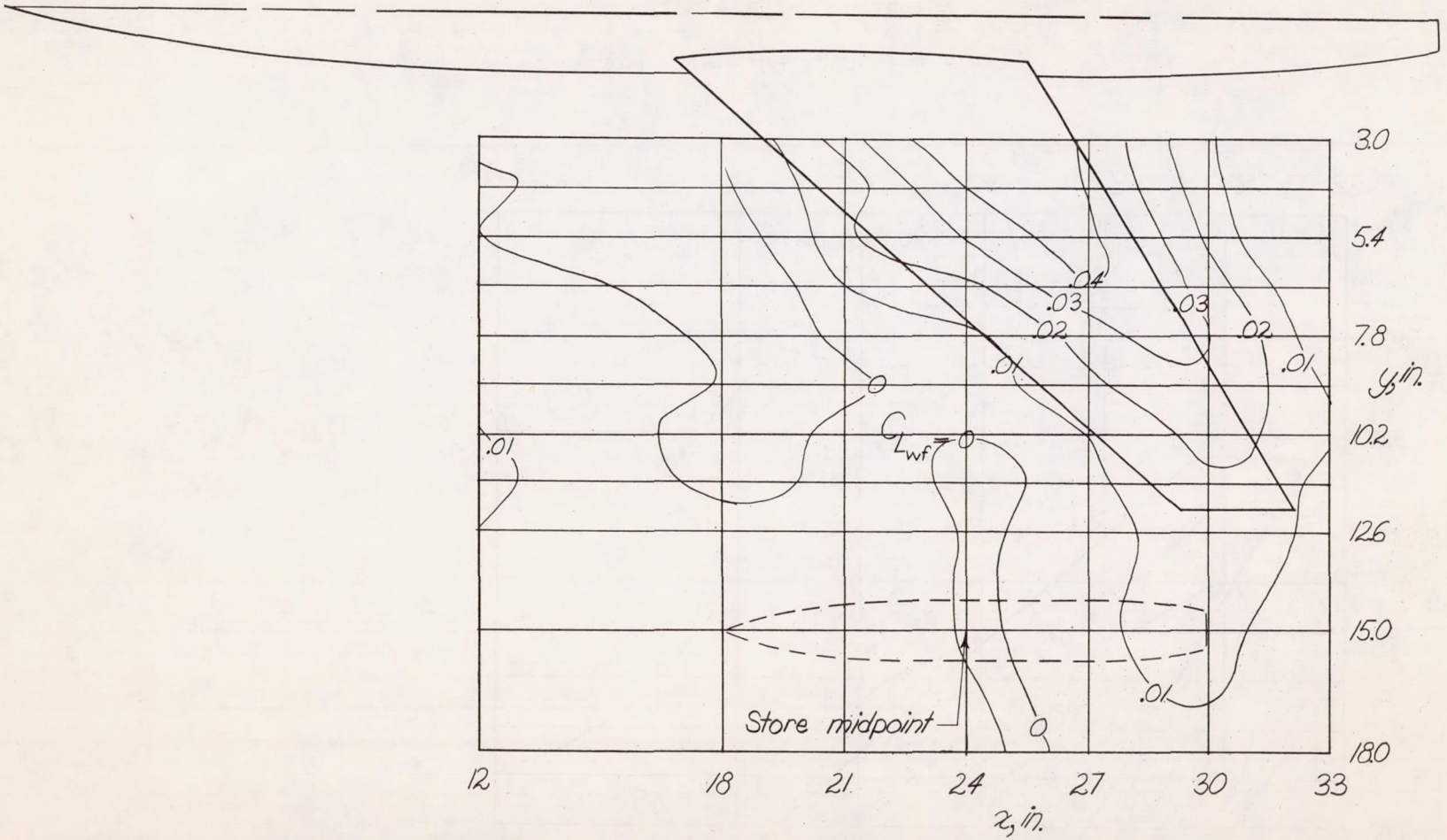
(c) z = 2.09 inches; $\alpha = 4^\circ$.

Figure 22.- Concluded.



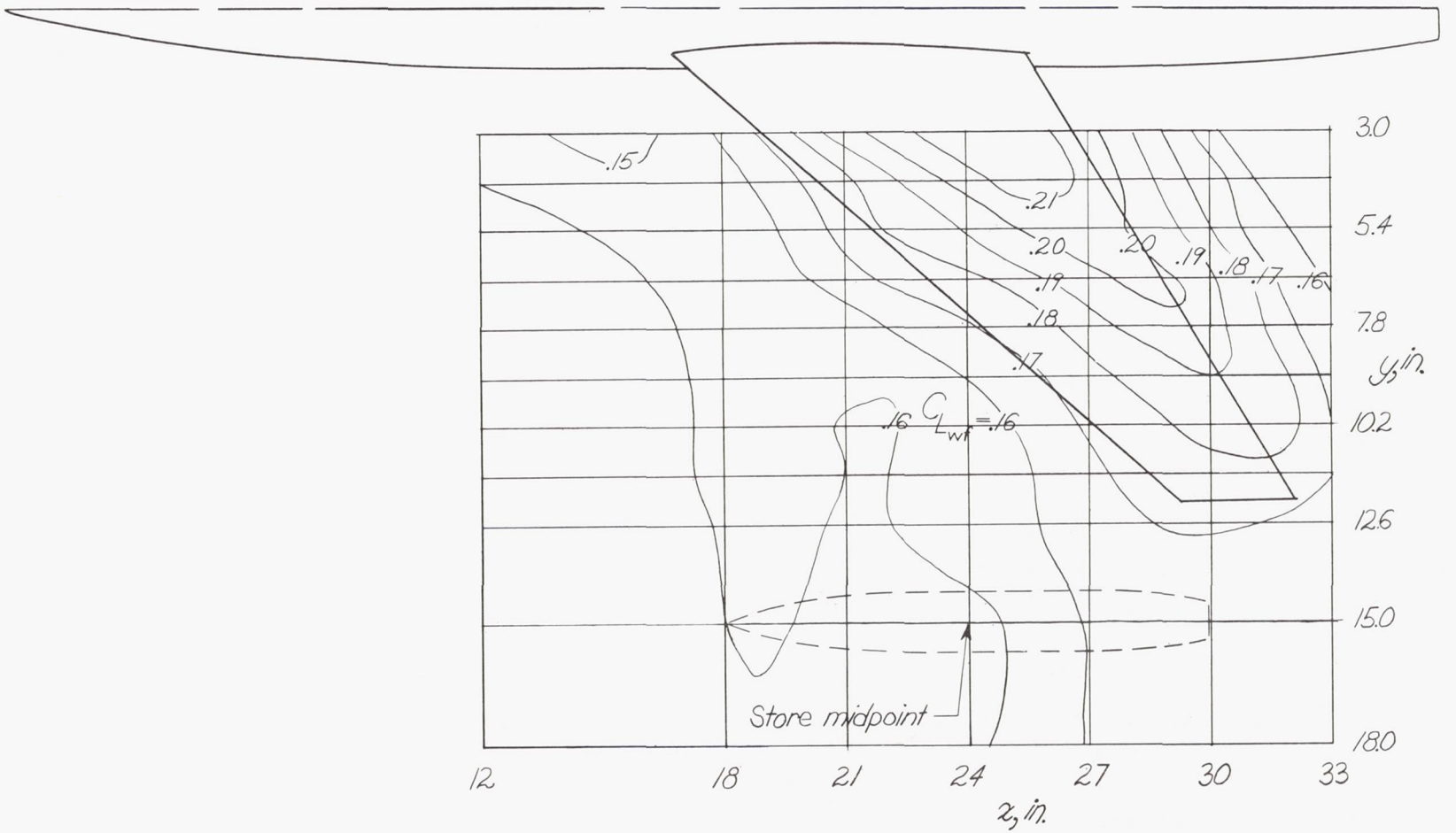
(a) z = 1.15 inches; $\alpha = 0^{\circ}$.

Figure 23.- Contour plot of the lift of the wing-fuselage combination in presence of store.



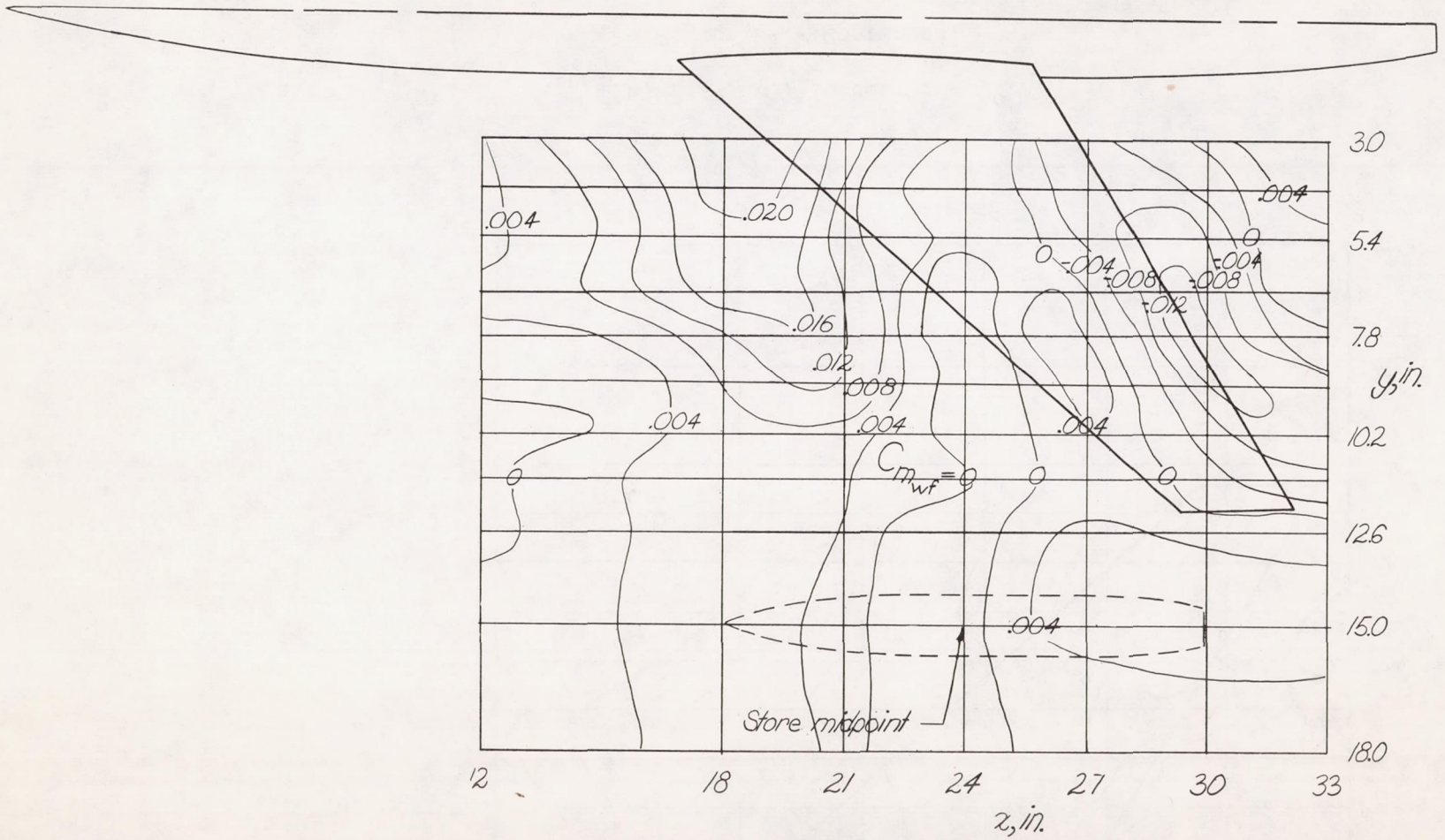
(b) z = 2.09 inches; $\alpha = 0^{\circ}$.

Figure 23.- Continued.



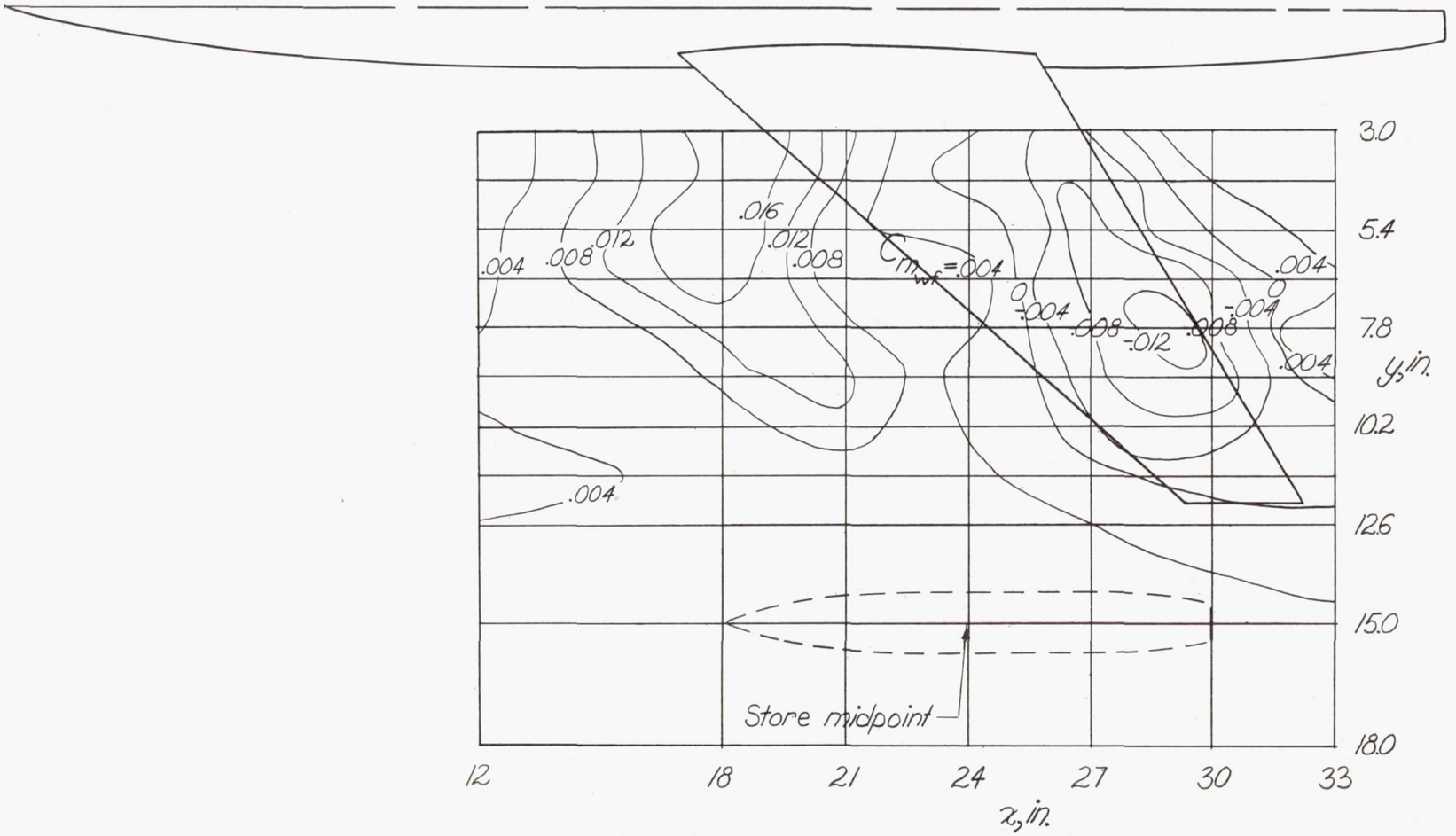
(c) z = 2.09 inches; $\alpha = 4^{\circ}$.

Figure 23.- Concluded.



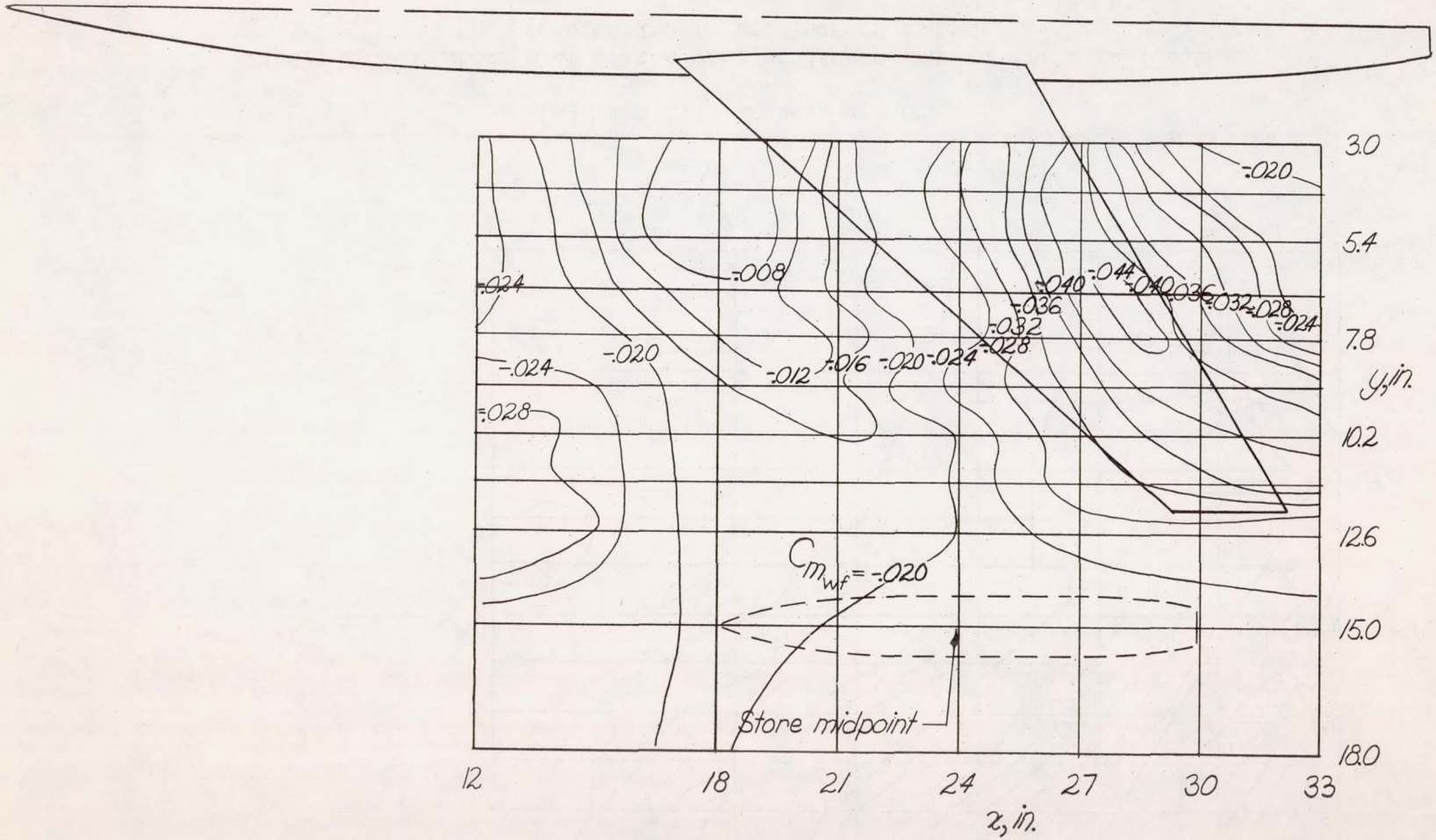
(a) z = 1.15 inches; $\alpha = 0^{\circ}$.

Figure 24.- Contour plot of the pitching moment of the wing-fuselage combination in presence of store.



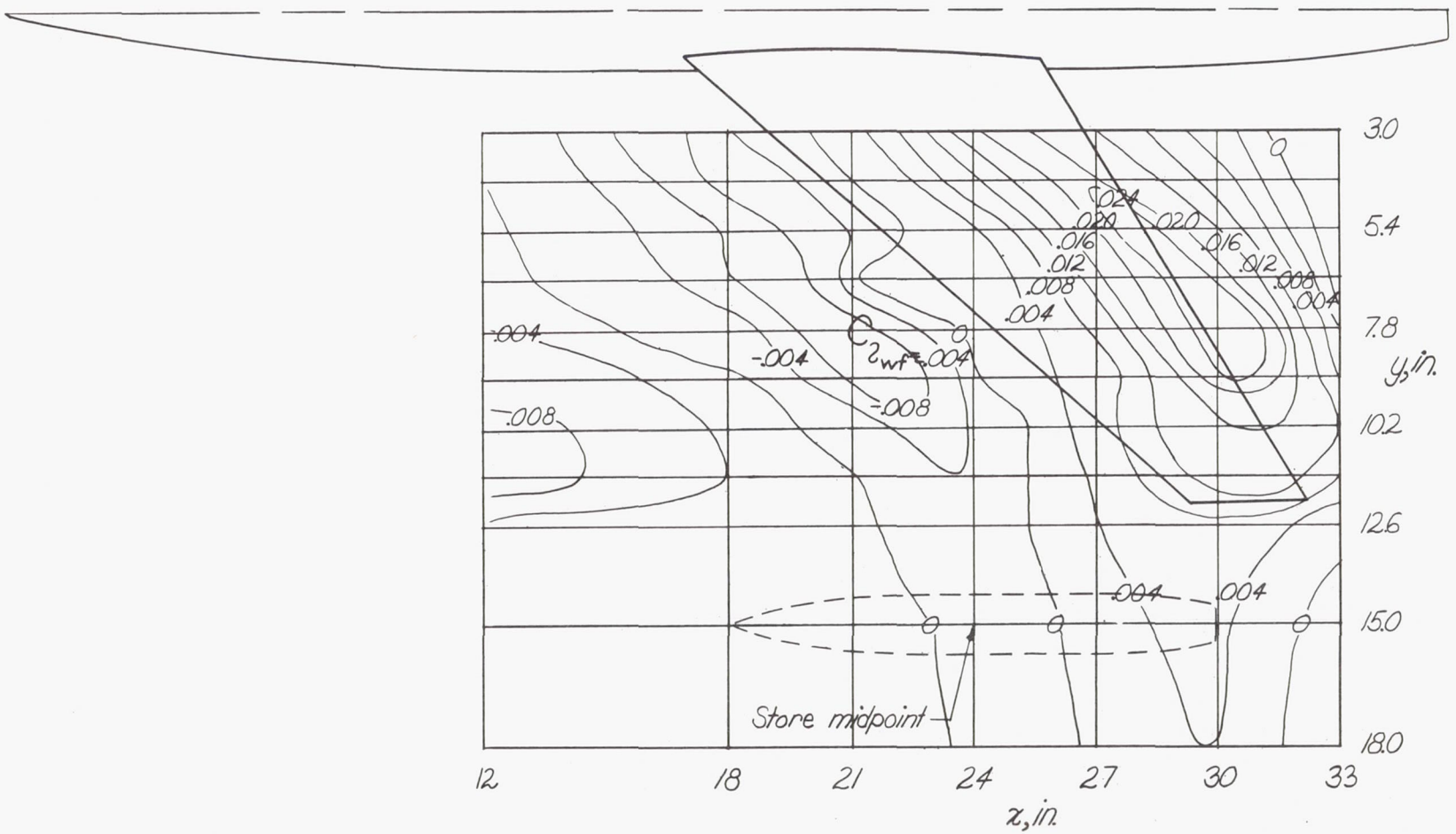
(b) z = 2.09 inches; $\alpha = 0^\circ$.

Figure 24.- Continued.



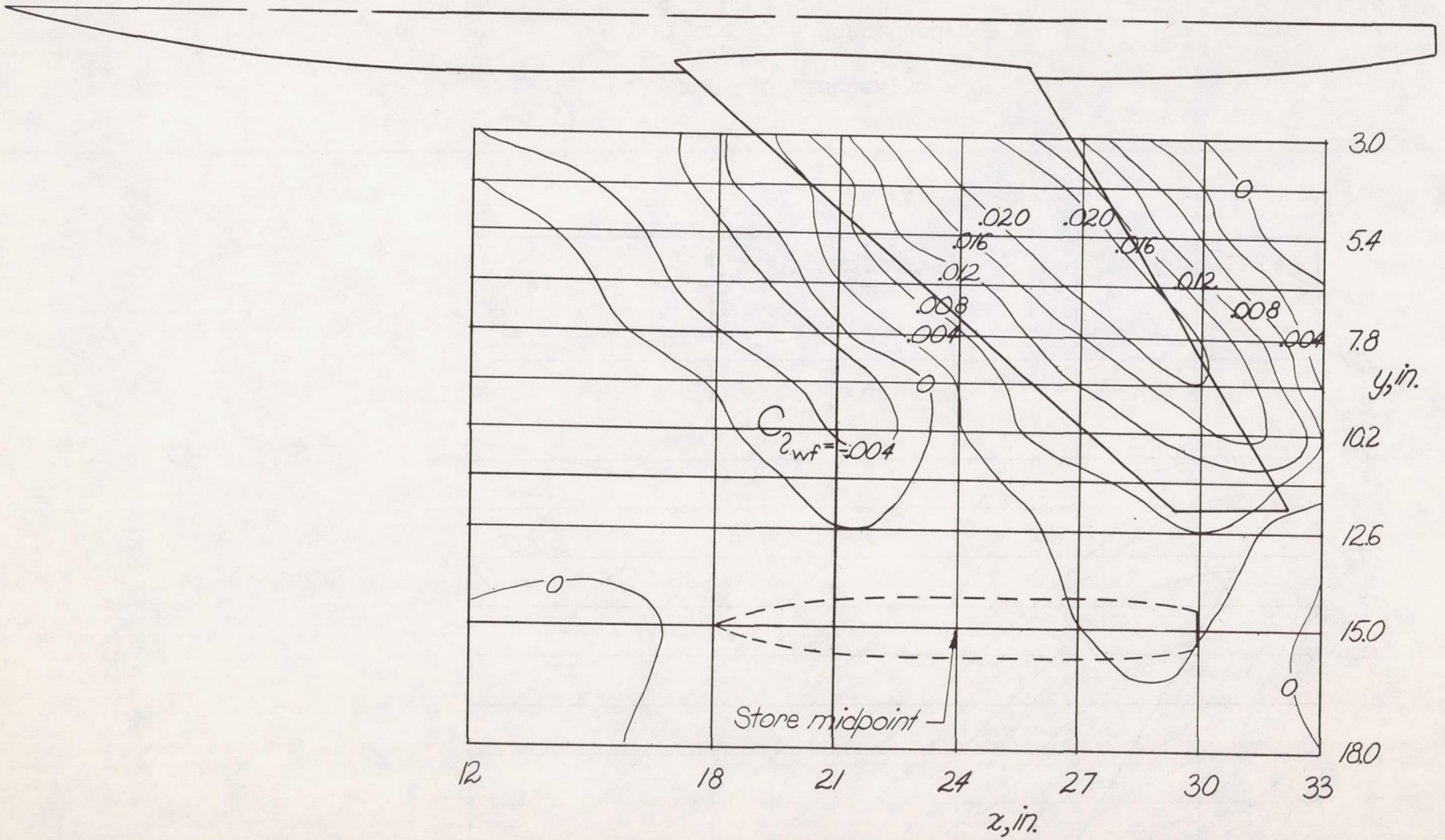
(c) z = 2.09 inches; $\alpha = 4^\circ$.

Figure 24.- Concluded.



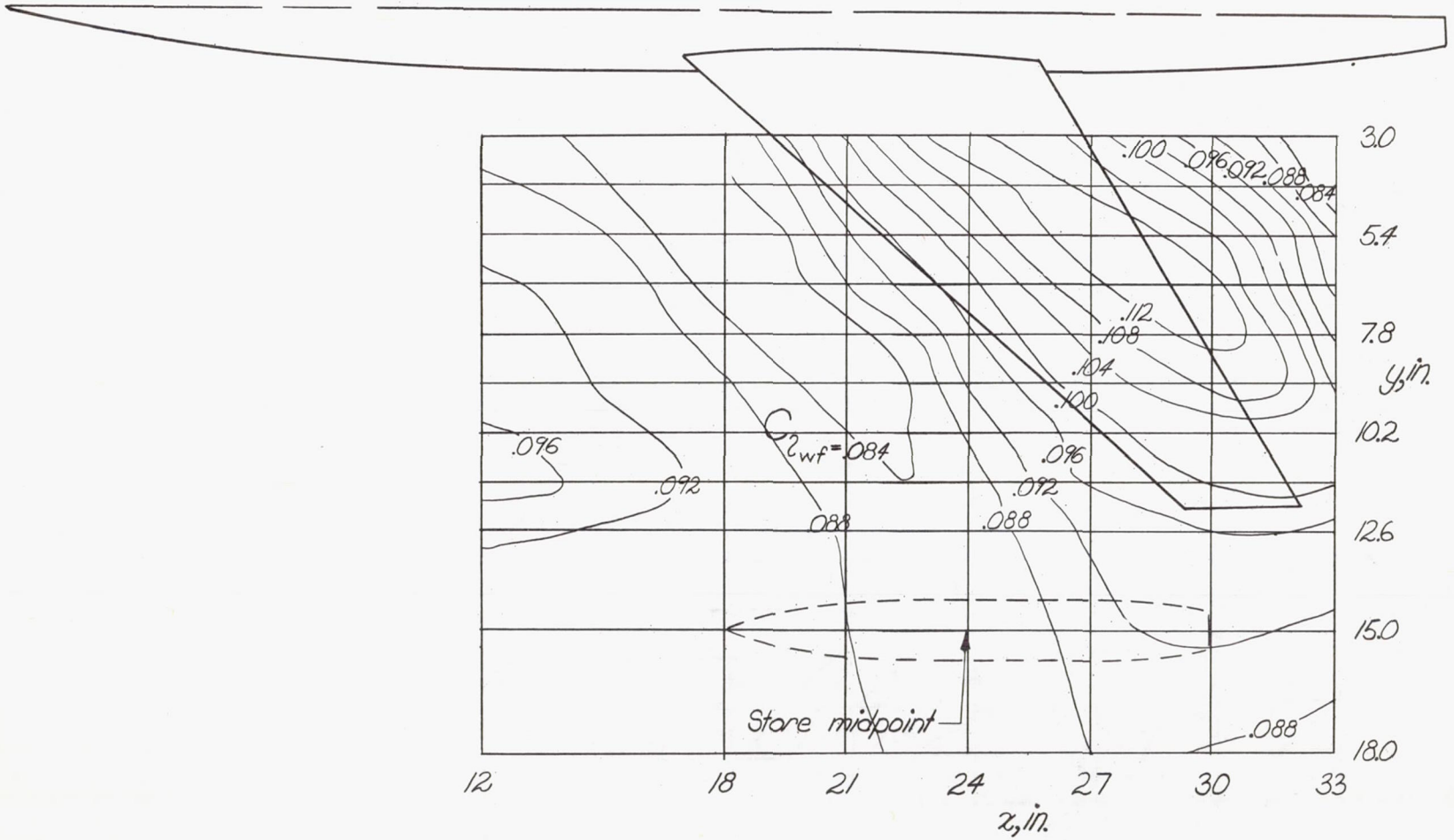
(a) z = 1.15 inches; $\alpha = 0^{\circ}$.

Figure 25.- Contour plot of the wing bending moment of the wing-fuselage combination in presence of store.



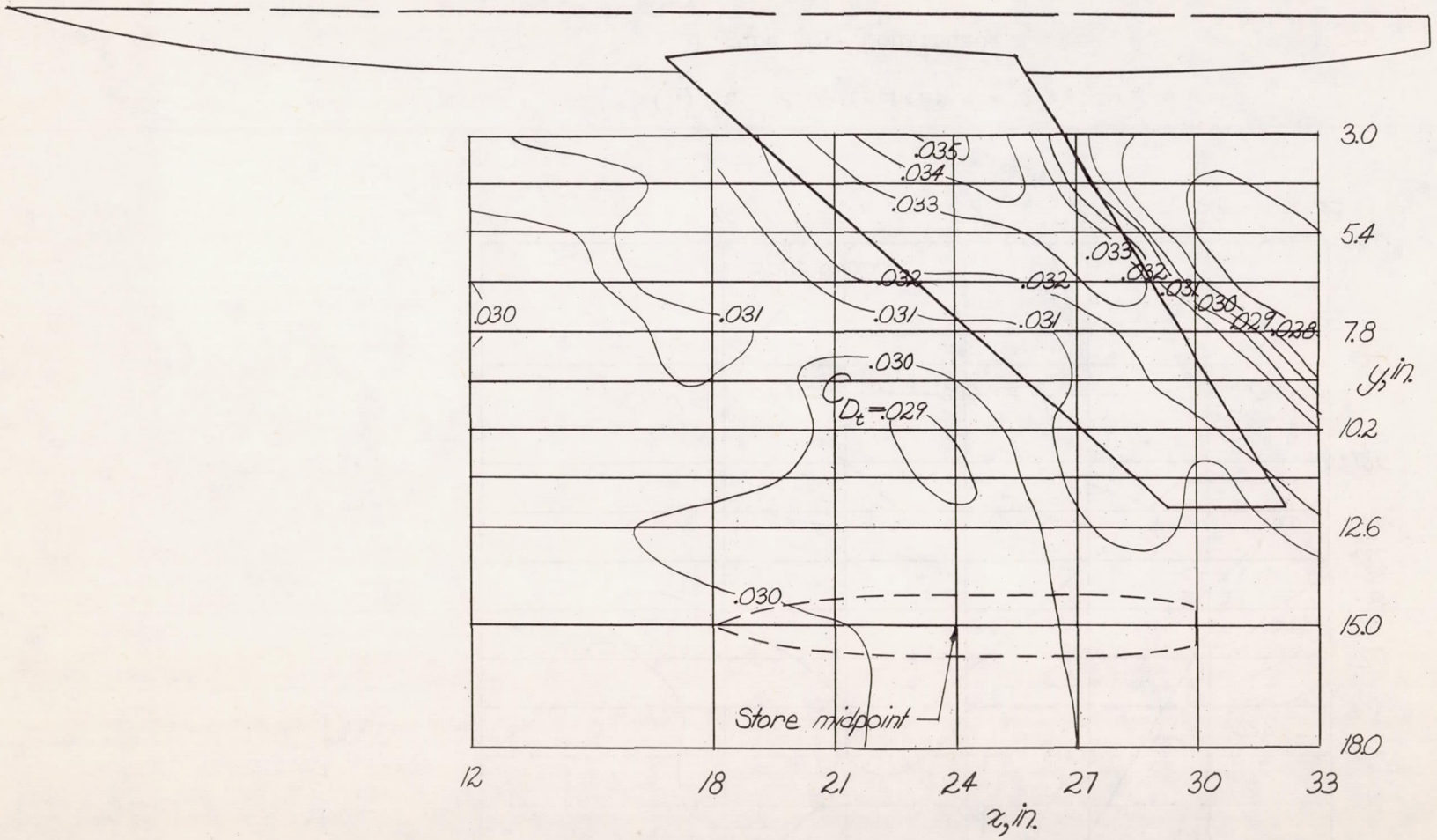
(b) z = 2.09 inches; $\alpha = 0^{\circ}$.

Figure 25.- Continued.



(c) z = 2.09 inches; $\alpha = 4^{\circ}$.

Figure 25.- Concluded.



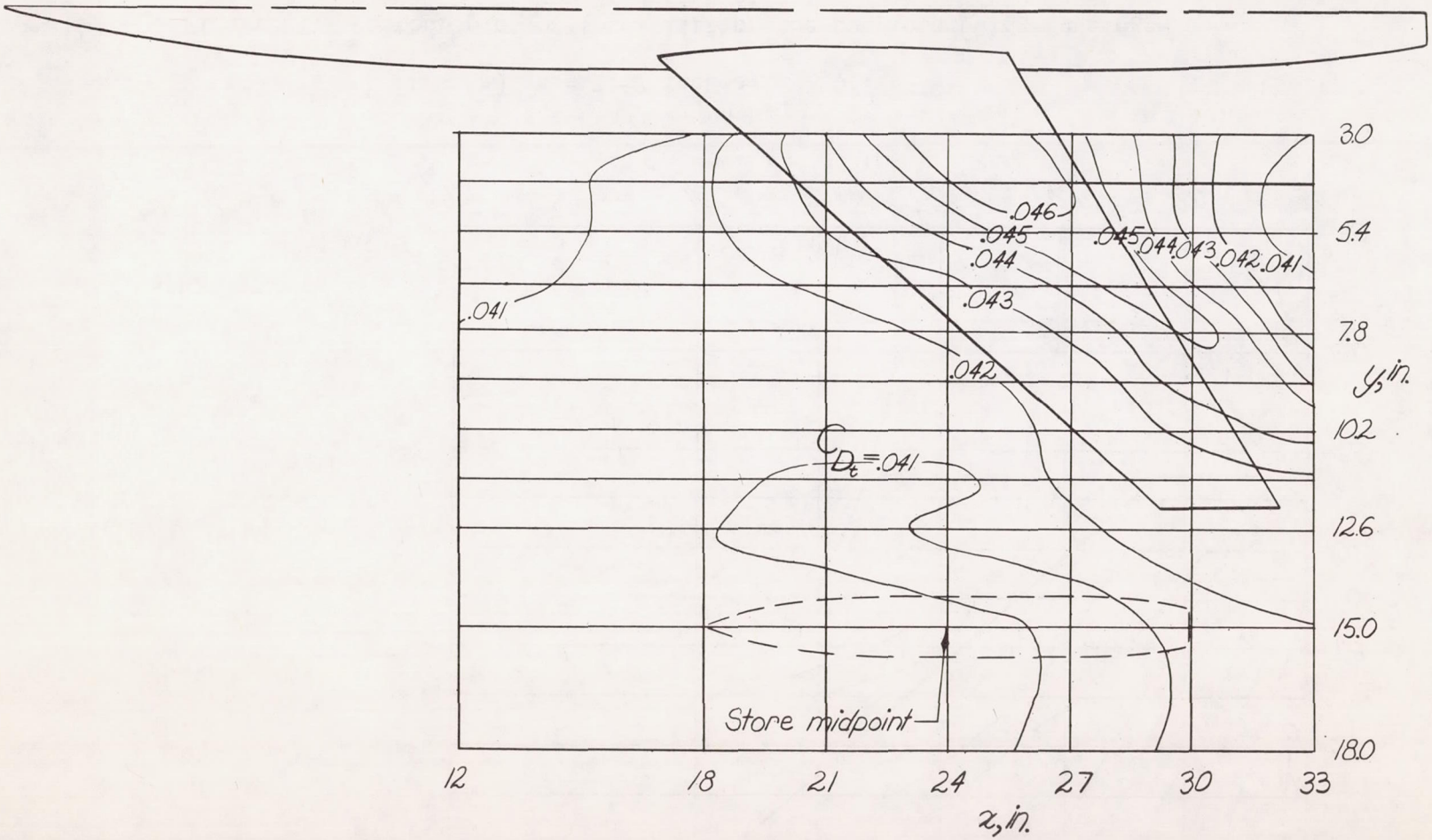
(a) z = 1.15 inches; $\alpha = 0^\circ$.

Figure 26.- Contour plot of the total drag of the complete (wing-fuselage-store) configuration.



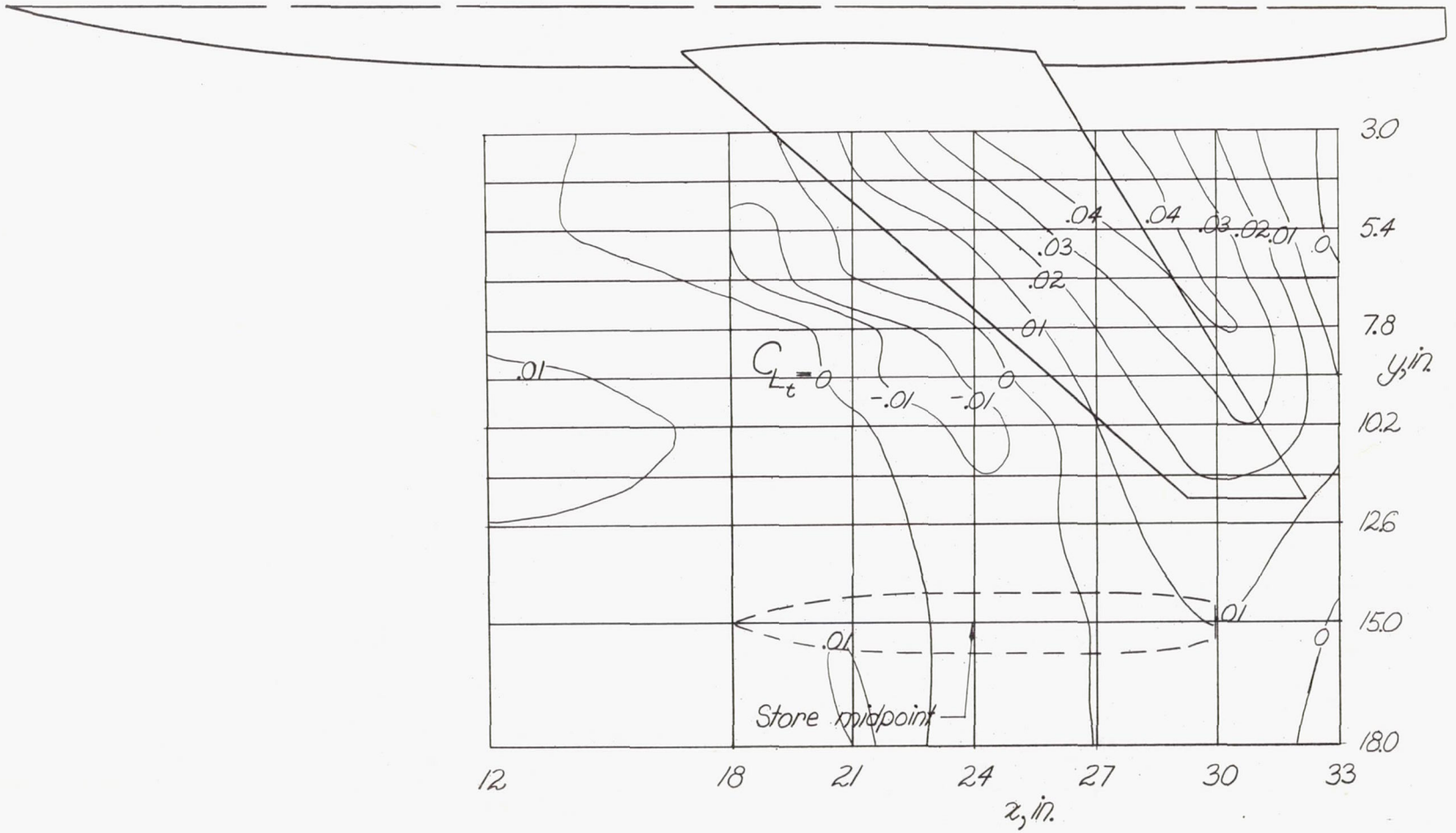
(b) z = 2.09 inches; $\alpha = 0^{\circ}$.

Figure 26.- Continued.



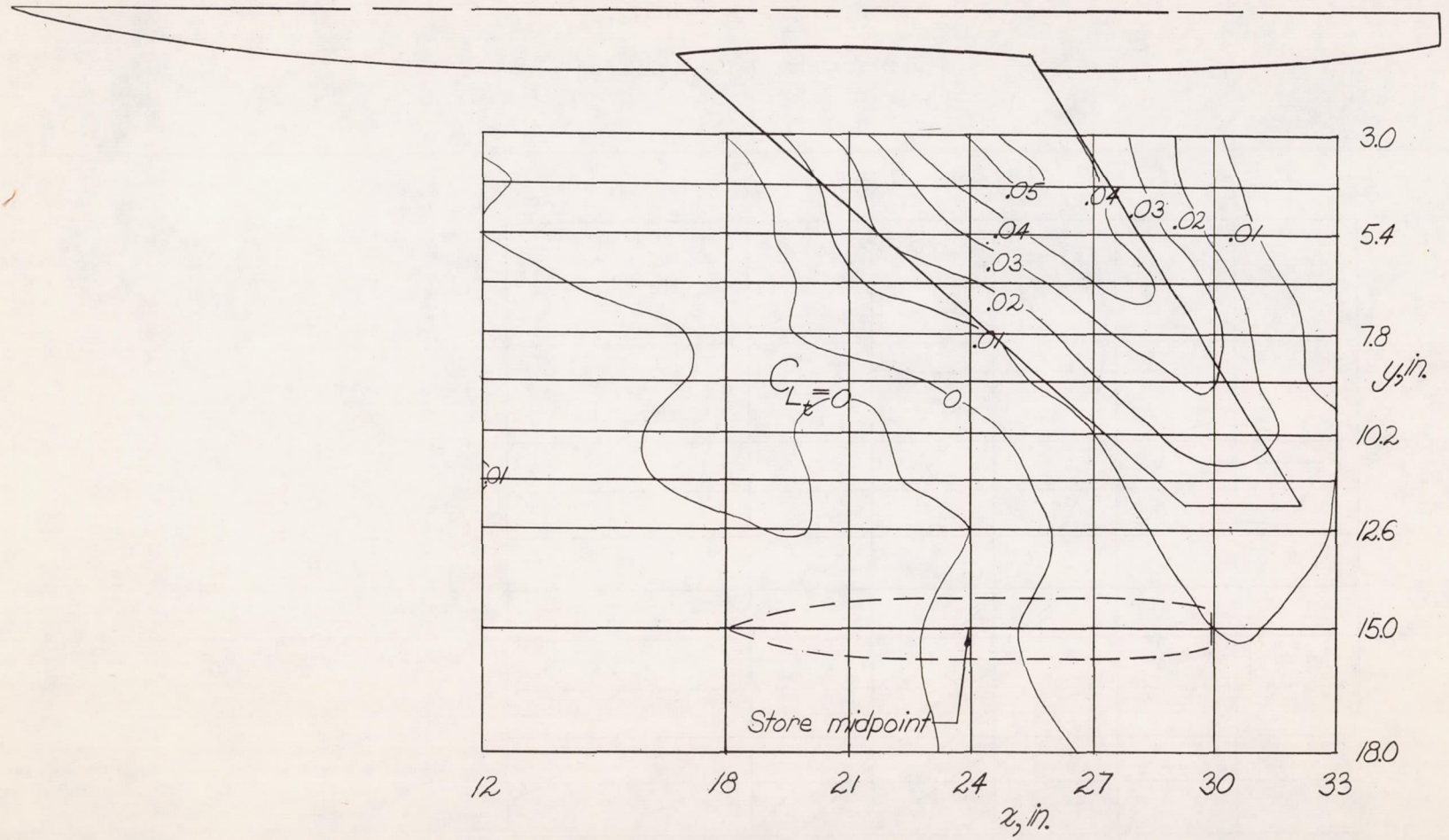
(c) z = 2.09 inches; $\alpha = 4^{\circ}$.

Figure 26.- Concluded.



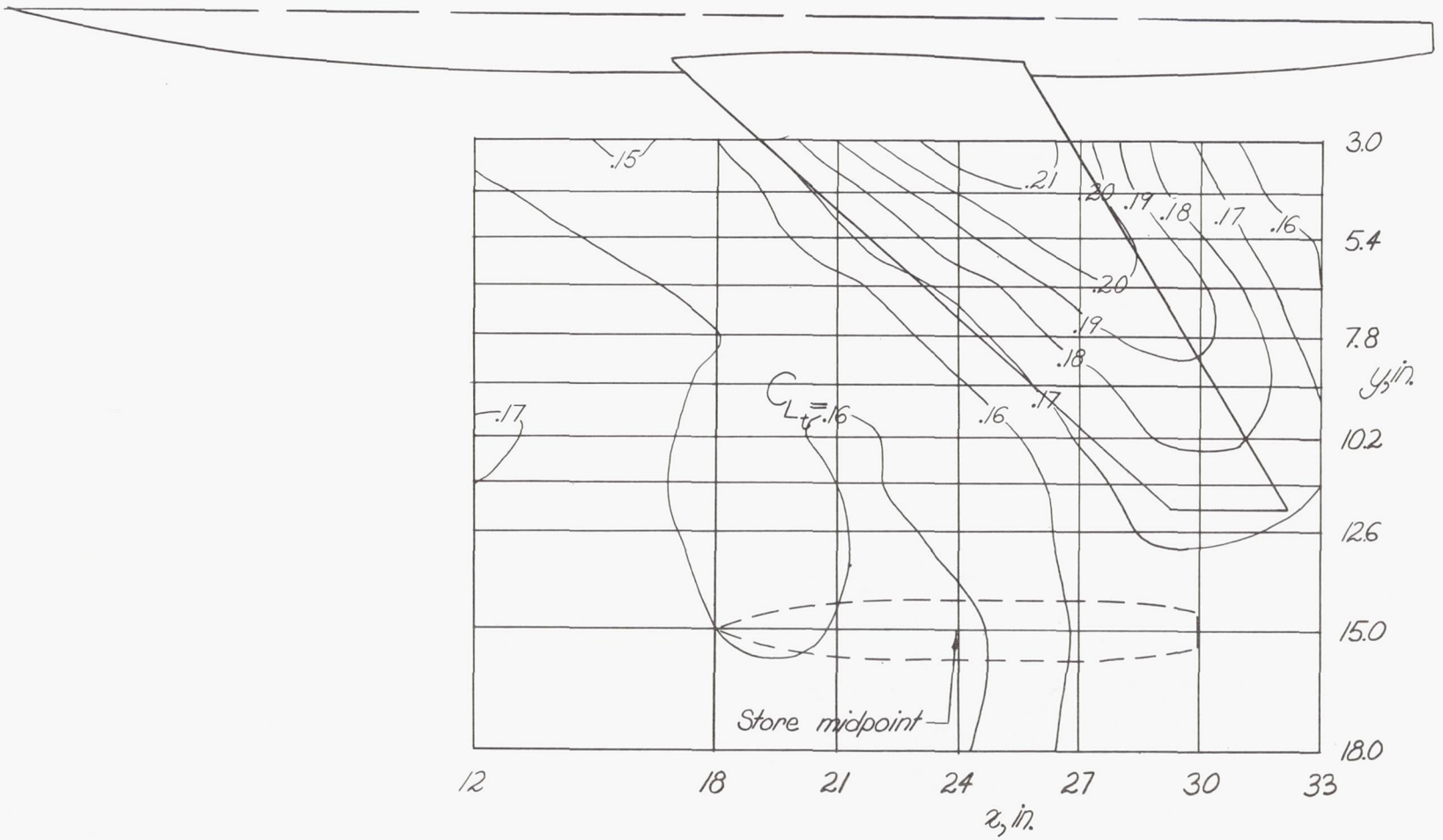
(a) z = 1.67 inches; $\alpha = 0^\circ$.

Figure 27.- Contour plot of total lift of the complete (wing-fuselage-store) configuration.



(b) z = 2.09 inches; $\alpha = 0^\circ$.

Figure 27.- Continued.



(c) z = 2.09 inches; $\alpha = 4^\circ$.

Figure 27.- Concluded.

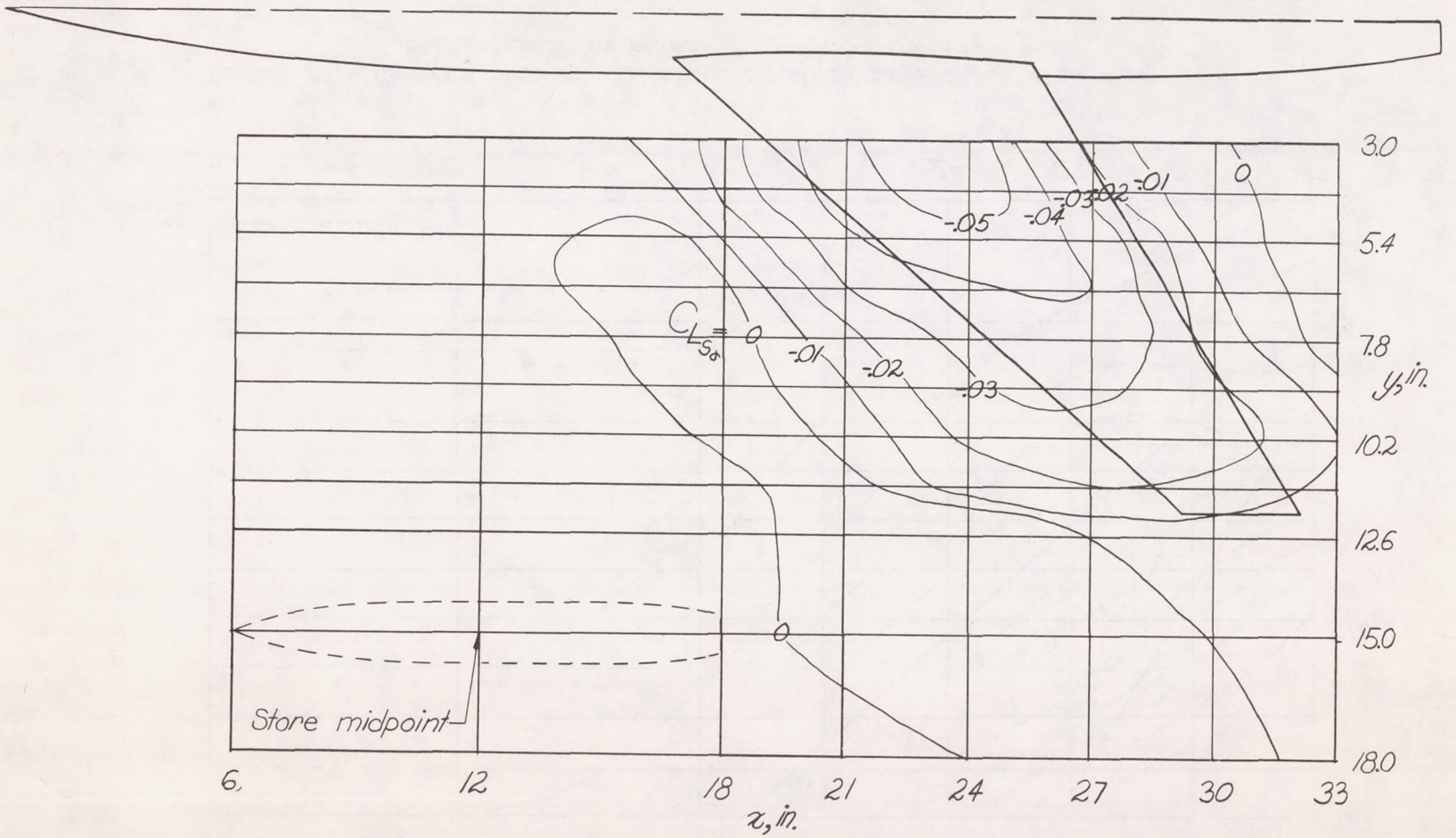


Figure 28.- Contour plot of the slope of store lift with wing-fuselage angle of attack. z = 2.09 inches.

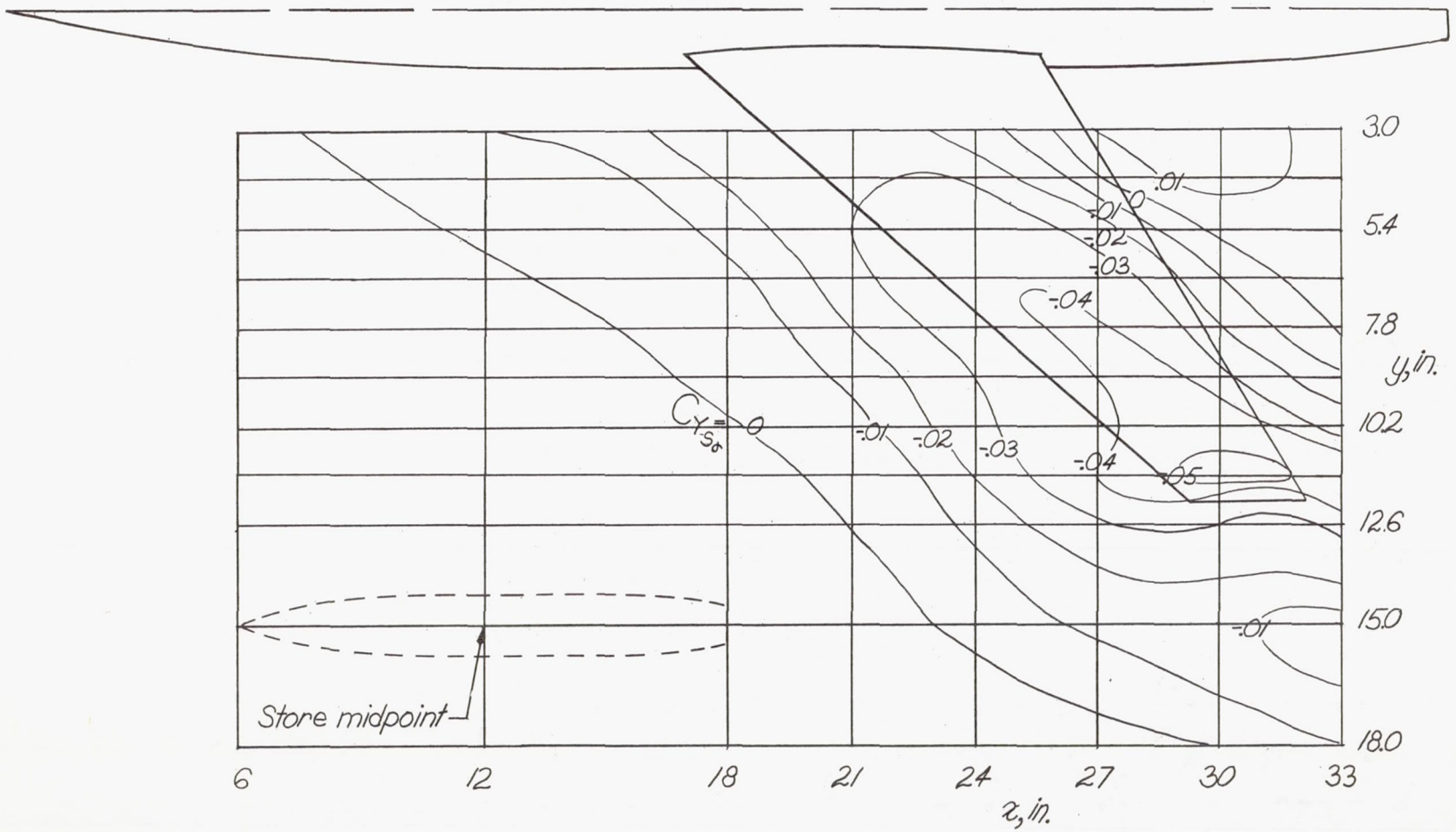


Figure 29.- Contour plot of the slope of store side force with wing-fuselage angle of attack. z = 2.09 inches.

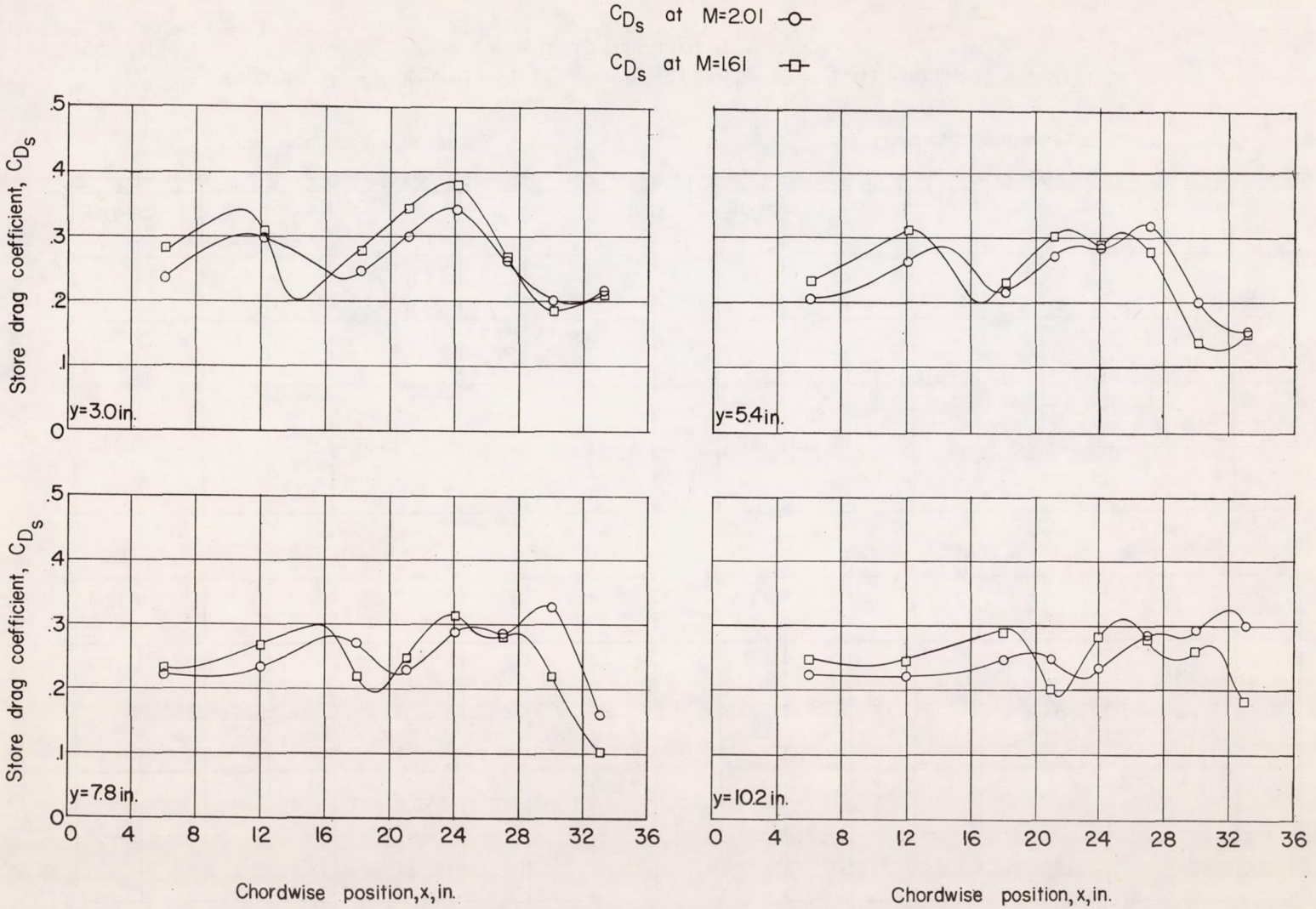


Figure 30.- Comparison of store drag at M = 1.61 and M = 2.01. z = 1.15 inches; $\alpha = 0^{\circ}$.

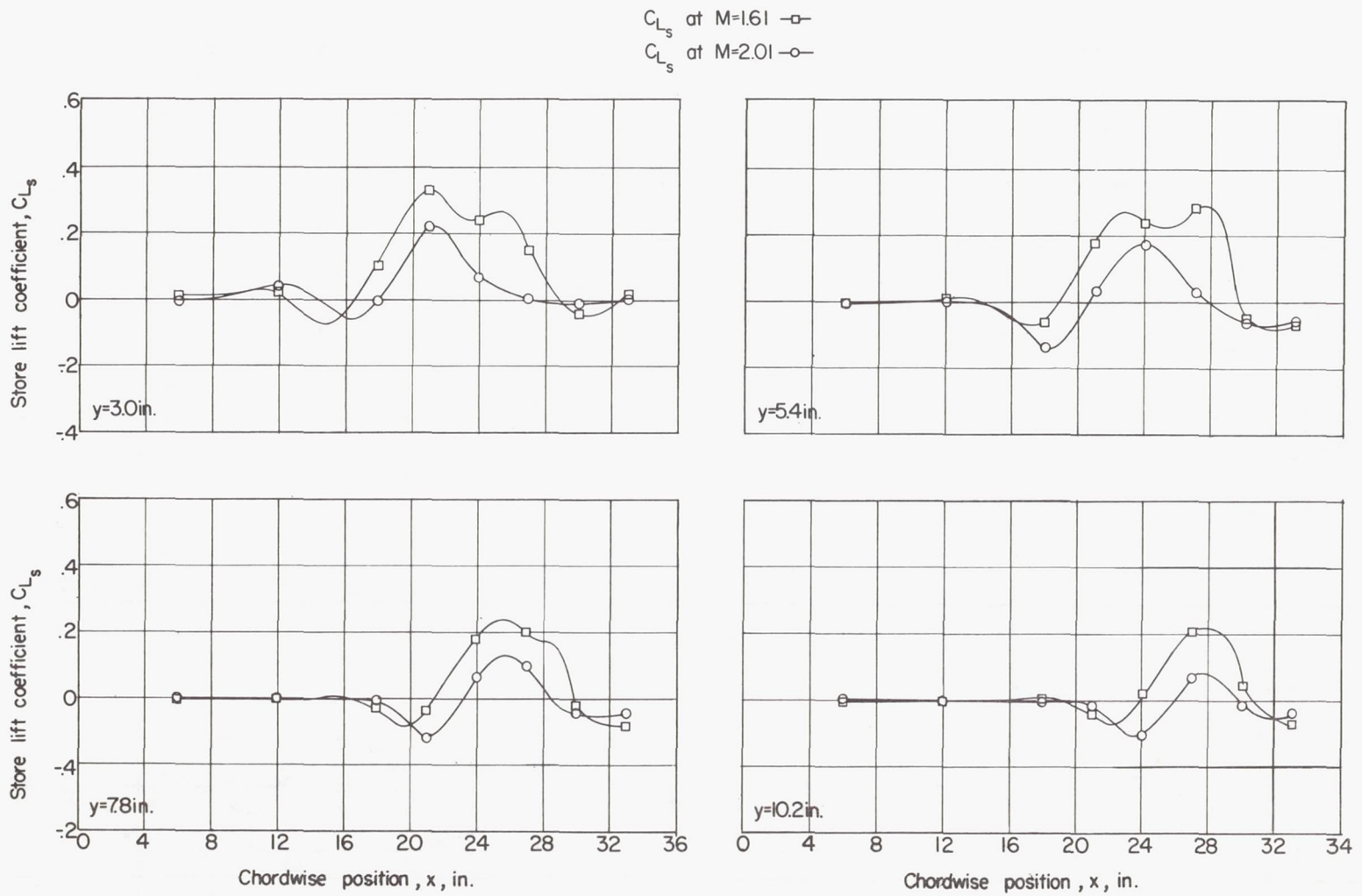


Figure 31.- Comparison of store lift at M = 1.61 and M = 2.01. z = 1.15 inches; $\alpha = 0^{\circ}$.

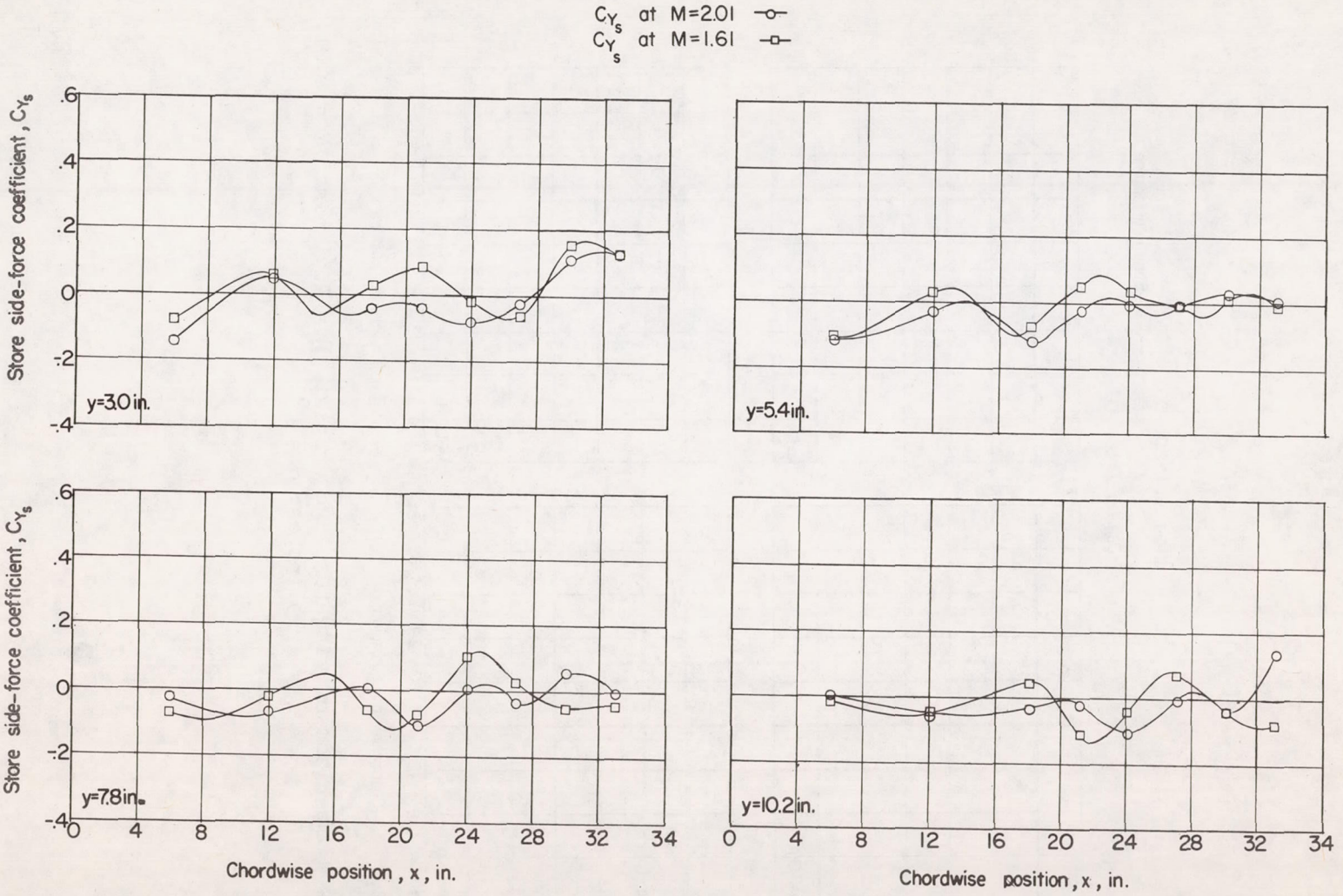


Figure 32.- Comparison of store side force at M = 1.61 and M = 2.01. z = 1.15 inches; $\alpha = 0^{\circ}$.

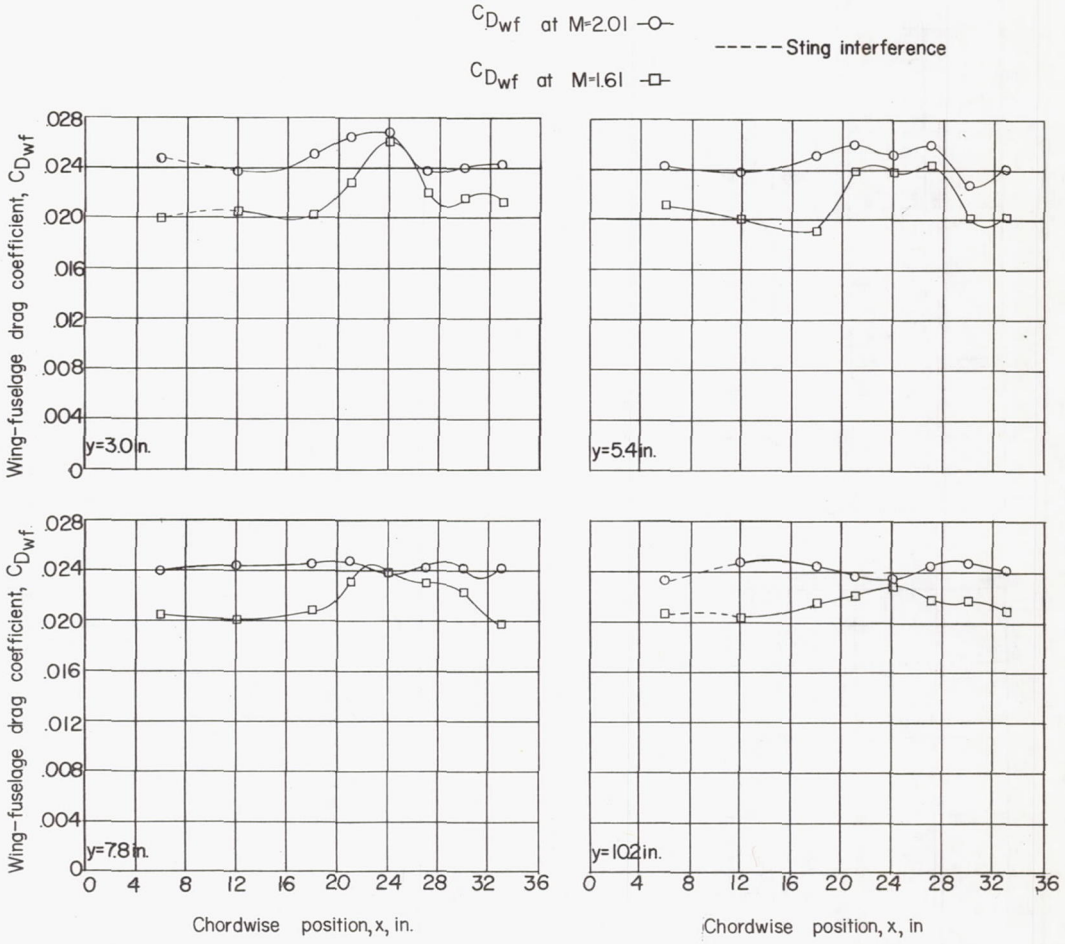


Figure 33.- Comparison of wing-fuselage drag at M = 1.61 and M = 2.01. z = 1.15 inches; $\alpha = 0^{\circ}$.

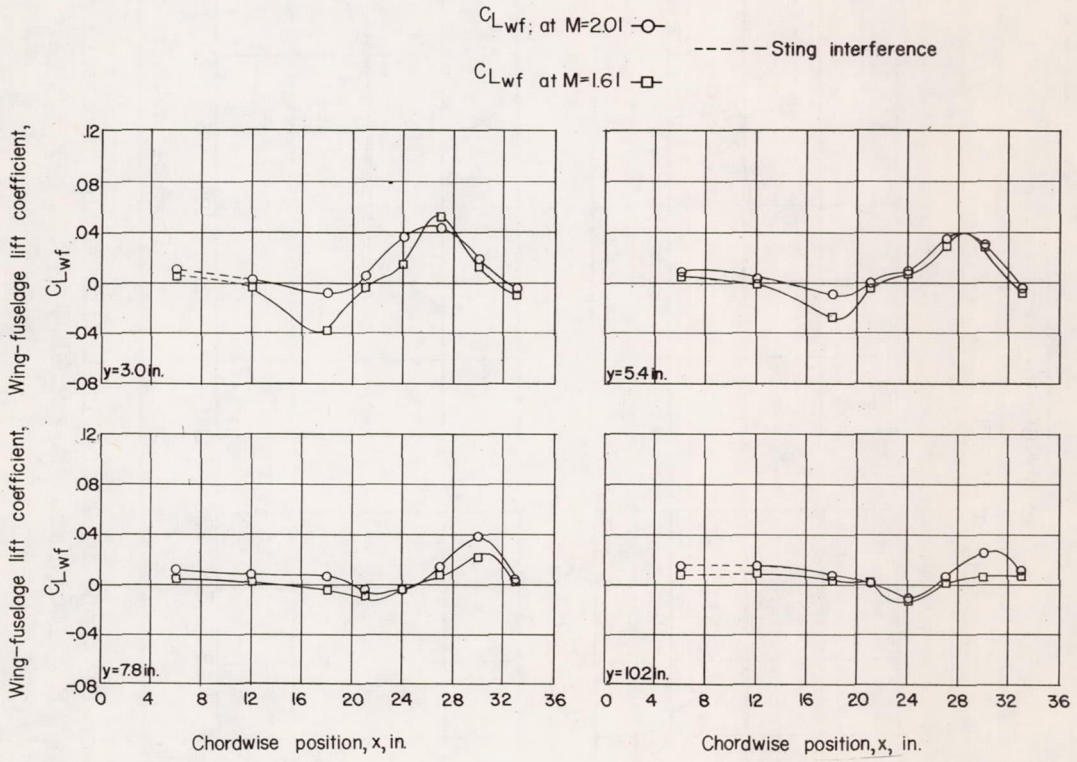


Figure 34.- Comparison of wing-fuselage lift at M = 1.61 and M = 2.01. z = 1.15 inches; $\alpha = 0^{\circ}$.

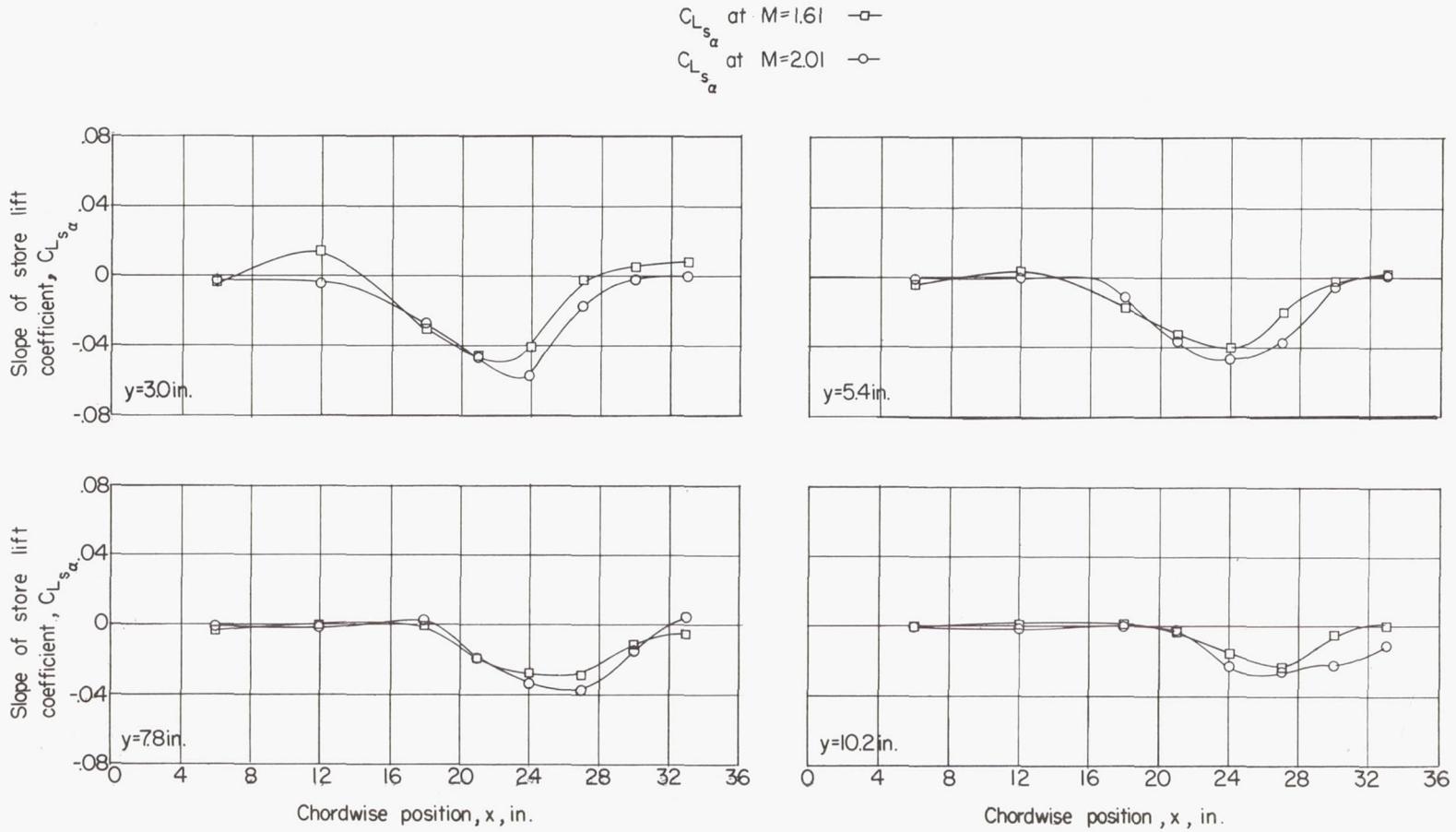


Figure 35.- Comparison of slope of store lift with angle of attack at M = 1.61 and M = 2.01.

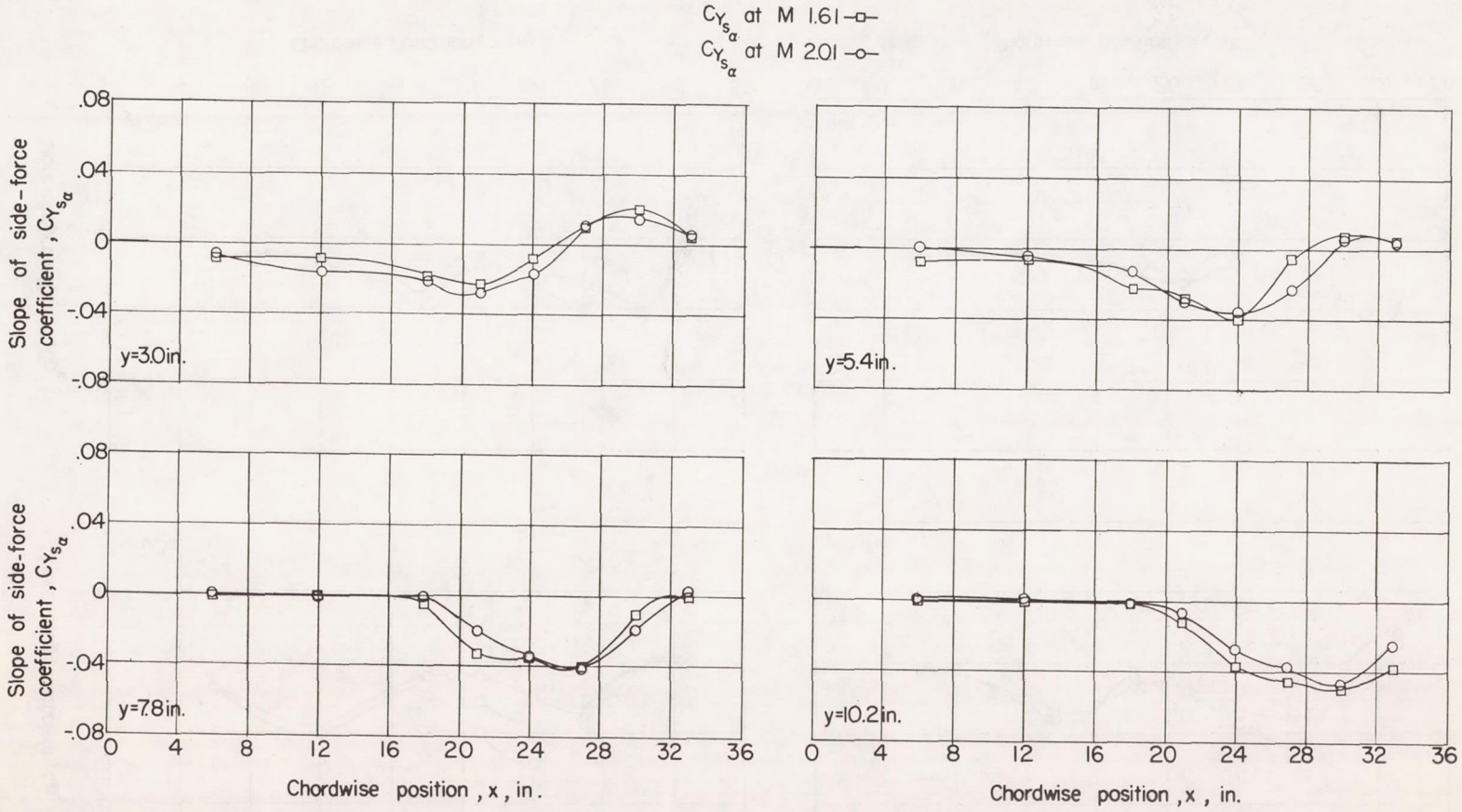


Figure 36.- Comparison of slope of store side force with angle of attack at M = 1.61 and M = 2.01.

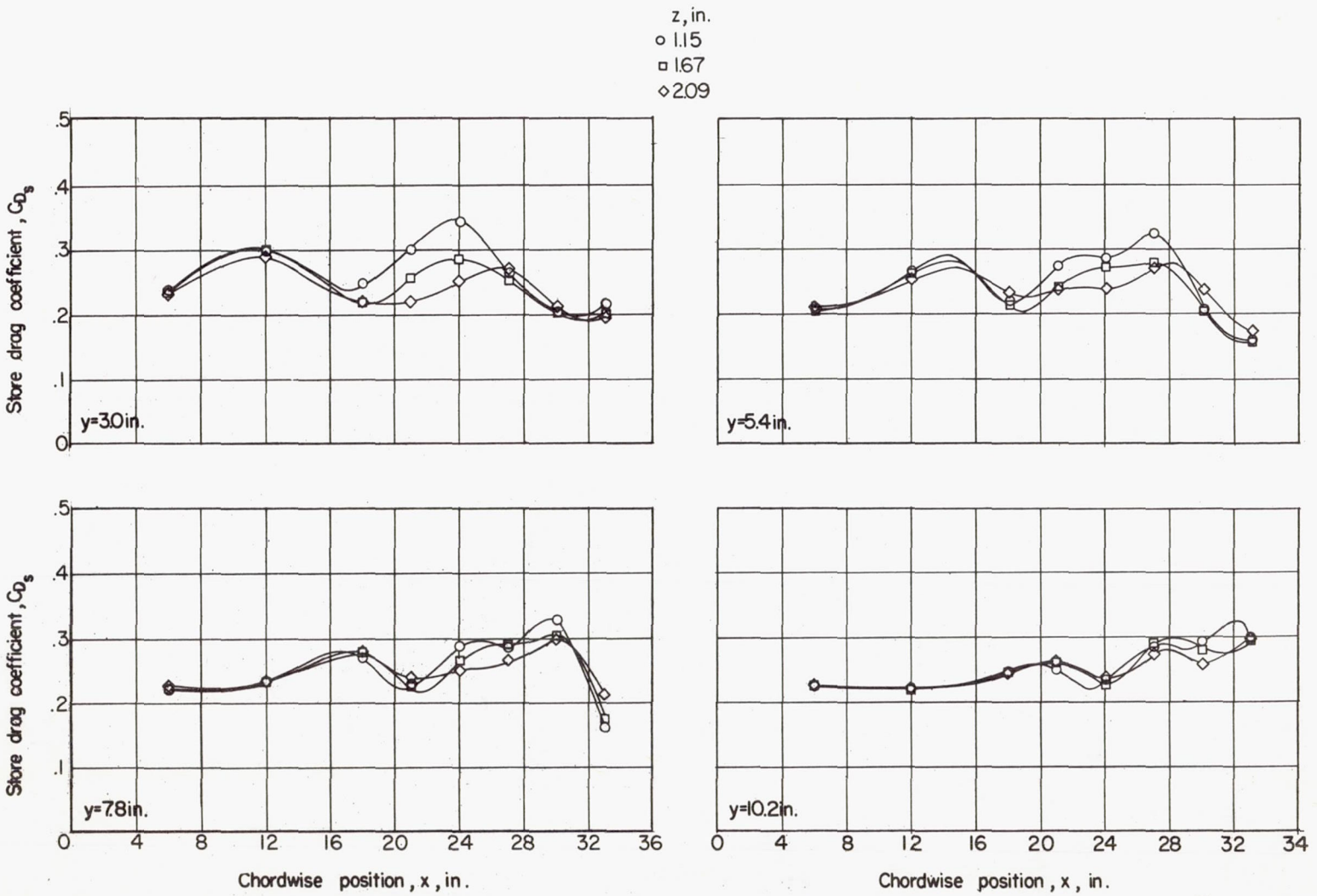


Figure 37.- Effect of store vertical location on store drag. $\alpha = 0^{\circ}$.

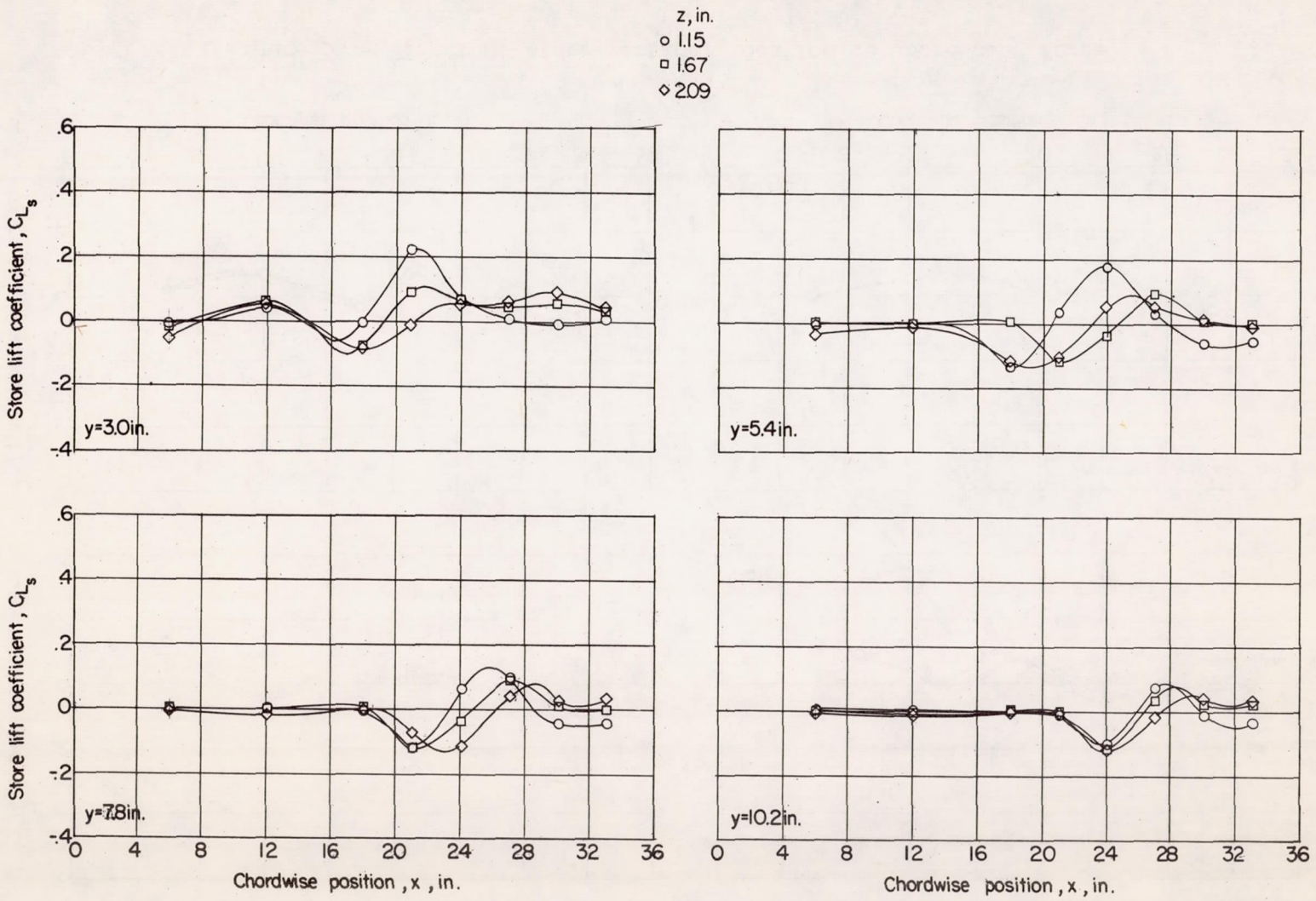


Figure 38.- Effect of store vertical location on store lift. $\alpha = 0^{\circ}$.

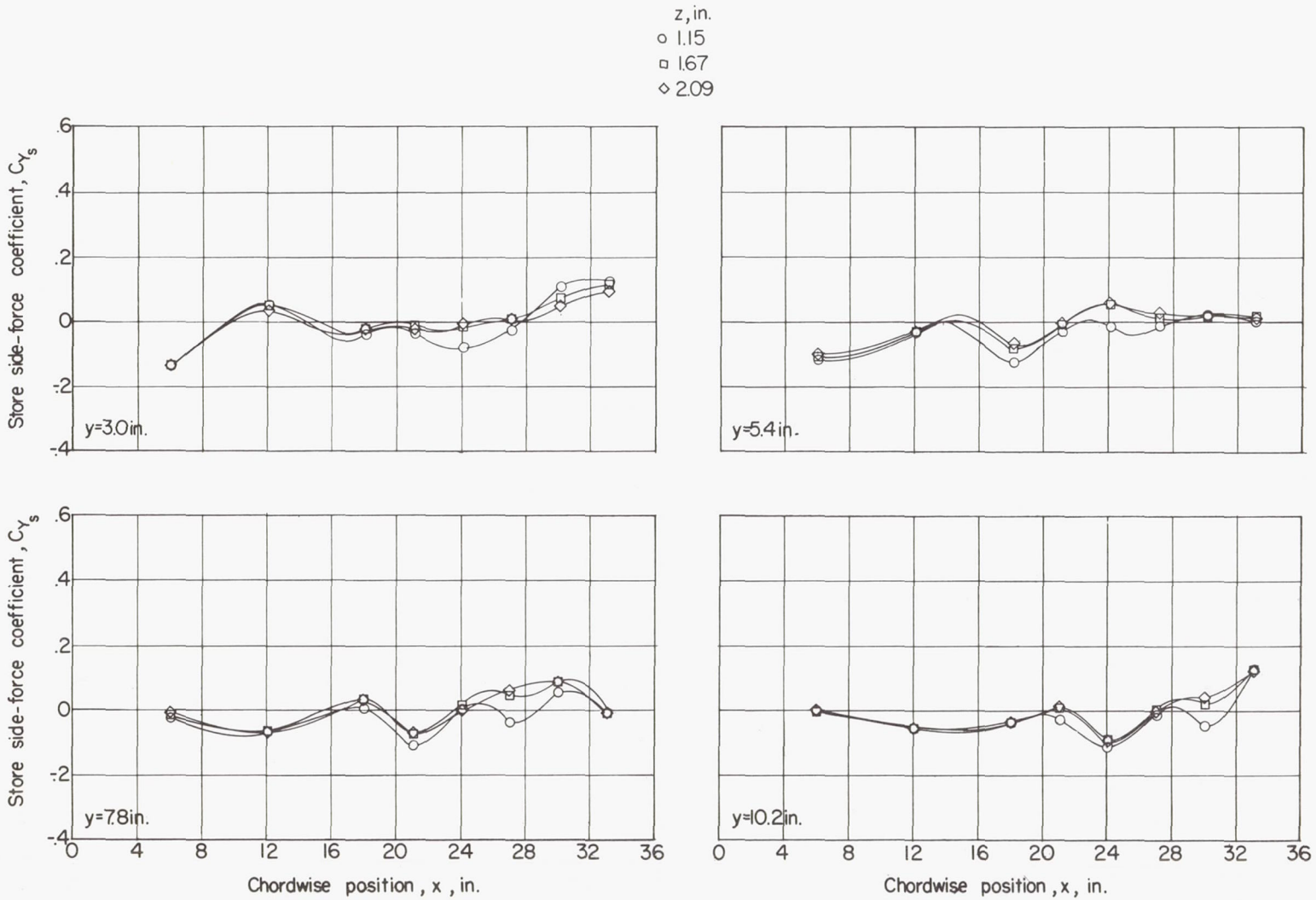


Figure 39.- Effect of store vertical location on store side force.

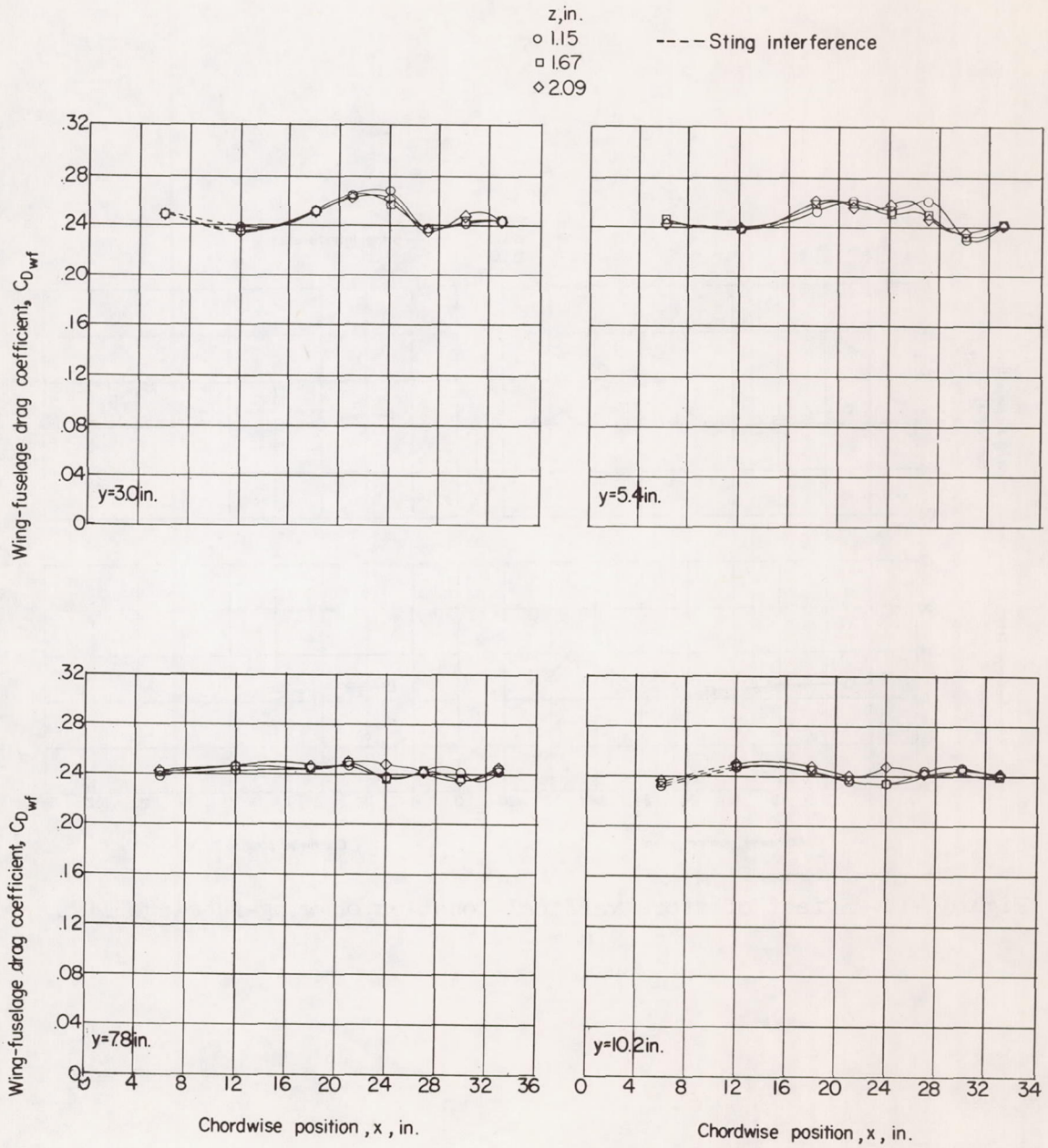


Figure 40.- Effect of store vertical location on wing-fuselage drag. $\alpha = 0^{\circ}$.

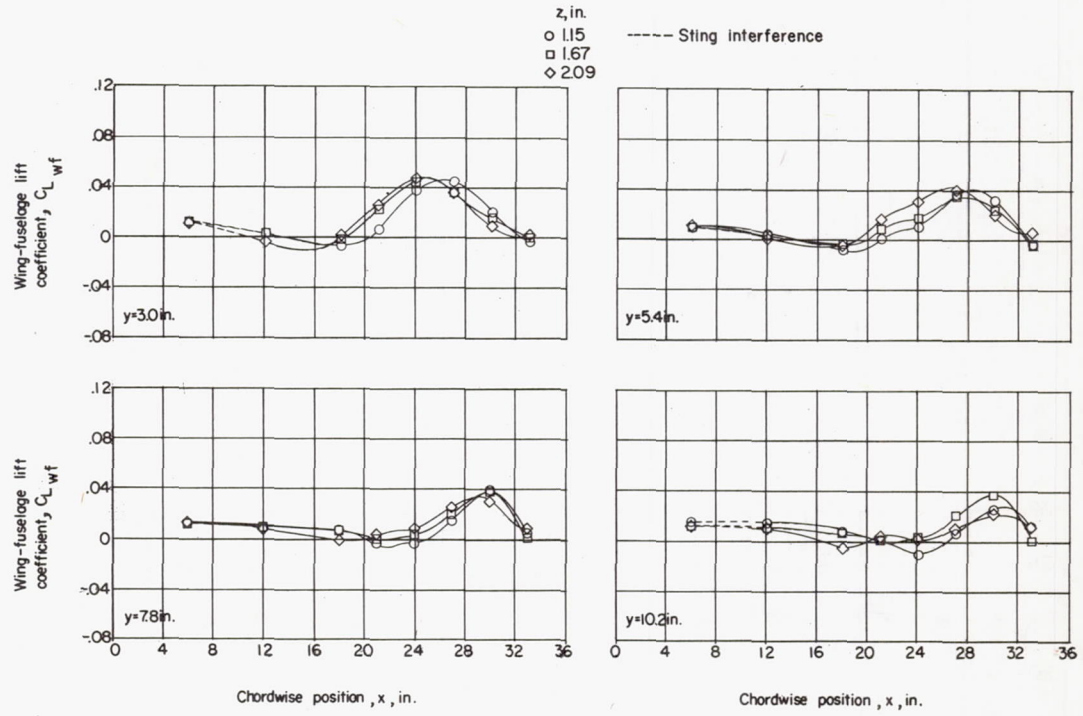


Figure 41.- Effect of store vertical location on wing-fuselage lift. $\alpha = 0^{\circ}$.

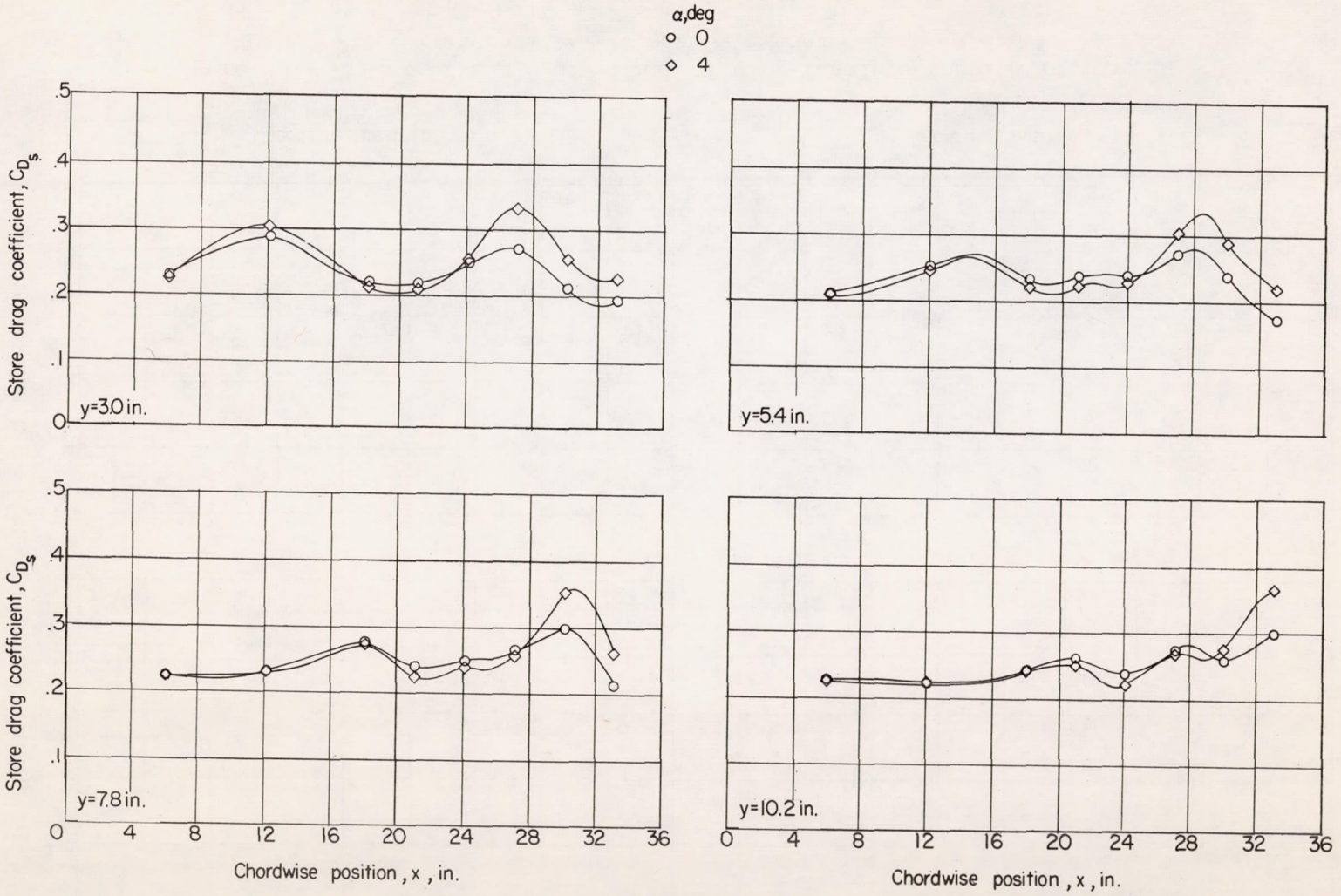


Figure 42.- Effect of angle of attack of wing-fuselage combination on store drag. z = 2.09 inches.

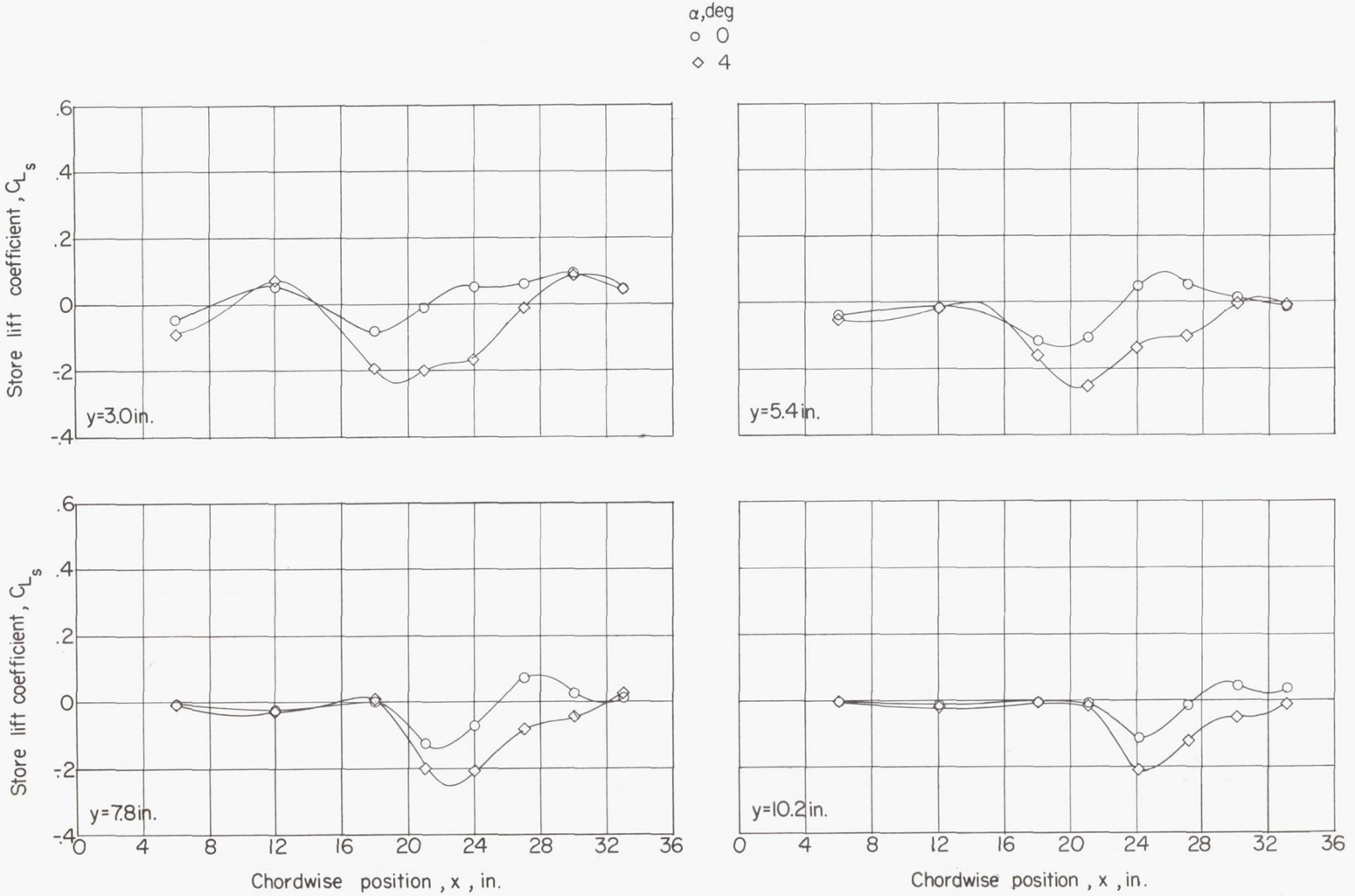


Figure 43.- Effect of angle of attack of wing-fuselage combination on store lift. z = 2.09 inches.

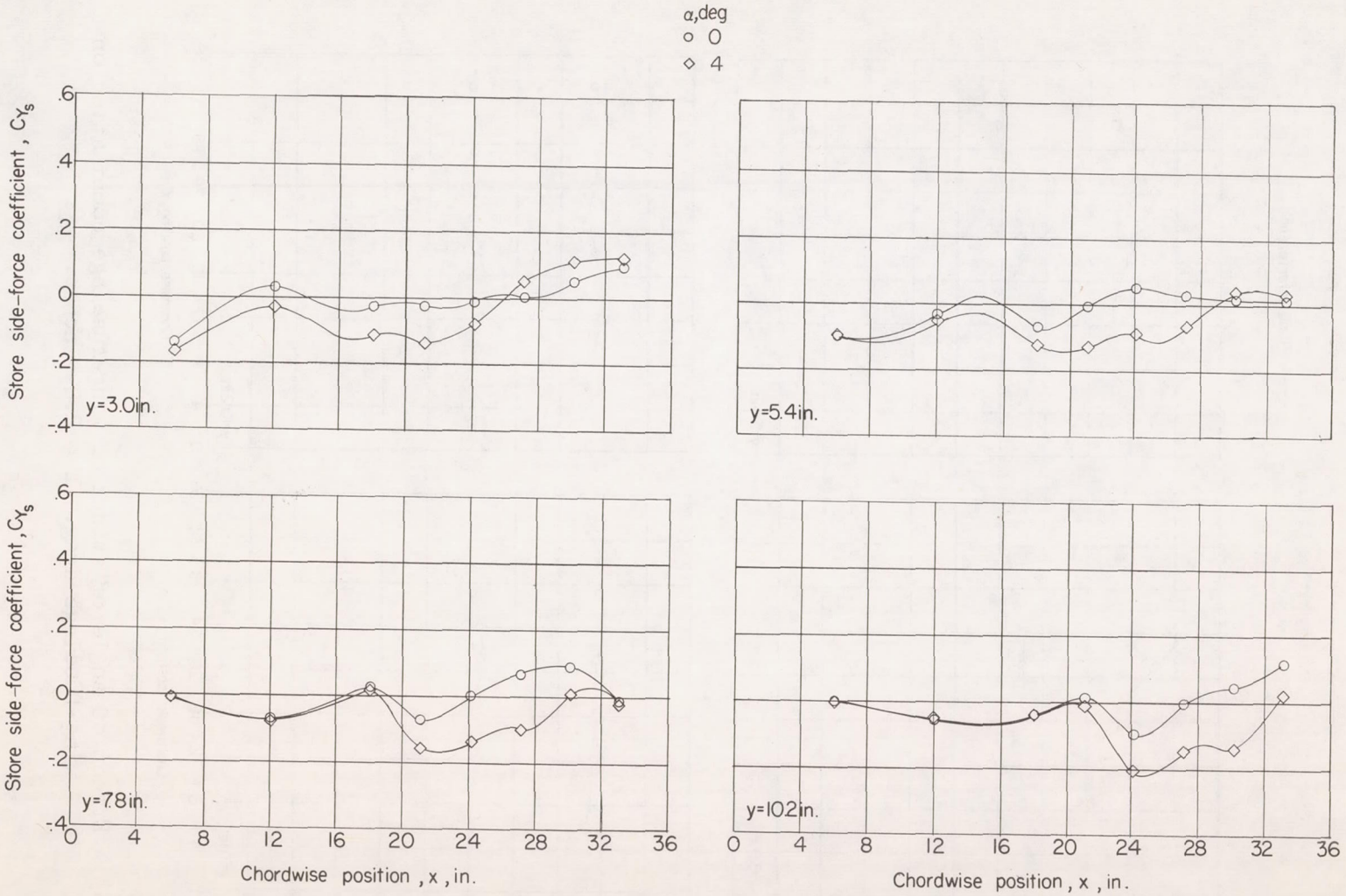


Figure 44.- Effect of angle of attack of wing-fuselage combination on store side force. z = 2.09 inches.

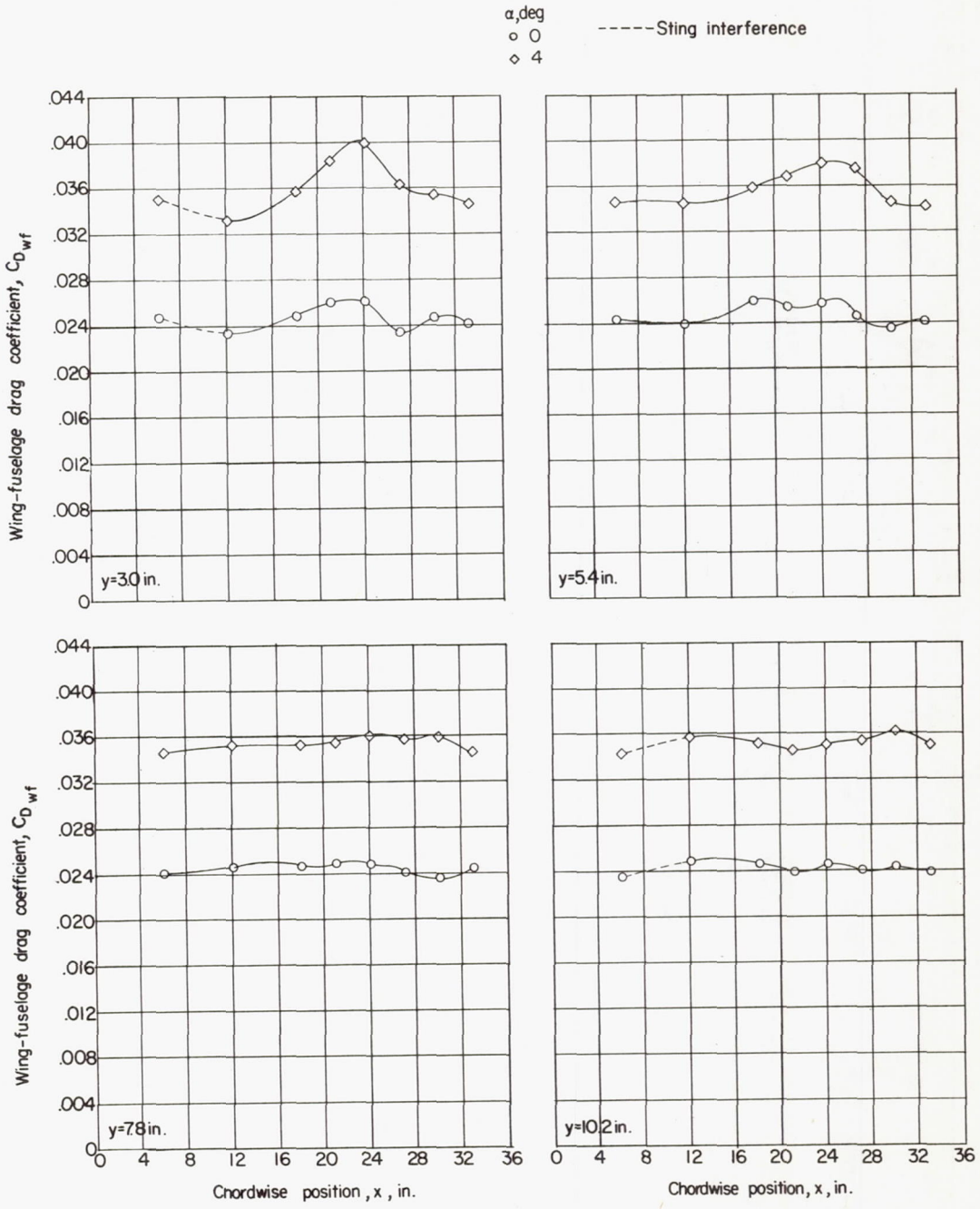


Figure 45.- Effect of angle of attack of wing-fuselage combination on wing-fuselage drag. z = 2.09 inches.

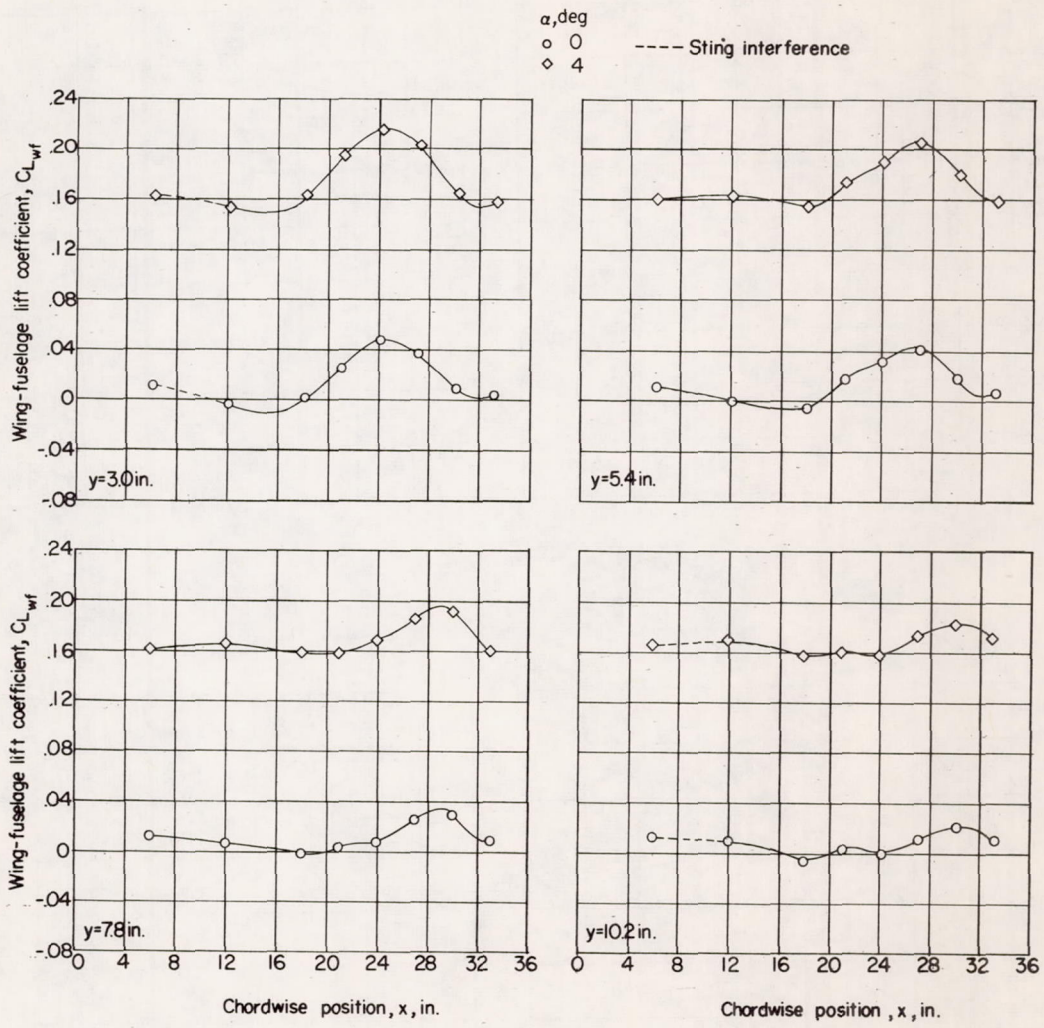


Figure 46.- Effect of angle of attack of wing-fuselage combination on wing-fuselage lift. z = 2.09 inches.

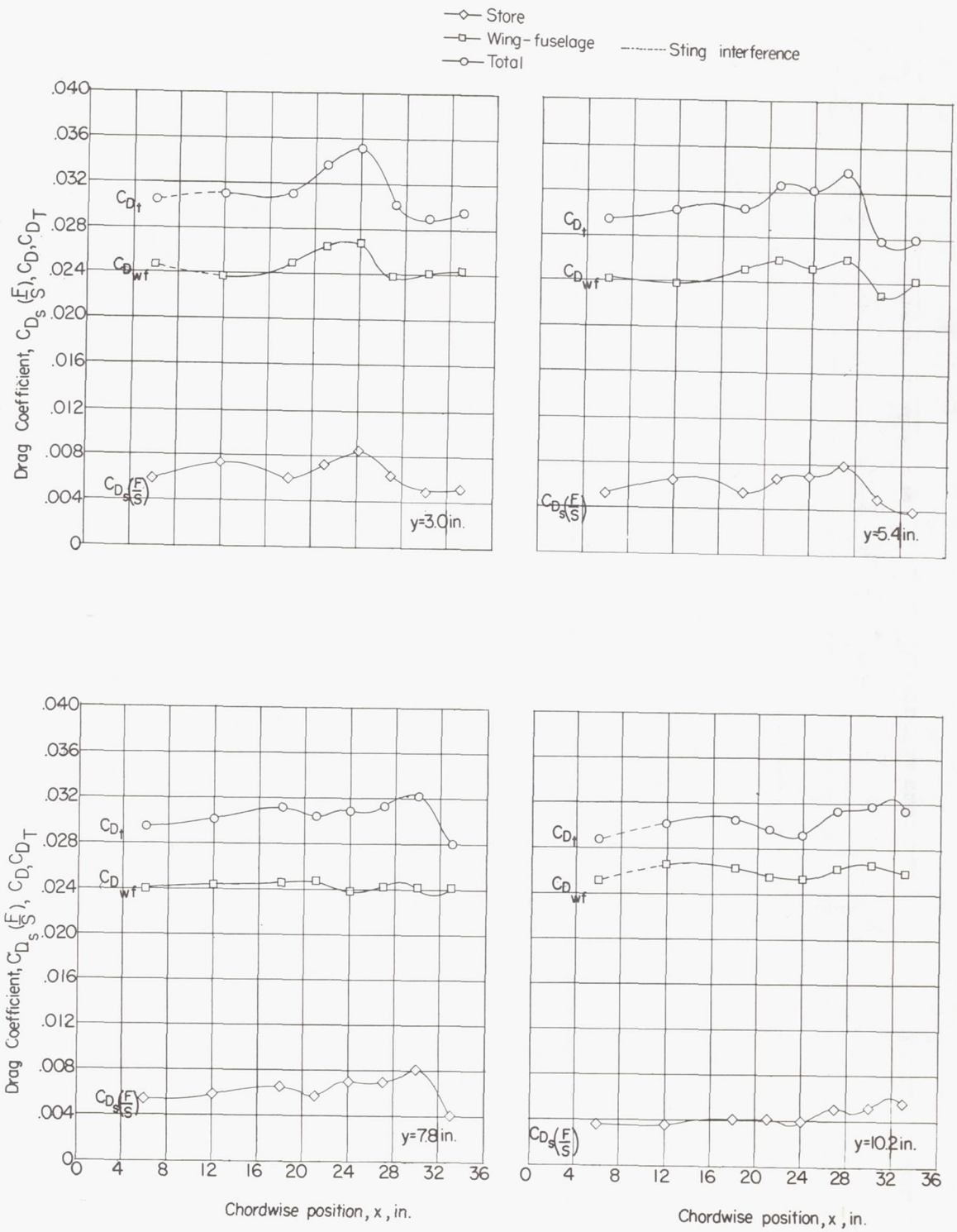


Figure 47.- Relative contribution of store and wing-fuselage drag to total drag. z = 1.15 inches; $\alpha = 0^{\circ}$.

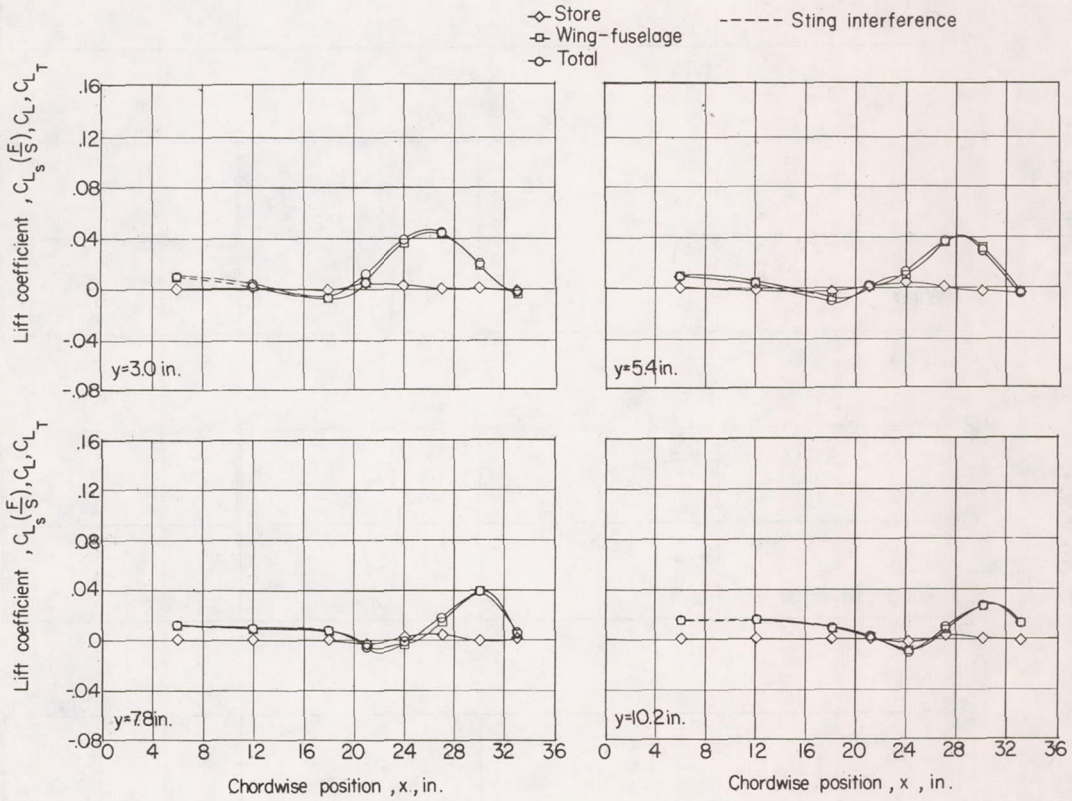
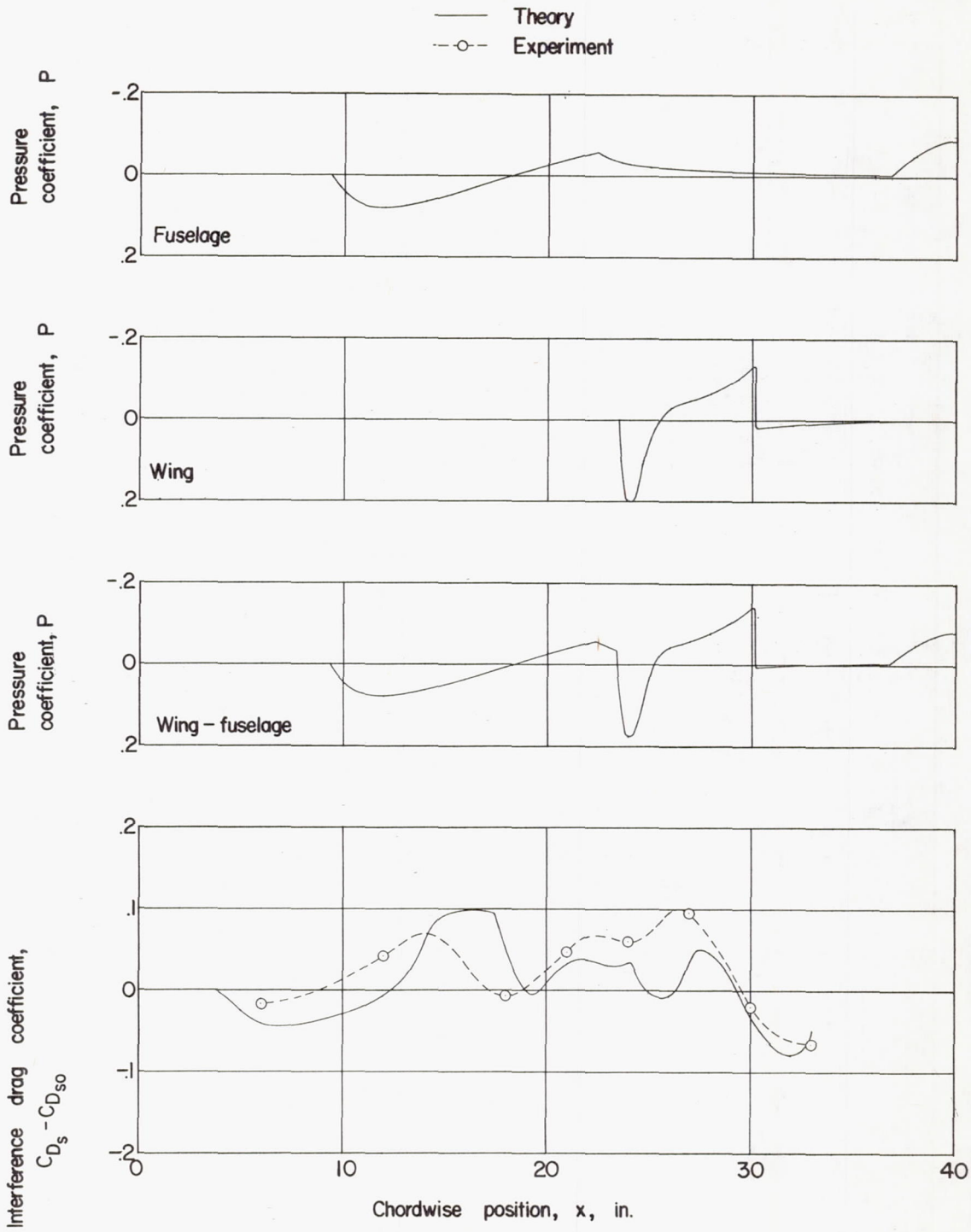
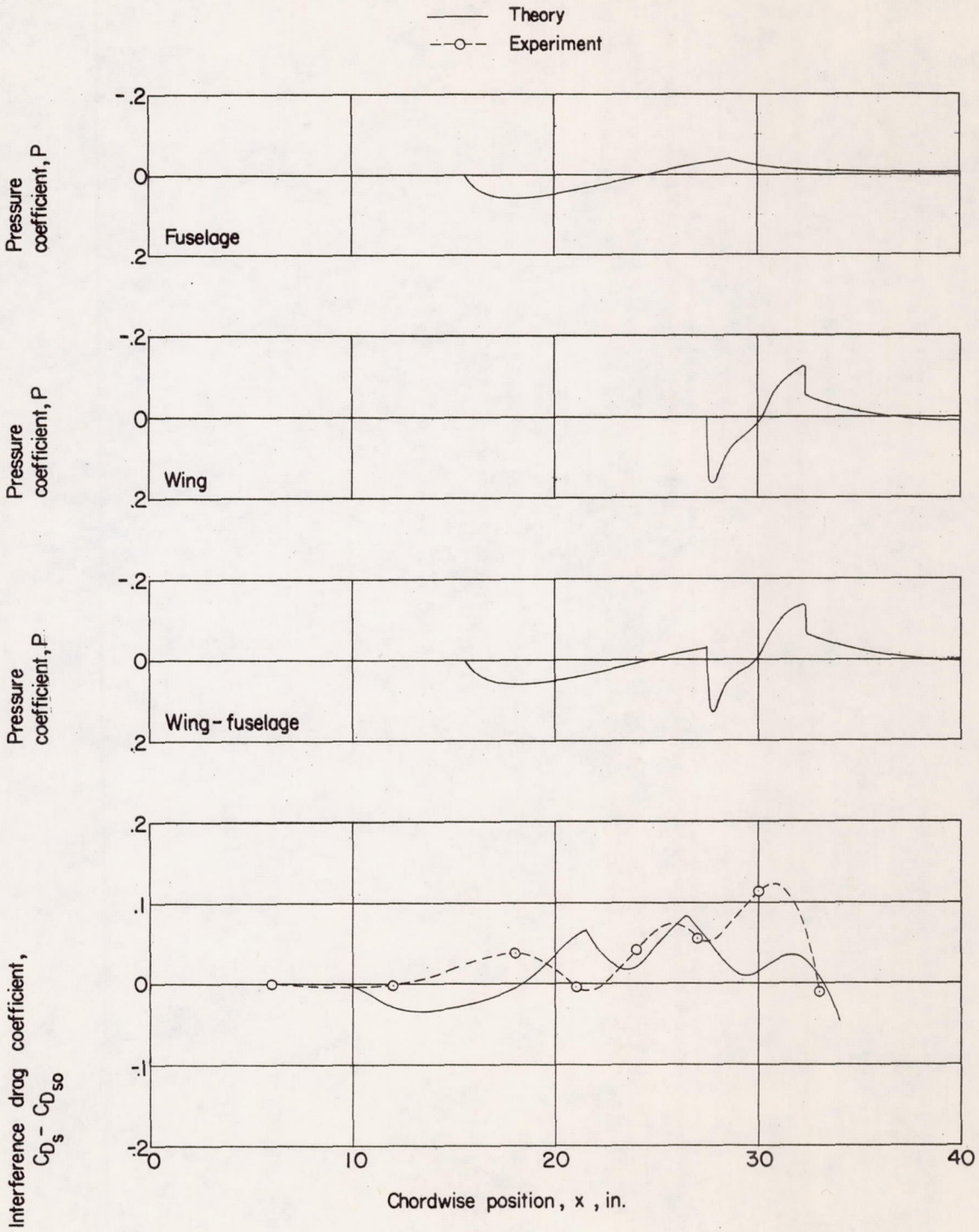


Figure 48.- Relative contribution of store and wing-fuselage lift to total lift. z = 1.15 inches; $\alpha = 0^{\circ}$.



(a) y = 5.4.

Figure 49.- Theoretical pressure distribution and a comparison of theoretical and experimental interference store drag. z = 1.15; $\alpha = 0^{\circ}$.



(b) y = 9.0.

Figure 49.- Concluded.